PREPARATION, CHARACTERIZATION AND APPLICATION OF ACTIVATED CARBON FROM AGRICULTURAL SOLID WASTES

NORLI BINTI UMAR

FACULTY OF SCIENCE
UNIVERSITI MALAYA
KUALA LUMPUR

2022

UNIVERSITI MALAYA

ORIGINAL LITERARY WORK DECLARATION

Name of Candidate: NORLI BINTI UMAR

Registration/Matric No: SMA190012 / 17202057

Name of Degree: Masters of Science (Chemistry)

Title of Project Paper/Research Report/Dissertation/Thesis ("this Work"):

PREPARATION, CHARACTERIZATION AND APPLICATION OF ACTIVATED CARBON FROM AGRICULTURAL SOLID WASTES

Field of Study: Chemistry

I do solemnly and sincerely declare that:

- (1) I am the sole author/writer of this Work;
- (2) This Work is original;
- (3) Any use of any work in which copyright exists was done by way of fair dealing and for permitted purposes and any excerpt or extract from, or reference to or reproduction of any copyright work has been disclosed expressly and sufficiently and the title of the Work and its authorship have been acknowledged in this Work;
- (4) I do not have any actual knowledge nor do I ought reasonably to know that the making of this work constitutes an infringement of any copyright work;
- (5) I hereby assign all and every right in the copyright to this Work to the Universiti Malaya ("UM"), who henceforth shall be owner of the copyright in this Work and that any reproduction or use in any form or by any means whatsoever is prohibited without the written consent of UM having been first had and obtained;
- (6) I am fully aware that if in the course of making this Work, I have infringed any copyright whether intentionally or otherwise, I may be subject to legal action or any other action as may be determined by UM.

Candidate's Signature	Date: 14th May 2022
	·
Subscribed and solemnly declared before,	
Witness's Signature	Date: 14 th May 2022
Name:	
Designation:	

PREPARATION, CHARACTERIZATION AND APPLICATION OF ACTIVATED CARBON FROM AGRICULTURAL SOLID WASTES

ABSTRACT

The purpose of this study was to prepare activated carbon (AC) from palm kernel shells (PKS) and coconut shells (CS) as soot adsorbents. The proximate, ultimate, and lignocellulosic background study was conducted to determine the composition of the starting material. Thermogravimetric analysis (TGA) was used to verify the lignocellulosic content and thermal stability of the biomass. Following this, an optimization study was conducted to produce AC with the desired properties. Fourier Transform Infra-red (FTIR) analysis was conducted as validation of the optimization study. Carbonization was followed by chemical activation (H₃PO₄, KOH and ZnCl₂) and finally microwave radiation treatment. The percentage yield was calculated to determine the efficiency of AC production. The surface area was determined using the Brunauer-Emmett-Teller (BET) method, and the surface acidity and basicity were determined using Boehm titration. Field Emission Scanning Electron Microscope (FESEM) was used to gain insight into the morphology of the AC. Energy Dispersive X - Ray analysis (EDX) was conducted to identify soot presence on the AC surface. The composition analysis reveals that despite the starting materials being from different plant species, both PKS and CS have similar chemical compositions except ash content. In this work, the ash content is found to be 2.16% and 0.24% for PKS and CS, respectively. In addition, PKS primarily comprised of lignin (40.7%) while CS mainly comprised of hemicellulose (38.9%). The optimal carbonization temperature used for preparation of biochar was 650°C and 600°C for PKS and CS, respectively. Each biochar or carbonized biomass was activated at a 1:1 w/w ratio of carbonized biomass and activating agent for 30 minutes at room temperature followed by 4 minutes of microwave radiation. After the optimized method was implemented, CS and PKS activated with ZnCl₂ and microwave radiation (MZCS and MZPKS) has the most suitable characteristic to be applied as a soot adsorbent. This is due to the BET surface area collected being the highest at 391.26 m²/g for MZCS and 367.12 m²/g for MZPKS. In addition, the percentage yield of both AC is acceptable and the morphology shown in FESEM images showed the most uniform pores. Through Boehm titration, it was discovered that the MZCS and MZPKS surface was predominantly acidic. After MZCS and MZPKS were exposed to soot emitted from paddy straw burning, MZCS shows the most visible physical adsorption and an even distribution of soot on the surface and within the pores. The MZCS maximum capacity was 30 minutes for approximately 23 g of paddy straw burning using 0.1 g of AC. Economic feasibility studies have been conducted and it has been determined that the laboratory scale price of AC is 4.78 USD / kg.

Keywords: activated carbon, agricultural waste, soot adsorption, palm kernel shell, coconut shell

PENYEDIAAN, PENCIRIAN DAN APLIKASI KARBON TERAKTIF DARI SISA PERTANIAN

ABSTRAK

Tujuan penyelidikan in dijalankan adalah bagi menyediakan karbon teraktif (AC) dari tempurung kelapa sawit (PKS) dan tempurung kelapa (CS) sebagai penjerap jelaga. Analisis proksimat, altimat and latar belakang lignoselulosa dijalankan bagi mengenalpasti komposisi bahan mula. Analisis Termogravimatrik (TGA) digunakan bagi mengesahkan kandungan lignoselulosa dan kestabilan termal biojisim. Kajian pengoptimuman dijalankan bagi menghasilkan AC dengan sifat dikehendaki. Analisis pengtransformasian Fourier infra – merah (FTIR) dijalankan sebagai validasi kajian pengoptimuman. Pengkarbonan dijalankan melalui pengaktifan kimia (H₃PO₄, KOH and ZnCl₂) diikuti radiasi gelombang mikro. Peratusan hasil dikira bagi mengenalpasti kecekapan produksi AC. Luas permukaan ditentukan melalui kaedah Brunauer – Emmett - Teller (BET) dan kadar asid dan bes permukaan ditentukan melalui pentitratan Boehm. Mikroskopi elektron pengimbasan pancaran medan (FESEM) digunakan bagi menilai morfologi permukaan AC. Analisis tenaga x – ray serakan (EDX) digunakan bagi mengenalpasti kehadiran jelaga pada permukaan AC. Analisis komposisi menunjukkan walaupun bahan pemula adalah daripada tumbuhan berbeza spesis, komposisi kimia adalah lebih kurang. Kecuali pada kandungan abu iaitu sebanyak 2.16% bagi PKS dan 0.24% bagi CS. Tambahan pula, PKS mengandungi lebih lignin (40.67%) berbanding CS mempunyai lebih banyak kandungan hemiselulosa (38.89%). yang pengoptimumam mendapati suhu pengkarbonan bagi PKS adalah 650°C dan CS 600°C. Setiap biojisim terkarbon diaktifkan pada nisbah 1:1 w/w biojisim terkarbon dan agen pengaktifan selama 30 minit pada suhu bilik diikuti oleh radiasi gelombang mikro selama 4 minit. Selepas kaedah optimum telah dijalankan, CS and PKS yang telah dikarbon dan diaktifkan dengan ZnCl₂ (MZCS dan MZPKS) dan melalui radiasi gelombang mikro

dipilih sebagai AC yang sesuai bagi menjerap jelaga. Ini berikutan luas permukaan BET yang tertinggi iaitu 391.26 m²/g bagi MZCS dan 367.12 m²/g bagi MZPKS. Selain dari ini, peratusan penghasilan bagi kedua – dua AC ini adalah baik dan morfologi yang ditunjukkan dalam imej FESEM menunjukkan penghasilan pori yang seragam. Melalui pentitratan Boehm, adalah dikenalpasti permukaan MZCS dan MZPKS bersifat asid. Setelah MZPKS dan MZCS didedahkan kepada jelaga yang dihasilkan dari pembakaran jerami padi, didapati MZCS menunjukkan penjerapan fizikal terbanyak dan sekata pada atas permukaan dan di dalam pori. Kapasiti maksimum penggunaan MZCS adalah 30 minit bagi pembakaran lebih kurang 23 g jerami padi menggunakan 0.1 g AC. Kajian kebolehlaksanaan ekonomi dijalankan dan didapati harga jualan peringkat makmal adalah pada 4.78 USD bagi setiap 1 kg AC.

Kata kunci: karbon teraktif, sisa pepertaniananian, penjerapan jelaga, tempurung kelapa sawit, tempurung kelapa

ACKNOWLEDGEMENT

I am extremely grateful for the opportunity that Allah S.W.T has presented to me by allowing me to pursue my studies in MSc (Chemistry), at the prestigious University of Malaya. I have been awarded with a full paid leave and scholarship named "*Hadiah Latihan Persekutuan*" sponsored by Malaysia Ministry of Higher Education. I wouldn't have written this without it.

My heartfelt thanks go to both my excellent supervisors Associate Professor Dr Cheng Sit Foon and Associate Professor Dr Nor Kartini Bt Abu Bakar for welcoming me as a student, guiding me without fail, continuing to support me in sharing their knowledge and helping me develop myself. My gratitude goes also to the Science Faculty, University of Malaya especially Department of Chemistry for providing me with such great facilities, conducive environment and amazing, helpful and committed staff to ease my study.

I am immensely blessed that my parents and family members provided me with a strong support system. My father, Dr. Umar Bin Man is my inspiration for my journey through life and my mother, Khatijah Binti Wan Ismail is my pillar of strength to support my every move. My sisters, brothers and in laws have always been there to give me every moral support I could get. My daughters, Ayra Rose Khadijah and Maryam Rose Amina have always been my motivation for me to be a better person. Lastly, my appreciation goes to my husband, thanks for everything sayang.

TABLE OF CONTENTS

ABST	TRACT	iii
ABST	TRAK	V
LIST	OF FIGURES	X
LIST	OF TABLES	xiii
LIST	OF SYMBOLS AND ABBREVIATIONS	xiv
CHAI	PTER 1: INTRODUCTION	1
1.1	Background of study	1
1.2	Problem statement	
1.3	Research questions	·3
1.4	Research objectives	
1.5	Scope and limitation of study	6
1.6	Outline of thesis	
CHAI	PTER 2: LITERATURE REVIEW	
2.1	Soot pollution	8
2.2	Agriculture waste and its impact	
	2.2.1 Palm waste	
	2.2.2 Coconut waste	11
	2.2.3 Lignocellulosic biomass	13
2.3	Introduction to activated carbon	17
	2.3.1 Preparation of AC	18
	2.3.2 Carbonization	19
	2.3.3 Activation	
	2.3.3.1 Chemical activation	25
	2.3.3.2 Microwave activation	29
2.4	Underlying mechanism of AC apllication	31
CHAI	PTER 3: METHODOLOGY	36
3.1	Materials and chemicals	36
3.2	Pre-treatment of agriculture biomass waste	38
3.3	Proximal analysis	38
3.4	Ultimate analysis	39
3.5	Thermogravimetric analysis (TGA)	39
3.6	Determination of lignocellulosic content	39
	3.6.1 Determination of extractive content	40
	3.6.2 Determination of hemicellulose content	40
	3.6.3 Determination of lignin content	40
	3.6.4 Determination of cellulose content	
3.7	Optimization study	
3.8	Carbonization	42
3.9	Activation of carbon	
3.10	Percentage yield	43

3.11	Fourier Transform Infrared (FTIR)	44
3.12	Boehm titration	44
3.13	Brunauer-Emmett-Teller (BET) surface area	45
3.14	Field Emission Scanning Electron Microscope (FESEM) and EDX	45
3.15	Evaluation of activated carbon prodiced as soot adsorbent	46
СНАН	PTER 4: RESULTS AND DISCUSSION	53
4.1	Background study of starting materials	53
4.2	Proximal analysis	53
4.3	Ultimate analysis	
4.4	Lignocellulosic content	
4.5	Thermogravimetric analyses (TGA) and DTG	58
4.6	FTIR of starting materials	
4.7	Carbonization of biomass	63
	4.7.1 Optimization carbonization temperature and duration	63
4.8	Activation of carbonized biomass	67
	4.8.1 Activation optimization (impregnation ratio and duration)	67
	4.8.2 Base activation of carbonized biomass	69
	4.8.3 Acid activation of carbonized biomass	71
	4.8.4 Metal salt activation of carbonized biomass	73
	4.8.5 Microwave activation (physical activation)	75
4.9	The percentage yield of carbonization and activation	
4.10	BET value of activated carbon	81
4.11	Boehm titration of activated carbon	85
4.12	Morphology of activated carbon	
4.13	Application of activated carbon on the smoke muffler	
4.14	Energy Dispersive X-Ray Analysis (EDX) of activated carbon	107
4.15	Econimic feasibility of prepared activated carbon	110
4.16	Comparison studies with other findings	112
СНАН	PTER 5: CONCLUSION	113
5.1	Conclusion	113
5.2	Recommendation for future work	115
REFE	RENCES	117
APPE	NDICES	128

LIST OF FIGURES

Figure 1.1: Flow chart of research activities	5
Figure 2.1: Schematic diagram of soot or black carbon emission sources	9
Figure 2.2: Chemical properties of particles from biomass burning	9
Figure 2.3: Structure of lignocellulose with cellulose, hemicellulose and lignin	13
Figure 2.4: Monomer in cellulose structure	15
Figure 2.5: Structure of glucomannan	16
Figure 2.6: Lignin polymer structure.	
Figure 2.7: An illustration of pores network	18
Figure 2.8: AC preparation methods	19
Figure 2.9: Mechanism of biomass conversion during the pyrolysis process	21
Figure 2.10: Reaction pathway for biochar formation	23
Figure 2.11: Active surface of AC from activation by ZnCl ₂	27
Figure 2.12: Reaction pathway of activation using KOH	29
Figure 2.13: Adsorption interaction on the activated carbon surface	32
Figure 2.14: Acidic and basic group that exist in AC surface	33
Figure 3.1: Palm kernel shells	36
Figure 3.2: Coconut shells	37
Figure 3.3: Paddy straws used for combustion to produce soot	37
Figure 3.4: Schematic design of the smoke muffler	48
Figure 3.5: Appearance of the smoke muffler	49
Figure 3.6: AC holder. AC inserted into AC holder	50
Figure 3.7: Paddy straw placed at the bottom of combustion chamber	51
Figure 3.8: The opening of the muffler	52
Figure 4.1: TGA and DTG curves of PKS	60
Figure 4.2: TGA and DTG curves of CS	60

Figure 4.3: Raw PKS FTIR spectra	61
Figure 4.4: Raw CS FTIR spectra	62
Figure 4.5: FTIR spectra of the raw PKS and the CPKS	64
Figure 4.6: FTIR spectra of the raw CS and the CCS	65
Figure 4.7: FTIR spectra of CCS at different carbonization time	66
Figure 4.8: FTIR spectra of different impregnation ratio of CCS	68
Figure 4.9: FTIR spectra of different impregnation duration	69
Figure 4.10: FTIR spectra of CPKS, BPKS and raw PKS	70
Figure 4.11: FTIR spectra of CCS, BCS and raw CS	71
Figure 4.12: FTIR spectra of CPKS, APKS and raw PKS	72
Figure 4.13: FTIR spectra of ACS	73
Figure 4.14: FTIR spectra of CPKS, ZPKS and raw PKS	74
Figure 4.15: FTIR spectra of CS, ZCS and raw CS	75
Figure 4.16: FTIR spectra of raw PKS, CPKS, BPKS and MBPKS	76
Figure 4.17: FTIR spectra of raw CS, CSS, BCS and MBCS	77
Figure 4.18: FTIR spectra of raw PKS, CPKS, APKS and MAPKS	77
Figure 4.19: FTIR spectra of ACS and MACS	78
Figure 4.20: FTIR spectra of raw PKS, CPKS, ZPKS and MZPKS	78
Figure 4.21: FTIR spectra of raw CS, CCS, ZCS and MZCS	79
Figure 4.22: Percentage yield of CCS and CPKS samples	80
Figure 4.23: Isotherm linear plot of MZCS (a) and MZPKS (b)	85
Figure 4.24: FESEM images of CPKS	87
Figure 4.25: FESEM images of CCS	88
Figure 4.26: FESEM images of MBPKS	90
Figure 4.27: FESEM images of MBCS	91
Figure 4.28: FESEM images of MAPKS	93

Figure 4.29: FESEM images of MACS	94
Figure 4.30: FESEM images of MZPKS	96
Figure 4.31: FESEM images of MZCS	97
Figure 4.32: FESEM images of MZPKS after combustion with paddy straw1	00
Figure 4.33: FESEM images of MZCS after combustion of paddy straw1	01
Figure 4.34: FESEM images of MZCS surface after 60 minutes of combustion1	03
Figure 4.35: FESEM images of blank filter paper before combustion	05
Figure 4.36: FESEM images of filter paper after 30 minutes of combustion1	06
Figure 4.37: FESEM images of soot sediment accumulated inside the smoke muffler l	08
Figure 4.38: EDX site on filter paper after combustion	09
Figure 4.39: EDX analysis on different spots on AC surface	10

LIST OF TABLES

Table 2.1: PKS content from other findings	11
Table 2.2: CS content from other authors	12
Table 2.3: Biopolymer components in CS and PKS	14
Table 2.4: Summary of reactions	26
Table 4.1: Proximal analysis of starting materials	56
Table 4.2: CHNS/O content of starting materials	57
Table 4.3: Lignocellulosic content of starting materials	58
Table 4.4: Comparison of conditions used for carbonization process	67
Table 4.5: Percentage yield after carbonization process	79
Table 4.6: Percentage yield of activation process	81
Table 4.7: BET value of prepared AC	84
Table 4.8: Different functional groups on the surface of AC	86
Table 4.9: Study of paddy straw mass that can be combusted within 30 minutes	99
Table 4.10: EDX analysis on filter paper and MZCS before and after combustion	107
Table 4.11: Estimation cost for lab-scale production	111
Table 4.12: A comparison between this study and other studies	112

LIST OF SYMBOLS AND ABBREVIATIONS

°C : Degree Celsius

μm : Micro meter

% : percentage

AC : Activated carbon

ACS : Acid activated coconut shell

APKS : Acid activated palm kernel shell

BET : Brunauer-Emmett-Teller

BCS : Base activated coconut shell

BPKS : Base activated palm kernel shell

CHNS/O : Carbon, hydrogen, nitrogen, sulphur, oxygen

CCS : Carbonized coconut shell

cm : Centimeter

CPKS : Carbonized palm kernel shell

CS : Coconut shell

EC : European commission

EDX : Energy Dispersive X-ray Analysis

et al. : et alia

FAO : Food and Agriculture Organization of the United Nations

FESEM : Field Emission Scanning Electron Microscope

FTIR : Fourier Transform Infra-red

g : Gram

IUPAC : International Union of Pure and Applied Chemistry

kg : Kilogram

KOH : Potassium hydroxide

H₃PO₄ : Phosphoric acid

i.e : Id est

MACS : Microwave acid activated coconut shell

MAPKS : Microwave acid activated palm kernel shell

MBCS : Microwave base activated coconut shell

MBPKS : Microwave base activated palm kernel shell

mL : Milliliter

mm : Millimeter

mmol : Milli mol

MZCS : Microwave zinc chloride activated coconut shell

MZPKS : Microwave zinc chloride activated palm kernel shell

N/A : Not available

n.d: No date

nm : Nano meter

PKS : Palm kernel shell

TGA : Thermogravimetric analysis

USD : United State dollar

 $ZnCl_2$: Zinc chloride

W : Watt

wt : weight

w/w : Weight per weight

CHAPTER 1: INTRODUCTION

1.1 Background of study

The present study utilizes agricultural wastes, namely, coconut shells (CS) and palm kernel shells (PKS), to produce activated carbon (AC). Preparation of AC includes carbonization of the selected agricultural wastes in an electric furnace, followed by chemical activation and microwave radiation. Characterization of the produced AC includes calculation of percentage, identification of functional group using Fourier transform infrared (FTIR) analysis, surface area identification using Brunauer-Emmett-Teller (BET) method, proximal and ultimate (CHNS/O) analysis, thermogravimetric analysis (TGA) and Field Emission scanning electron microscopy (FESEM). Lastly, the AC was tested using a custom-made smoke muffler.

1.2 Problem statement

Agricultural commodities play a significant role in human daily needs, with a global output of 23.7 million tonnes per day providing a key economic source and employment creator worldwide (Ritchie & Roser, 2020; FAO, 2017). As a result, the agricultural sector has become one of the main sources of biomass production (EC, 2015). Major crops in Malaysia include 34.56% oil palm and 6.34% coconut, with an estimated 168 million tonnes of biomass waste produced annually in Malaysia (Zafar, 2019). Quantitatively, only 27% of agricultural waste is reused and rendered into items such as fibreboard, while the rest is disposed of, typically by burning (Zafar, 2019).

The combustion process is necessary for some industries, especially in agriculture.

According to California Air Resources Board, agriculture burning is carry out in

vegetation management to remove crop residue, control pest and diseases (California Air Resources Board, n.d). However, it causes a problem from the emission of soot by various burning conducted. Burning agricultural waste is the simplest way of disposal (Gummert *et al.*, 2020). He *et al.* (2019) reported that open incineration of agricultural waste led to one of the key sources of air pollution. The highest concentration of particulate matter in South and East Asia is reported from agricultural residues burning (Wei *et al.*, 2020). It is estimated that 20 million tonnes of carbon dioxide were released due to agricultural burning during the two - month haze in 2015 (Tacconi, 2016). It has caused increased death, where an estimated excess of 6500 death reported in Malaysia during the affected time (Koplitz *et al.*, 2016). A more recent case has occurred in Alor Setar in September 2019 where paddy hay was burned for the preparation of paddy replanting. This act has raised the nearby city's air pollution index to unhealthful levels (Bernama, 2019).

To mitigate the effect of the burning process, a trapping device can be implemented to limit soot output. The method of trapping can be used to reduce the release of soot particles directly into the atmosphere. Activated carbon (AC) is a well-known adsorbent that can be used in trapping systems due to its high adsorption effectiveness.

AC production has been widely studied over the decade. However, in most of these studies, the production of AC recorded high energy consumption. For example, raw material carbonization required a temperature up to 1000°C for 120 minutes (Huang *et al.*, 2015). Therefore, the present study has successfully prepared AC with lower carbonization temperature (600 to 650°C) and shorter impregnation time (30 minutes).

The novelty of this research lies in the ability of AC prepared to adsorb soot. There is a lack of study on soot adsorption as the majority of the research carried out on AC was targeted at aqueous adsorption, *i.e.*, adsorption of dye, methyl blue, wastewater treatment

and dye removal (Jadhav & Mohanraj, 2016; Yaacaubi & Songlin, 2019). This study presents a new viewpoint that is not commonly explored in the current application.

In general, this study is based on two issues, namely, underutilized agricultural waste and soot produced from combustion processes, *i.e.*, agricultural activities, being released to the environment causing reduction of air quality. The two issues will, therefore, be dealt with in this study. The possible solution includes the study of using agricultural waste to produce AC. The AC produced will then be used as adsorbents to reduce soot particles from combustion processes. As mentioned, the present study emphasizes the reduction of carbonization and activation temperature and duration. Novel use of AC as a soot adsorbent is also aimed. The AC is hypothesized to act as a soot adsorbent to keep out soot particles from escaping into the atmosphere. The use of AC from agricultural waste not only provides a solution for dealing with agricultural waste but, at the same time, adds new applications of AC by the implementation of a waste resource development system.

1.3 Research questions

Research questions that are investigated in this study include:

- 1. What is the optimum condition to produce AC?
- 2. How will the preparation methods influence the properties of the prepared AC?
- 3. How does the produced AC adsorb soot particles from the combustion process?

1.4 Research objectives

The objectives of this study are as follows:

- To prepare activated carbon from palm kernel shell (PKS) and coconut shell (CS) by physicochemical activation with lower carbonization temperature, shorter impregnation and activation time.
- 2. To investigate the properties of the starting materials and the activated carbon prepared by FTIR, Boehm titration, BET, proximate and ultimate analysis, TGA analysis, percentage yield and FESEM.
- 3. To apply the prepared activated carbon for soot particles adsorption using a smoke muffler.

Figure 1.1 depicts the research activities of the present study in reference to the objectives outlined.

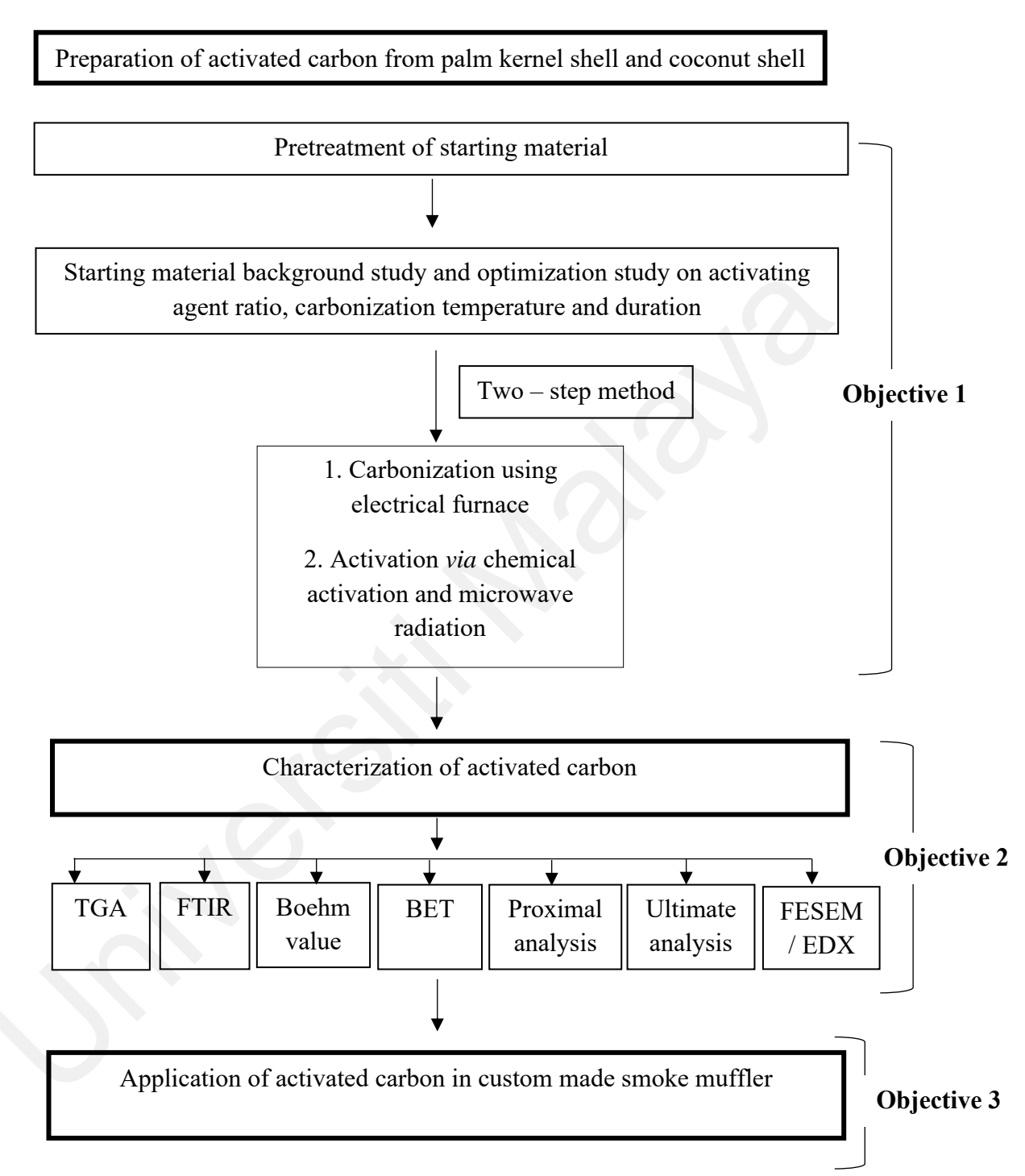


Figure 1.1: Flow chart of research activities

1.5 Scope and limitation of study

This study is limited to focusing on the production, characterization and application of the final products obtained. Development of AC carried out includes CS obtained from the coconut milk industry in Kuching, Sarawak. Palm biomass used is from PKS obtained from Sime Darby Plantation Sdn Bhd, East Oil Mill, Pulau Carey, Selangor.

Background study on the starting material was first conducted. This is to study the characteristics of the selected biomass. For this, FTIR analysis has been conducted on raw biomass to determine the functional group. Proximal analysis gives information on moisture and ash content followed by CHNS/O content of the starting materials. Lignocellulosic content has also been determined and TGA data on both biomasses were also collected. TGA data obtained gives information on fixed carbon and volatile content.

The technique used was the carbonization of precursors followed by a two-step activation process. First chemical activation step using KOH, H₃PO₄ and ZnCl₂ accompanied by microwave radiation to improve pore formation. Due to the difference in the lignocellulosic biomass content, the carbonization temperature was adjusted to obtain an optimum carbon skeleton. The optimal biochar was produced when reduction of FTIR signal from biomass functional groups occurs following a carbonization process. All precursors have undergone the same activation method.

Characterization of AC has been conducted and data obtained were analyzed. The first characterization was the calculation of the percentage yield. FTIR spectroscopy was performed to investigate the changes in the functional group of raw material, carbonized starting material and finished product. Following this, the BET method was conducted and this has provided information on the micropore surface area, pore size and volume of AC. Boehm titration was conducted to study the surface functional group. The FESEM images were collected to analyses the surface of the AC produced.

To apply the AC, it was loaded into a custom-made smoke muffler. Combustion of paddy straw will take place within the combustion chamber and soot produced will be filtered through AC. After the filtration process has been carried out, FESEM images and EDX data on the AC surface was collected.

1.6 Outline of thesis

There are five chapters in this thesis to present the research done. Chapter One discusses the background of the study, problem statement, research questions, and objectives, as well as the scope of the study and limitations.

Chapter Two contains a review of the literature on soot pollution and agricultural waste, as well as information on each agriculture waste used in this study, namely, coconut waste and palm waste. This chapter discusses the preparation of lignocellulosic biomass and activated carbon, which involves the carbonization and activation processes. The science of chemical activation and microwave activation is represented. Additionally, the AC application mechanism is described.

Chapter Three reports the methodology used in this study. This includes preparing, characterizing, and testing the AC produced. This chapter contains a detailed explanation of the methodology used throughout this research.

Chapter Four discusses the preparation, characterization, and testing results. Proximate and ultimate analysis, Boehm titration, percentage yield, FTIR spectrum, TGA data, BET surface area, EDX analysis and FESEM surface images are included in the results.

Chapter Five summarizes this research and makes recommendations for future research.

CHAPTER 2: LITERATURE REVIEW

2.1 Soot pollution

The agricultural industry is one of the industries that practice the combustion process. According to He *et al.* (2019), open incineration of agricultural waste is a significant source of air pollution. A recent study by Wei *et al.* (2020) reports agriculture is responsible for the highest concentration of particulate matter in East and South Asia. Wildfires and agricultural burning account for one-third of the world's carbon aerosol (Bond *et al.*, 2013). Biomass combustion accounts for up to 38% of global carbonaceous aerosol production (Liu & Mishchenko, 2020). The combustion of biomass produces soot which is a small aerosol particle. Such aerosols consist of inorganic and organic components as well as black carbon, also referred to as soot (Liu & Mishchenko, 2020).

Soot or light adsorbing black carbon particles causes atmosphere warming and deteriorates the earth's climate (Adler *et al.*, 2019). Soot can be defined as a carbonaceous material that is formed in flames, emitted into the atmosphere, and exhibits a range of physical properties (Lack *et al.*, 2014). As a result of the incomplete burning of hydrocarbons, soot is composed of both incipient molecular particles (nanoparticles of organic carbon with liquid-like properties) and larger-sized elemental carbon particles (D'Anna, 2015). The source of soot and its effects on the earth are depicted in Figure 2.1. The size of soot emitted during the burning process varies between 10 µm to less than 1 µm (Posfai *et al.*, 2003; Phairuang *et al.*, 2019). Due to the ability of soot to absorb light in the UV – visible spectrum, it can cause harm to the earth's atmosphere. Another characteristic of soot particles studied by Pye *et al.* (2020) is their acidic nature, as illustrated in Figure 2.2 The same study also reported the presence of ionized species, indicating that biomass soot contains H⁺ particles.

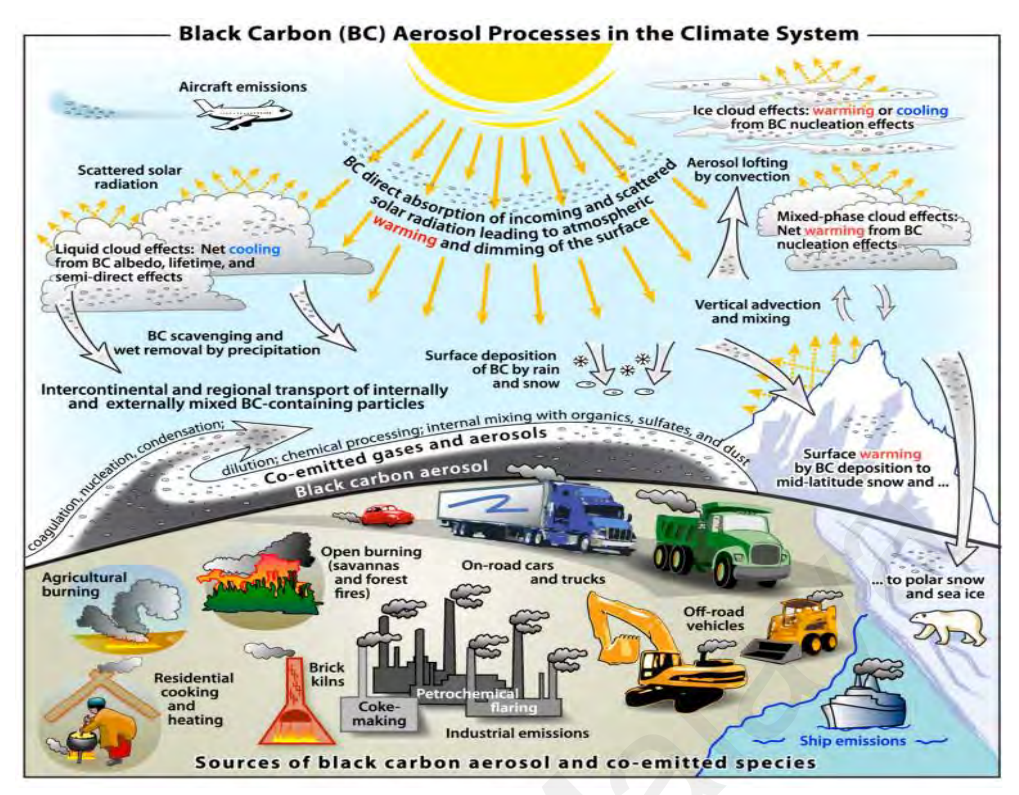


Figure 2.1: Schematic diagram of soot or black carbon emission sources (Bond *et al.*, 2013)

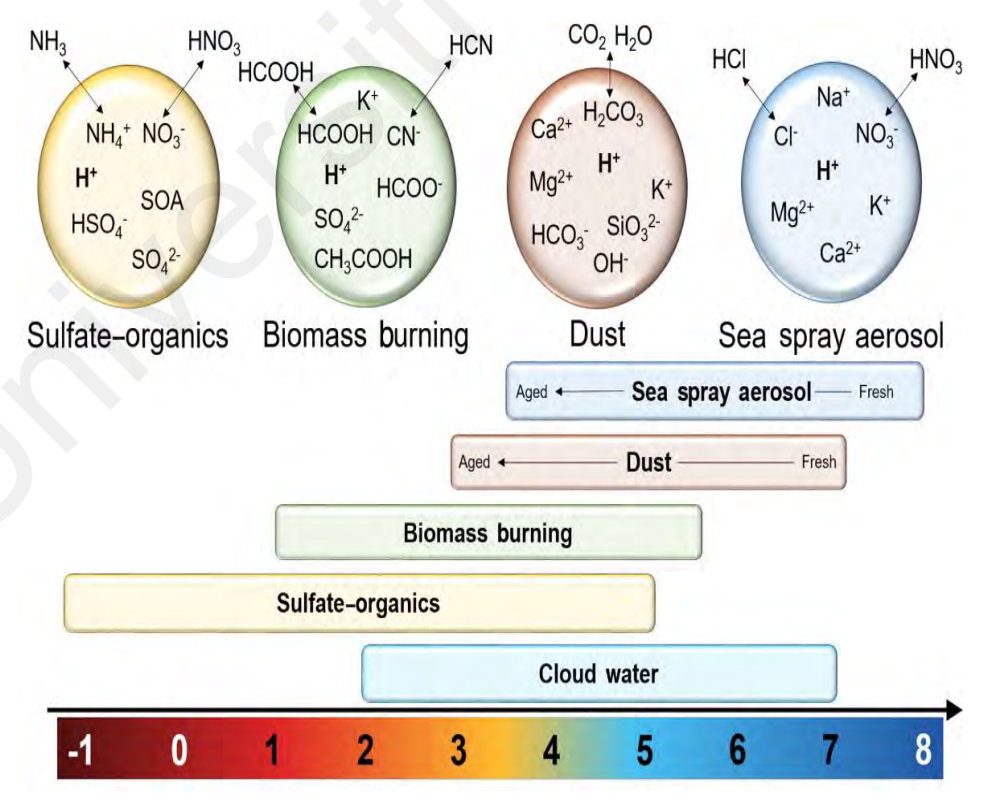


Figure 2.2: Chemical properties of particles from biomass burning (Pye et al., 2020)

2.2 Agriculture waste and its impact

Ramirez-Garcia (2019) defines agricultural waste as any product that results from agricultural activities such as agriculture or plantation, as well as animal manure. Agriculture has developed into a significant source of biomass production (EC, 2015). This sector generates waste at several stages: harvesting, cultivation, processing, and consumption (Bedoic *et al.*, 2019). Given the volume of waste produced by agricultural activities, it is critical to promote waste conversion to value-added products.

2.2.1 Palm waste

Malaysia is a market leader in the palm oil industry, ranking as the world's second largest producer of palm oil (Ge *et al.*, 2020). Additionally, it is anticipated that by 2021, palm oil industries will account for approximately USD 93 billion of the global market value (Liew *et al.*, 2019). According to the Malaysian Department of Statistics, the oil palm industry is a significant contributor to the country's gross domestic product, accounting for 39.9% of the agriculture sector (Agriculture, 2019). Naturally, the waste products from this massive commodity accumulate to a significant extent. Out of 1 million tons of palm waste, 0.4 million tons come from palm kernel shells (PKS) (Ge *et al.*, 2020). This study will, therefore, use PKS as one of the starting materials for the production of activated carbon. The content of PKS as determined by ultimate and proximate analysis in previous studies is tabulated in Table 2.1.

Table 2.1: PKS content from other findings

Table 2.1. I KS content from other intungs					
Content	Nizamuddin	Arami-Niya	Kamarul	Liew et al.	
percentage (%)	et al. (2015)	et al. (2011)	Zaman <i>et al</i> .	(2018)	
/ Author			(2018)		
С	49.70	50.01	48.85	51.00	
Н	5.90	6.85	6.32	3.00	
N	2.50	1.90	0.49	7.00	
C	2.20	NT/A	0.16	0.00	
S	2.20	N/A	0.16	0.00	
0	34.10	41.15	44.17	39.00	
	37.10	71.13	77.1/	37.00	
Fixed carbon	13.80	18.70	12.40	40.00	
	20100				
Volatile matter	34.80	72.47	81.50	53.00	
Ash	9.30	7.96	2.80	3.00	
Moisture	15.10	1.10	6.10	4.00	
C - 111	NT/A	20.70	NT/A	20.00	
Cellulose	N/A	29.70	N/A	30.00	
Hemicellulose	N/A	47.70	N/A	22.00	
Ticilicciulosc	11/71	77.70	1 1/ / 1	22.00	
Lignin	N/A	53.4	N/A	48.00	
<i>9</i>					

2.2.2 Coconut waste

Cocos nucifera or coconut is classified in the Aceraceae family. Malaysia is reported to have planted approximately 142 000 ha of coconut trees (Mohd Din et al., 2009). Coconut fruit is the most consumed fruit per capita in 2019 as recorded by the Department of Statistic Malaysia (Agriculture, 2019). Coconut is primarily used to extract milk from the meat of the coconut and to collect coconut water. Following that, the shell is discarded. Attributed by its lignocellulosic structure, it is ideal to convert as an adsorbent. CS content as studied by other authors is presented in Table 2.2. Husseinsyah & Zakaria (2011) reported that the composition of the coconut shell (CS) consisted of lignin (29.4%), pentosan (27.7%), cellulose (26.6%), moisture (8%), solvent extracts (4.2%), uranic anhydrides (3.5%) and ash (0.6%). However, this number varies between coconut trees since the fruit and planting climate can alter the shell composition.

For example, Rahman *et al.* (2012) reported that the coconut shell contains 33.7% hemicellulose, 10.35% cellulose and 15.2% lignin. Three additional studies, namely, Andrade *et al.* (2018), Prauchner & Reinoso (2012) and Freitas *et al.* (2019), have shown that coconut shells consist mainly of hemicellulose. According to Dhyani & Bashkar (2018), CS is 36.3% cellulose.

Table 2.2: CS content from other authors

Content	Andrade et	Dhyani &	Freitas <i>et al</i> .	Prauchner
percentage (%)	al. (2018)	Bashkar	(2019)	& Reinoso
/ Author	,	(2018)		(2012)
		` ′		
С	N/A	50.20	N/A	52.00
Н	N/A	5.70	N/A	6.00
N	N/A	0	N/A	0.10
S	N/A	0	N/A	0.00
О	N/A	43.4	N/A	40.90
Fixed carbon	N/A	N/A	N/A	N/A
Volatile matter	N/A	8.02	N/A	N/A
Ash	2.61	0.70	N/A	1.00
Moisture	N/A	8.02	N/A	N/A
Cellulose	10.35	36.30	36.00	43.00
Hemicellulose	33.70	25.10	25.00	8.00
Lignin	15.20	28.70	28.00	49.00

2.2.3 Lignocellulosic biomass

Due to its ease of availability and abundance as agricultural waste, lignocellulosic biomass is frequently used as a starting material for the production of AC. All agricultural waste has one feature in common that qualifies it for AC preparation: the lignocellulosic biomass composition (Figure 2.3). Lignocellulose is a polysaccharide matrix composed primarily of cellulose, hemicellulose, and lignin (Figure 2.3). Acetyl groups, minerals and phenolic compounds are also frequently present (Isikgor & Becer, 2015). The general lignocellulosic component of both starting materials used in this study is shown in Table 2.3.

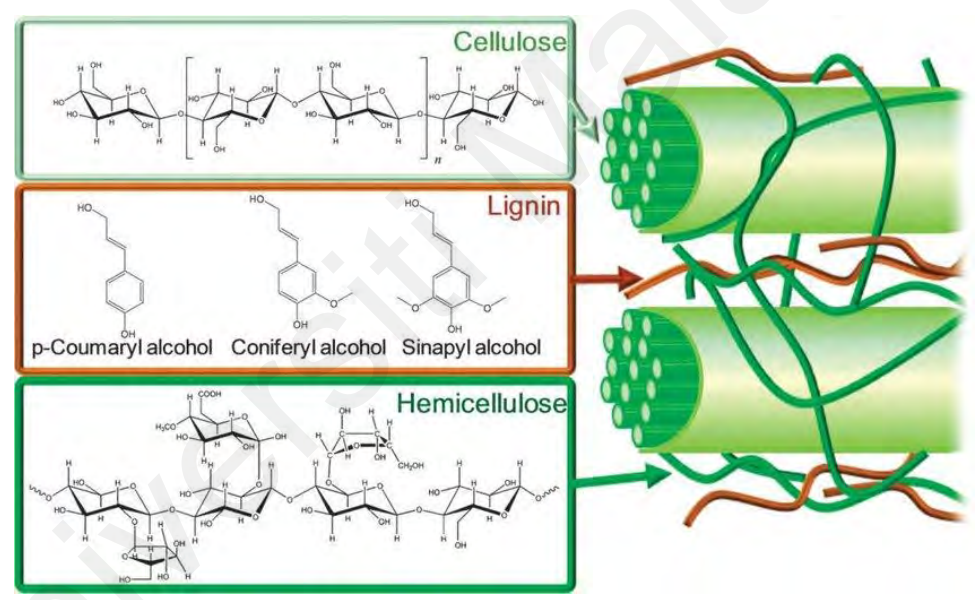


Figure 2.3: Structure of lignocellulose with cellulose, hemicellulose and lignin present (Alonso *et al.*, 2012)

Table 2.3: Biopolymer components in CS and PKS (Husseinsyah & Zakaria, 2011; Rahman *et al.*, 2012; Dhyani & Bashkar, 2018; Andrade *et al.*, 2018; Prauchner & Reinoso, 2012; Freitas *et al.*, 2019)

Agriculture waste/ components	Hemicellulose (%)	Cellulose (%)	Lignin (%)
CS	8 – 34	10 – 43	15 – 49
PKS	21 – 47	30	48 – 53

Cellulose contains both highly ordered crystalline and amorphous structures (Collard and Blin, 2014). Cellulose monomers contain two units of β-glucopyranose that form a linear homopolysaccharide called cellobiose (Figure 2.4). Hemicellulose is an amorphous heteropolysaccharide. Glucomannans are usually present in gymnosperm plants where the main chains are rarely acylated at C2 or C3 (Alen *et al.*, 1996; Grondahl *et al.*, 2003). Figure 2.5 shows the glucomannan structure. Lignin is an amorphous polymer with building blocks (Figure 2.6) such as p-hydroxyphenyl, guaicyl and syringyl (Collard & Blin, 2014). The building blocks contain a hydroxyl group in the para position of the alkyl chain (Collard & Blin, 2014). Alkyl chain in lignin may also contain functional groups such as ether, alcohol, carboxylic acid and carbonyl, with the proportion of each group dependent on lignocellulosic species (Jakab *et al.*, 1995; Shen *et al.*, 2010). Lignin is a rigid structure that acts as "glue" in binding polysaccharide fibers together (Dhyani & Bhaskar 2018; Isikgor & Becer, 2015). Lignin is also the most heat resistant component and will require higher energy to break compared to hemicellulose or cellulose (Collard & Blin, 2014).

This biopolymer plays a significant role in the formation of activated carbon. Fragmentation of these compounds due to high temperatures can cause the formation of pores. Fragmentation will occur as non-carbon elements such as oxygen and hydrogen are volatilized. Pores will grow as these elements disperse from the surface of the starting materials during the carbonization process (Selvaraju & Abu Bakar, 2017). The pores

that have been formed contain an active site resulting from reactions that occur on the surface of biomass (Liu *et al.*, 2016). The active site is a critical component of the adsorption process. The active site, which involves the formation of ions from polymer defragmentation, as well as free hydrogen and oxygen, has led to the interaction between adsorbate and AC. Section 2.4 will discuss the adsorption of AC in greater detail.

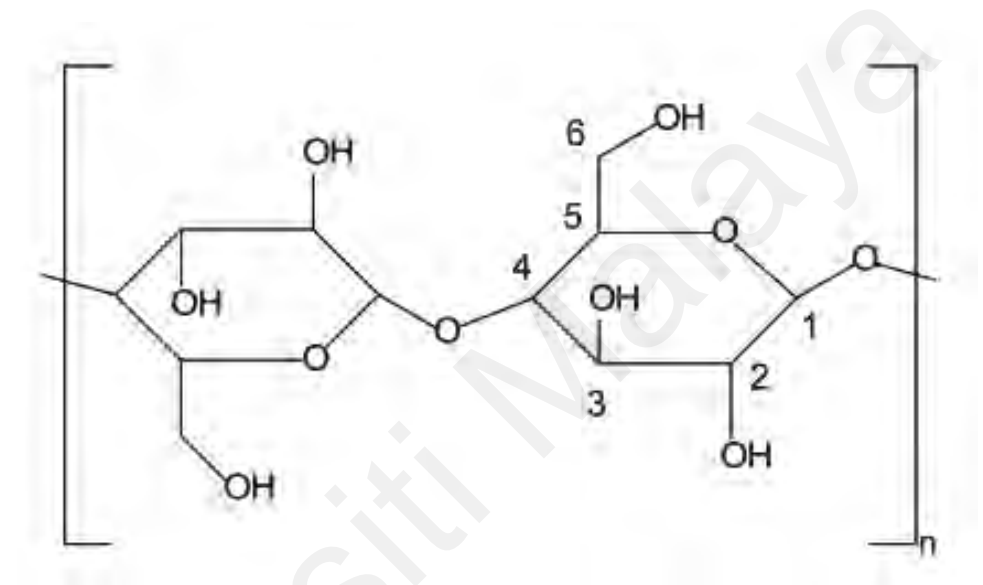


Figure 2.4: Monomer in cellulose structure that consists of two units of $\beta\mbox{-}$ glucopyranose (Collard & Blin, 2014)

Figure 2.5: Structure of glucomannan that exists in hemicellulose of gymnosperm plants (Collard & Blin, 2014)

$$H_3CO$$
 OH OCH $_3$ HO OCH $_3$ HO OCH $_3$ HO OH OCH $_3$ HO OH OH

Figure 2.6: Lignin polymer structure. Hydroxyl group exist in this structure at the para position or fourth carbon

2.3 Introduction to activated carbon

AC was first used in 3750 BCE by both Sumerians and Egyptians to aid in the reduction of zinc, tin, and copper ores (Derbyshire & Jagtoyen, 1995). Quick on to 1881, R. Von Ostrejko was recognized as the father and inventor of AC for his proprietary AC production methodology (Derbyshire & Jagtoyen, 1995). The methodology was carbonization with metal chloride and mild carbon dioxide gasification with steam or carbon dioxide (Rodriguez–Reinose, 1997).

Today, the term "activated carbon" is frequently used to refer to a highly developed porous structure. The International Union of Pure and Applied Chemistry (IUPAC) defines AC as porous carbon material that has been subjected to reactions with an activating agent such as gases, the addition of chemicals before, during or after carbonization to improve adsorptive properties (McNaught & Wilkinson, 1997). According to the Gonzalez-Garcia (2018) definition, AC is a substance with a highly enhanced surface area, an internal porous structure with wide size distribution and a diverse variety of functional groups consisting of oxygen. In a nutshell, AC is a carbonaceous material that has undergone chemical reactions to form a porous material with highly activated surfaces.

According to IUPAC, there are three major pore size groups measured by its diameter: macropores (more than 50 nm), mesopores (between 2 and 50 nm) and micropores (less than 2 nm). Figure 2.7 shows the pore structure in AC. The macropores are the huge pore opening on the outer surface. Moving deeper into the AC, one will find mesopores and, eventually, micropores.

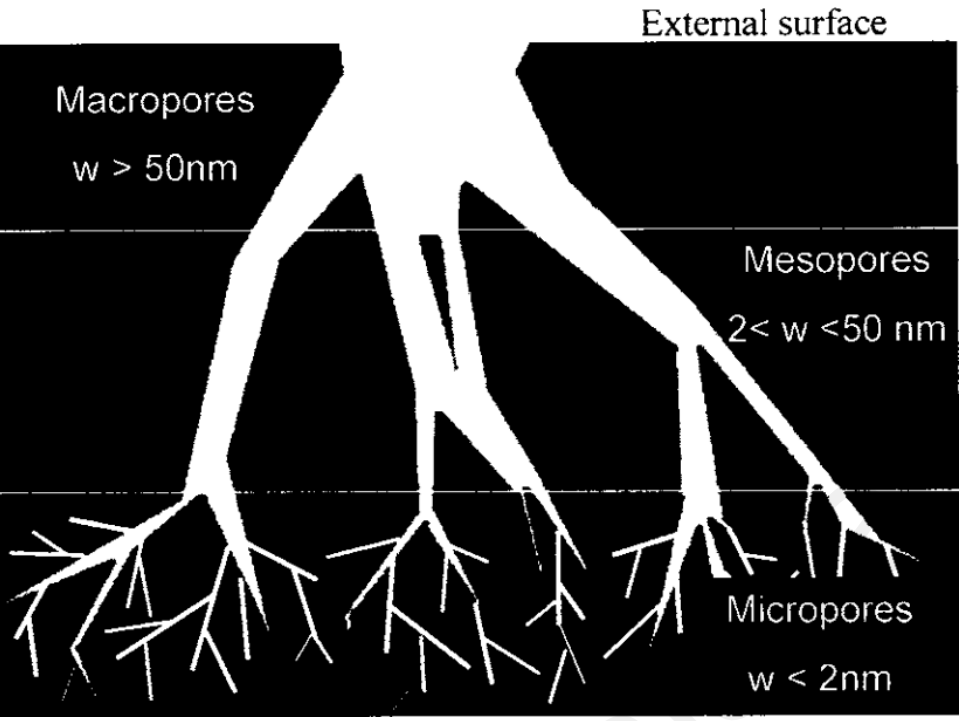


Figure 2.7: An illustration of pores network (Menendez-Diaz & Martin-Gullon, 2006)

2.3.1 Preparation of AC

AC can be prepared in a variety of ways. General methods of production include pretreatment of starting material, such as cleaning with water, drying and reduction of size. Carbonizing and activating the starting material will follow. Activation can be achieved *via* three pathways, namely, chemical, physical and combined routes of physiochemical activation. The general flow of the AC preparation is shown in Figure 2.8.

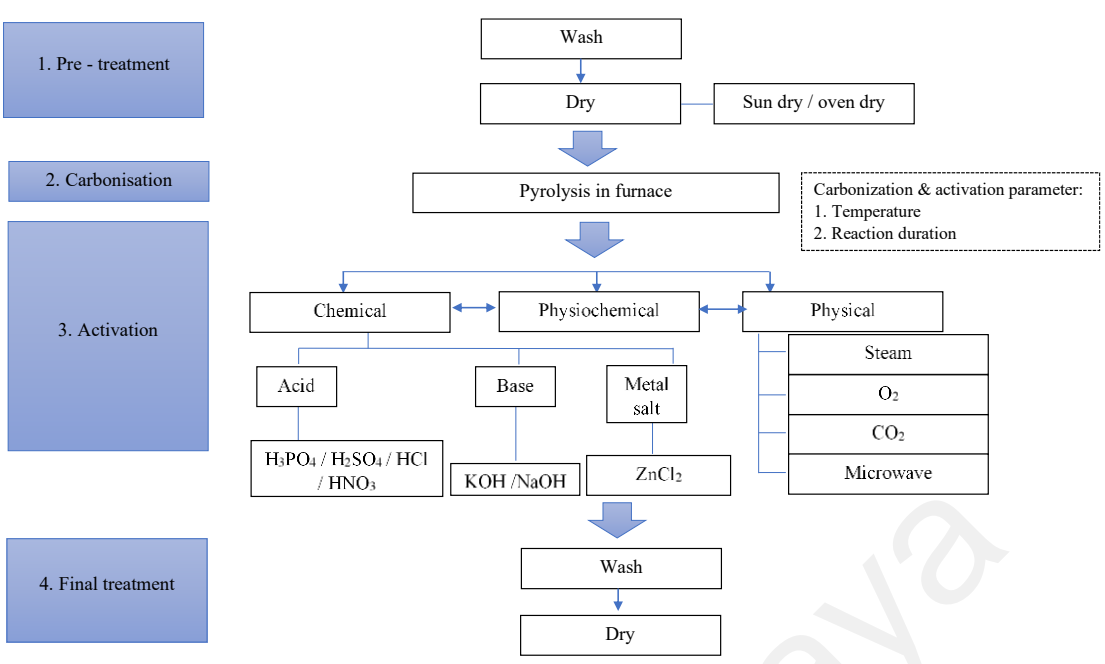


Figure 2.8: AC preparation methods

2.3.2 Carbonization

Carbonization is an elevated temperature process used to produce a charred product called biochar. The aim is to produce a carbonaceous and fixed carbon skeleton. Heat ranges from low temperature ($300 - 400^{\circ}$ C), moderate temperature ($500 - 700^{\circ}$ C) and high temperature ($800 - 1000^{\circ}$ C). Carbonization factors that have an impact on the quality of the final product include the heating temperature, inert air presence and residence time (Ioannidou & Zabaniotou, 2007).

Heating temperature varies according to the biomass used. Starting materials such as wood and shells may require higher carbonization temperature up to 1000°C (Bhungthong *et al.*, 2018). Seeds, husks, and fibrous starting materials, on the other hand, require a lower temperature. This is due to the chemical components in the biomass. Rigid structures require higher temperatures to be broken down to form a carbonaceous mass.

Carbonization in an inert atmosphere such as nitrogen or vacuum is preferred for most AC preparations. This is done to ensure that biomass does not react adversely with air

molecules. However, this is not compulsory as carbonization will still be a success even without an inert heating environment. Meanwhile, for the next parameter which is the residence time of carbonization, fragmentation of raw material must be completed to ensure a quality char is produced. As a result, a sufficient period of carbonization is also a determining factor in the production of AC. Carbonization duration ranges from 30 minutes to 3 hours.

Carbonization is important for modifying the natural binding properties of lignocellulosic by tempering the cellulose-hemicellulose-lignin matrix at high temperatures (Isikgor & Becer, 2015). Carbonization induces material decomposition through heat treatment. Volatilization of low molecular weight compounds on the surface, carbonization or depolymerization of materials due to reactions such as alkylaryl bond rupture and fragmentation of polycyclic structures are all examples of reactions that occur (Hidayu & Muda, 2016; Sharma *et al.*, 2010; Vargas *et al.*, 2010; Collard & Blin, 2014; Cazetta, 2011).

Collard & Blin (2014) reported that reactions, namely, char formation, depolymerization, and fragmentation occur during carbonization (Figure 2.9). During the formation of char, a rearrangement reaction occurs between the intra- and intermolecular units. The aromatic rings mixture forms polycyclic rings. By breaking polymer bonds, monomer units are formed during depolymerization. At elevated temperatures, defragmentation of the monomer units results in the formation of gases and non-condensable structures. Tan *et al.* (2017) and Bello & Ahmad (2012) previously demonstrated that fragmentation of polymer structures results in the formation of CO₂, CO, CH₄, C₂H₄ and C₂H₆. These gases are released at varying temperatures depending on the polymers in the biomass.

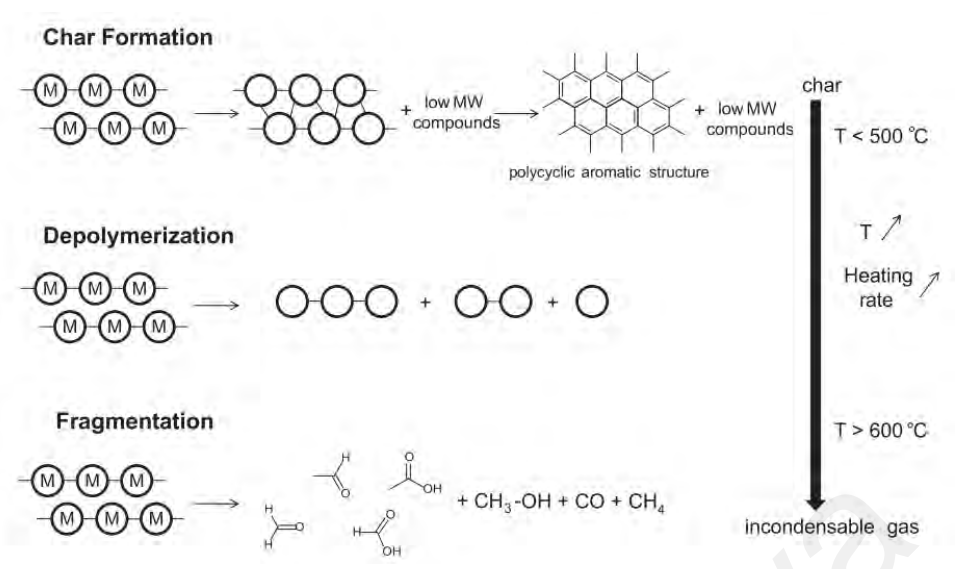


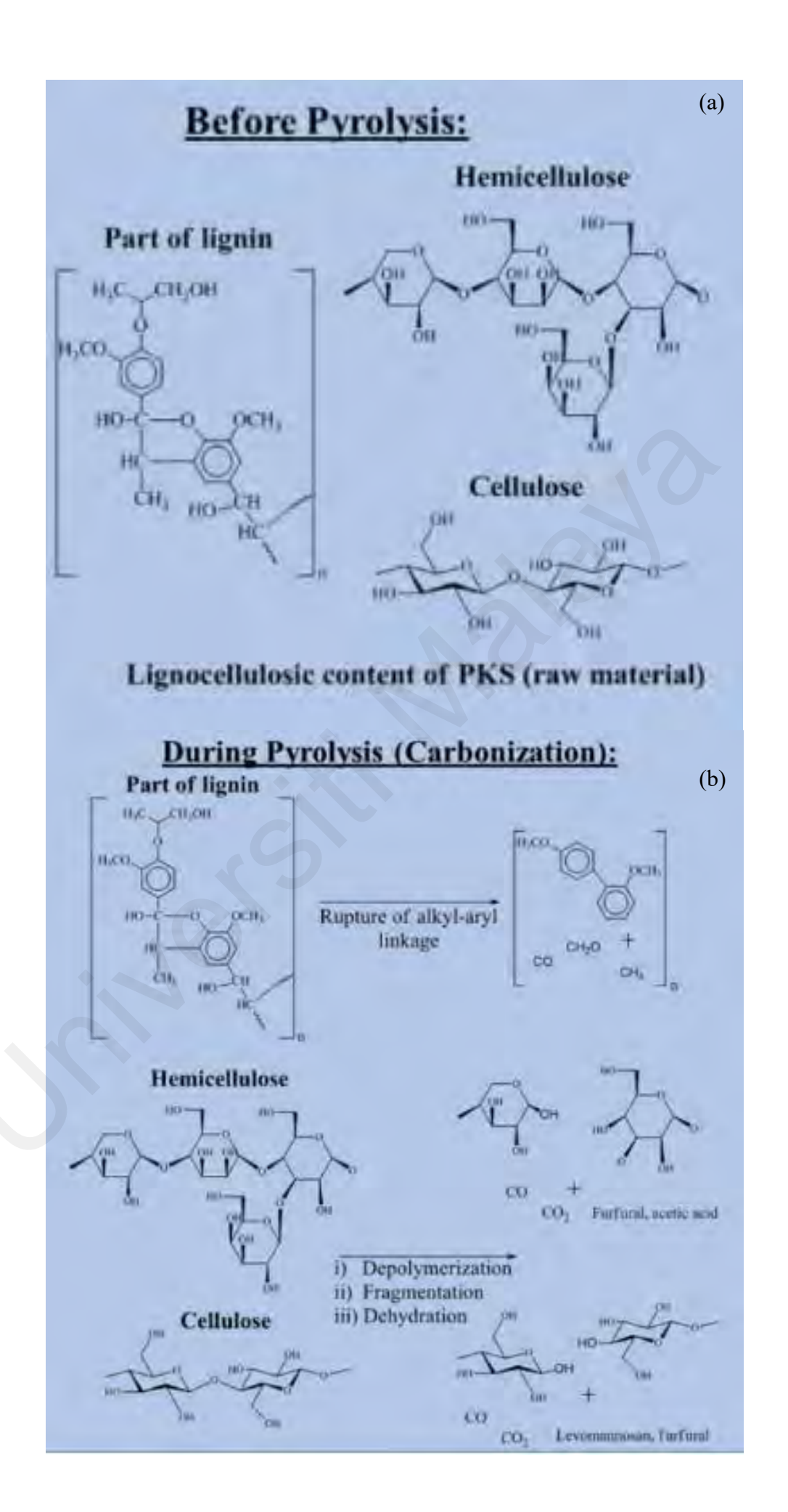
Figure 2.9: Mechanism of biomass conversion during the pyrolysis process whereby M: monomer, MW: molecular weight (Collard & Blin, 2014)

Numerous studies begin with carbonization and end with activation, while others reverse the order. Each method has distinct advantages. Prioritizing activation first will have an advantage over the removal of oxygen and hydrogen compounds that will help increase yields (Sanni *et al.*, 2017). Meanwhile, practising the carbonization step first will contribute to a better cross-linked matrix in the direct reaction of carbon atoms on the charred surface and reduce the reaction with impurities, thus prohibiting the formation of slurry on the charcoal surface (Mohd Din *et al.*, 2009). Additionally, carbonization allows the release of aliphatic side chains within the biomass system, increasing the skeleton density before activation (Prauchner *et al.*, 2016). Figures 2.9 and 2.10 and equations (2.1) to (2.3) from Kan *et al.* (2016) highlighted the possible reaction that took place from the starting material to biochar formation. This reaction occurs during the stage of carbonization. Certain routes combine activation and carbonization in a single step of preparation, which saves energy and reduces time by eliminating the need to perform two separate procedures.

Agriculture waste \rightarrow Volatiles + Scorched residue (2.1)

Scorched residue \rightarrow Tar + non-condensable gases + biochar (2.2)

Biochar \rightarrow Sintered-char + Ash (2.3)



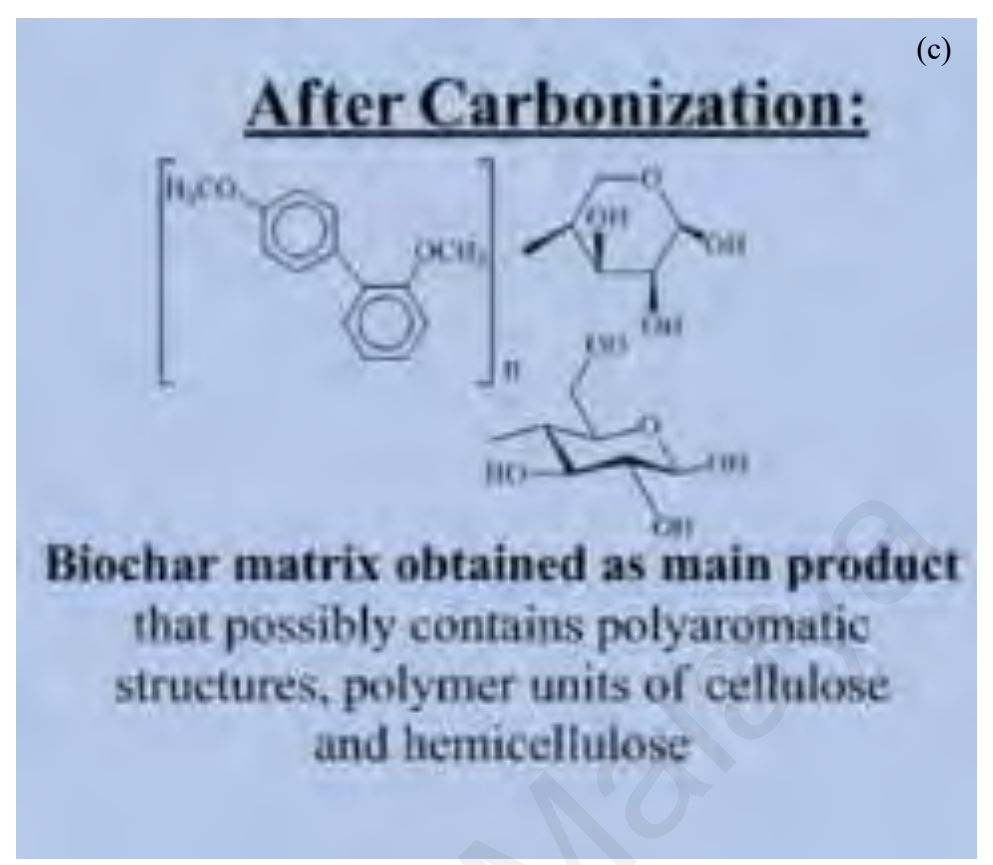


Figure 2.10 (a)(b)(c): Reaction pathway for biochar formation (Liew et al., 2018)

2.3.3 Activation

An activation step is needed to enhance pore formation. Pore formation occurs when hydrocarbons are removed or modified to increase the absorption capacity (Huang *et al.*, 2015). Factors that affect the activation process includes activating duration, activating ratio and type of activating agent.

The duration of activation is dependent on the starting materials, the type of activating agent used, and the activation temperature. As reviewed by Heidarinejad *et al.* (2020), the most optimal activation duration is between one hour to 3 hours. However, activation times of up to 24 hours have been reported, as proved by Saleem *et al.* (2017). Thus, the duration of the activation is a factor that should be considered to obtain the AC with the desired characteristics.

In chemical activation, the activating agent ratio to starting material is a crucial parameter. The most optimized ratio varies according to the biomass used in each study. As studied by Koyuncu *et al.* (2018), the optimum ratio is 2.0 when orange shells are used as precursors. According to the study, a ratio that is either too low or too high results in a lower BET value. The same conclusion was reached in Heidarinejad *et al.* (2020) whereby in the review study it is discovered that a high ratio of 3.0 is the optimum ratio for activating date pits, but a ratio of 0.75 is suitable for potato peels. In summary, optimization on the ratio between an activating agent and a starting material must be considered to obtain the desired results because the ratio of each study is unique, depending on the biomass used in the work.

The type of activation agent will determine the characteristics of the pores formed. As Ukanwa et al. (2019) concluded, there is no ideal activating agent; rather, the agent reacts differently with distinct types of biomasses, and the AC produced is target dependent. Chemical activating agents include acid, base and metal salts. Chemical activation provides several benefits in AC production as it is faster, high product yield and provide AC with a high surface area (Kumar *et al.*, 2020). Physical activation involves steam, carbon dioxide and microwave radiation. Physical activation excludes the usage of harmful chemicals but sometimes required high preparation conditions such as a vacuum environment and high temperature. Physical activation has reported the production of AC with micropores such as described by Zhao *et al.* (2018) and Rashidi *et al.* (2012). To obtain the desired AC, some studies, including this one, combine chemical and physical activation. This process is known as physicochemical activation.

2.3.3.1 Chemical activation

Metal salts, strong acids and strong bases are used to facilitate oxidation or reduction, dehydration, hydrolysis, condensation or to act as a catalyst in the chemical activation process. Pores are formed as a result of these chemical reactions. Chemical activation has several advantages, including low energy consumption and improved pore formation (Sanni *et al.*, 2017; Prauchner & Reinoso, 2012). It is an excellent method for creating micropores because it requires little activation energy and does not result in a decrease in the carbon skeleton body density (Prauchner *et al.*, 2016; Prauchner & Reinoso, 2012; Sharma *et al.*, 2010). High mechanical strength of AC can be obtained because chemical incorporation can be done through the impregnation step without the need for a heating process (Prauchner & Reinoso, 2012).

The activating agent will cause chemical bonds to weaken or break into smaller fractions such as CO₂, CH₄, OH⁻, Cl⁻ or H⁺. Chemical agents work by attacking the polymer units (cellulose and hemicellulose) in biochar biomass (Collard & Blin *et al.*, 2014). Decomposition into gases such as CO₂ and CH₄ will take place. The activation process in the present study is conducted *via* chemical activation using phosphoric acid, H₃PO₄, potassium hydroxide, KOH and zinc chloride, ZnCl₂. Table 2.4 summarizes reactions that occurred by using different activating agents in the production of AC.

Table 2.4: Summary of reactions that occurs during chemical treatment involving ZnCl₂, H₃PO₄ and KOH (Prauchner& Reinoso, 2012; Ma, 2017; Kumar *et al.*, 2020; Foo & Hameed., 2012; Sanni *et al.*, 2017)

ZnCl ₂	H ₃ PO ₄	КОН
1. Dehydration:	1. Dehydration on biomass	1. Redox reaction of
Zn ²⁺ donate proton to char	surface	KOH and lignocellulosic
surface		surface
2. Charging of particles:	2. Cross-linking:	2. Decomposition of
Formation of an acid site	Condensation of acid to	KOH under heat induces
that enables ion-exchange	produce polyphosphoric	other reactions.
adsorption	acid	
3. Electrolytic action that	3. Splitting of cellulose	
causes the breakdown of	fiber	
cellulose molecules		
4. Polymerization:	4. Depolymerization of	
Induces the formation of	hemicellulose and lignin	
hydrogen bond and		
aromatic condensation		
5. Direct reaction with		
ZnCl ₂ : Decomposition of		
the activating agent under		
thermal treatment		

Previous studies revealed that ZnCl₂ functions as an activating chemical reagent by promoting dehydration on the surface of the sample (Jain *et al.*, 2014; Andrade *et al.*, 2018; Prauchner & Reinoso, 2012; Prauchner *et al.*, 2016). ZnCl₂ has a Bronstead acidity characteristic, which will induce the donation of a proton to break structures of polymer compounds (Sanni *et al.*, 2017). ZnCl₂ will also cause the charging of particles and result in acid site formation, which induced ion-exchange adsorption.

In addition, ZnCl₂ causes electrolytic action which induces the breakdown of cellulose molecules that will promote cavities formation on the surface and inner part of biomass (Saka, 2012). Polymerization can occur in ZnCl₂ activation when it acts as Lewis's acid that induced hydrogen deformation and causes aromatic condensation (Heidarinejad *et al.*, 2020; Sun *et al.*, 2018). The formation of these sites promoted dehydrogenation and dehydrocyclization of alkanes and alkenes groups in lignocellulosic biomass (Sun *et al.*, 2018). Functional groups containing oxygen will induce hydrogen bonding for adsorption to take place as seen in Figure 2.11.

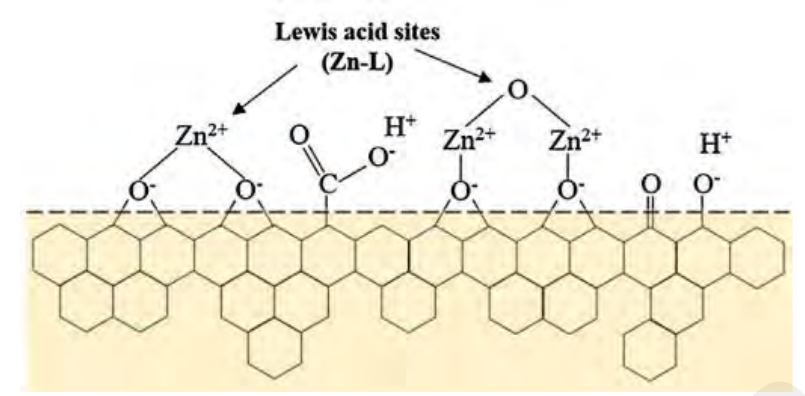


Figure 2.11: Active surface of AC from activation by ZnCl₂ (Sun et al., 2018)

Ma (2017) indicates that two reactions may occur during the activation process. First is the direct reaction of ZnCl₂ with polymer units in biomass whereby zinc oxide chloride (Zn₂OCl₂·2H₂O) is formed. Then, the same compound will be decomposed under thermal treatment and formed ZnCl₂ whereby the thermoplastic phase will take place and create pores. The reaction equation suggested by Ma (2017) using ZnCl₂ activation on lignocellulosic biomass with the heating process occurs as depicted in equations (2.1) and (2.2):

$$\begin{split} & \text{Lignocellulose} \left(C_x H_y O_z \right) + 2 Z n C l_2 \xrightarrow{\Delta} C_x H_{y\text{-}6} O_{z\text{-}3} + Z n_2 O C l_2 \cdot 2 H_2 O + 2 H C l + Tar \; (2.1) \\ & Z n_2 O C l_2 \cdot 2 H_2 O \xrightarrow{\Delta} Z n C l_2 + Z n O + 2 H_2 O \; (2.2) \end{split}$$

The reaction of biomass with a strong acid such as H₃PO₄ will cause dehydration and cleavage of bonding, hydrolysis, and condensation, which refine the lignocellulosic matrix by a cross-linking process (Kumar *et al.*, 2020; Foo & Hameed., 2012; Sanni *et al.*, 2017; Prauchner & Reinoso, 2012). Cross linkage is successfully done by the conversion of acid to polyphosphoric acid (H_{n+2}P_nO₃₊₁) and water, which will speed up the release of moisture and induce pores formation (Foo & Hameed, 2012). The possible cross-linking reaction reported by Foo & Hameed (2012) is shown in Equations (2.3) and (2.4). Equation (2.3) suggests that phosphoric acid conversion to polyphosphoric

acid and this compound can cause cross-linkages with the alcohol group that is available in the biomass matrix.

$$nH_3PO_4 \rightarrow H_{n+2} P_nO_{3n+1} + (n-1) H_2O (2.3)$$

$$-C-OH + H_3PO_4 \rightarrow -C-O-PO(OH)_2 + H_2O (2.4)$$

Since hemicellulose is prone to acid attack, phosphoric acid causes an immediate reaction upon contact with biomass (Jadhav & Mohanraj, 2016). Besides, phosphoric acid will also split cellulose fibres and the depolymerisation of hemicellulose and lignin will take place (Sanni *et al.*, 2017). The reaction will loosen the mechanical resistance between polymers making it easier for more cross-linkage to occur between the aromatic compound inside the lignocellulosic matrix (Sanni *et al.*, 2017; Prauchner & Reinoso, 2012).

Redox reaction due to alkaline decomposition occurs according to equation (2.5) to (2.11) (Hassan *et al.*, 2014). The oxidation, reduction, hydration and dehydration reaction will cause structure intercalation as depicted in Figure 2.12.

$$2KOH \to K_2O + H_2O (2.5)$$

$$C + H_2O \to H_2 + CO (2.6)$$

$$CO + H_2O \to H_2 + CO_2 (2.7)$$

$$K_2O + CO_2 \to K_2CO_3 (2.8)$$

$$K_2O + H_2 \to 2K + H_2O (2.9)$$

$$K_2O + C \to 2K + CO (2.10)$$

$$K_2CO_3 + 2C \to 2K + 3CO (2.11)$$

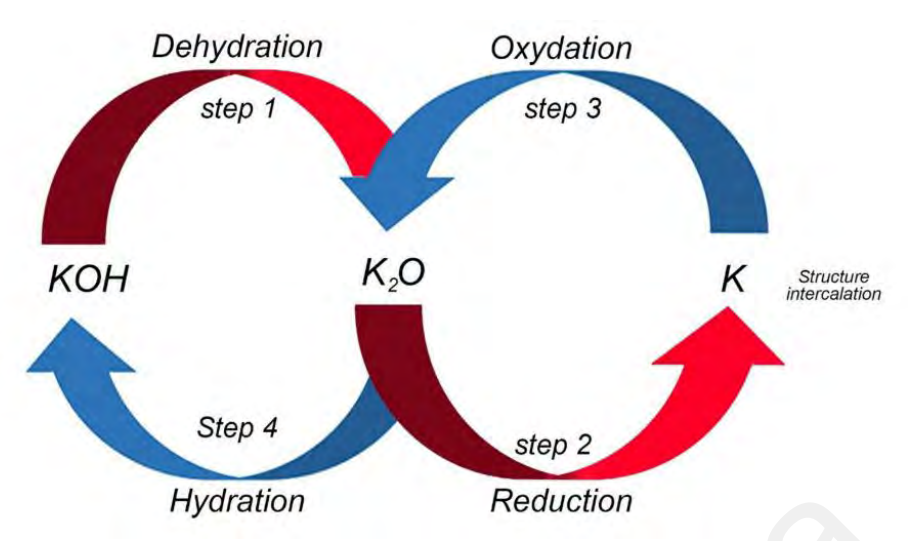


Figure 2.12: Reaction pathway of activation using KOH (Tounsadi et al., 2016; Heidarinejad et al., 2020)

2.3.3.2 Microwave activation

Physical activation using microwave utilises radiation as an activating agent. Microwave is a type of radiation method that uses electro heating at a frequency ranging from 0.3 GHz to 300 GHz and wavelength ranging from 1 mm to 100 cm (Abioye & Ani, 2017; Metaxas 1991). Microwave heating offers a variety of advantages in the heating process, including the uniform heating of the inner part of the sample using electromagnetic waves that cause a non–contact heating, lower reaction time but still at a high heating rate (Rouzitalab *et al.*, 2020; Xin-hui *et al.*, 2011; Jones *et al.*, 2002; Zhang *et al.*, 2009). Microwave radiation can reduce the heating rate by directly heating the internal centre of materials, which provides direct interaction that leads to faster volumetric heating (Rouzitalab *et al.*, 2020; Xie *et al.*, 1999).

Foo & Hameed (2012) investigated the effect of microwave power, demonstrating that power levels below 180W are insufficient to form pores. Additional power increases to 800W will have a detrimental effect on the formation of pores, including the destruction of pores due to aggressive devolatilization, dehydration and structural decomposition. This assertion is backed up by a study conducted by Hesas *et al.* (2015) which found that radiation above 850W causes carbon burn-off and damages pore structures. The duration

of microwave treatment is also likely to affect pore formation as prolonged exposure can cause temperature acceleration, which will increase the response rate, encourage porosity, and pore network (Foo & Hameed, 2012).

Activation using microwave works by adsorption of radiation through dipole rotation and ion conduction, which causes the temperature to rise evenly from the inside to the outside surface (Ganesapillai *et al.*, 2014; Ahmed, 2016). Radiation from electromagnetic energy emitted will directly interact with interior particles causing heat transfer in dielectric materials (Xie *et al.*, 1999; Ahmed, 2016). Since carbon is a dielectric material that is an excellent microwave adsorbent, this radiation technic provides an effective way to ensure that inner pores are formed (Abioye & Ani, 2017; Ahmed, 2016). Hesas *et al.* (2015) discovered that activating agents such as KOH also absorb MW radiation, thereby facilitating the formation of pores.

To maximize the benefits of both activation methods, microwave activation is typically combined with chemical activation (Jawad *et al.*, 2017; Nasri *et al.*, 2019; Mohammed *et al.*, 2014; Mohammed *et al.*, 2015). This physicochemical method is accomplished by exposing the precursor material to radiation following its impregnation with a chemical activator. Additionally, the impregnated chemical will act as a dielectric absorber, ensuring success of the precursor radiation (Abioye & Ani, 2017). Therefore, both chemical and physical activation methods are combined in this study, indicating two significant AC characteristics are elicited. Chemical activation can induce the formation of surface pores while the formation of inner pores is ensured by microwave radiation.

A chemical reaction that could occur during the radiation process is the reaction of carbon with water molecules because of chemical impregnation, as described in the following equation (2.12). As a result, carbon monoxide and hydrogen gas are released, and consequently, pores are formed.

 $C + H_2O \rightarrow CO + H_2 \tag{2.12}$

2.4 Underlying mechanism of AC application

In fact, the strength of adsorption is not selective in terms of the material it can adsorb. Suhas *et al.* (2016) clarified that this phenomenon is due to the attraction of Van der Waals that reside in the pore itself. This interpretation is also consistent with Menendez-Diaz & Martin-Gullon (2006) where pores should be considered as the key physical properties that render AC as it is. Pores formed by activated carbon are also different in size. In the previous studies, Bansal & Goyal (2005) reported that the enhancement of polar and non-polar adsorbates by AC enhanced the interactions. AC has a well-developed porous structure and surface chemical flexibility on its surface, which enables it to interact with both polar and non-polar adsorbates (Bansal & Goyal, 2005).

The adsorption process begins with the presence of a functional group from the activation process that is involved in the adsorption process, either chemically or physically activated (Yang *et al.*, 2019). These functional groups will form the interaction between adsorbent and adsorbate as depicted in Figure 2.13. Typically, functional groups are divided between heteroatoms such as oxygen, nitrogen, phosphorus, halogen groups and sulphur.

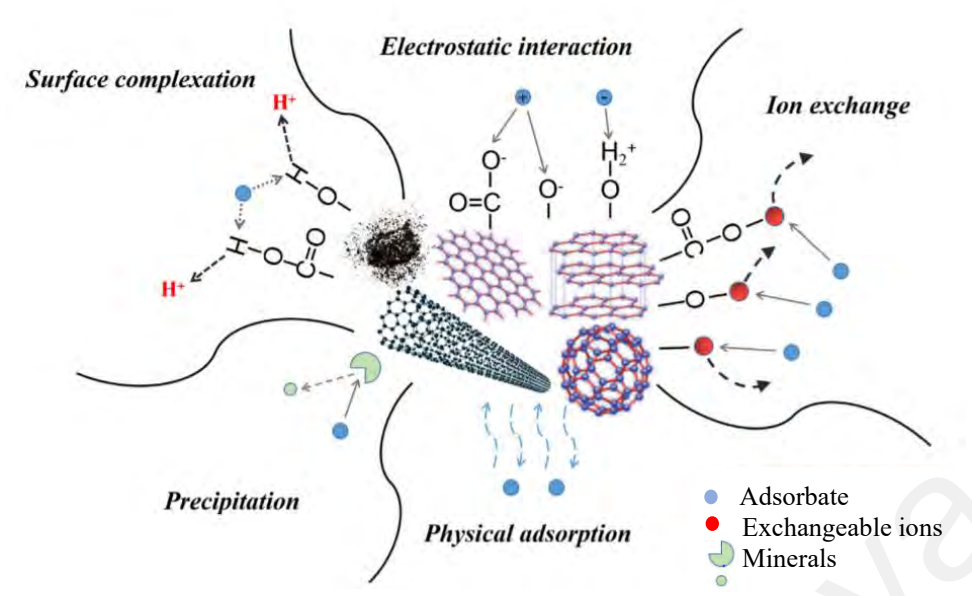


Figure 2.13: Adsorption interaction between a functional group in lignocellulosic matrices and the adsorbent on the activated carbon surface (Yang et al., 2019)

The functional groups influenced the acidity and basic properties of the activated carbon surface. The most important surface functioning group of AC is oxygen containing group that will determine the surface polarity, hydrophilic and acidic character. Boehm (2002) distinguishes four types of acidic groups on AC surfaces; strong carboxyl group, weak acidic carboxyl group, phenolic hydroxyl group and a carbonyl group. Figure 2.14 depicted the acid and basic group on the AC surface. These heteroatoms will form interactions between the AC surface and adsorbate for adsorption to occur.

Figure 2.14: Acidic and basic group that exist in AC surface (Li et al., 2011)

Apart from the presence of functional groups on AC surfaces, the surface area of the adsorbent is also significant in AC applications. A high surface area ensures that AC has enough active sites for adsorption to take place. AC surface area can reach 3000 m² g⁻¹. AC with a large surface area is typically more effective at adsorbing ions (adsorbates) and small molecules such as phenols, carbon dioxide, and volatile organic compounds (Mohammed *et al.*, 2015; Lewicka, 2017).

AC adsorption is mediated by two distinct mechanisms, chemisorption and physisorption. Chemisorption is a general term that refers to processes such as surface complexation, ion exchange, and precipitation. On the other hand, physisorption is a process that involves electrostatic interaction and physical adsorption on the surface of AC. Figure 2.13 illustrates the physisorption and chemisorption adsorption that occurs between a functional group on the AC surface and the adsorbate.

Chemisorption creates a strong force between the surface and adsorbate (Yunus *et al.*, 2020). Surface complexation is usually a predominant mechanism in heavy metal

adsorption between AC and heavy metal (Yang et al., 2019). Multiatom complexes are formed on the surface with metal functioning group that binds it on the surface (Peng et al., 2017). The ion exchange mechanism occurs through the exchange of ions on the carbon surface, which is primarily dependent on the size of the ion and feature groups of the AC surface (Yang et al., 2019; Yunus et al., 2020). Precipitation occurs in an aqueous phase where the solid residue is formed during the adsorption process that is highly dependent on the pH of the solution (Yang et al., 2019; Yunus et al., 2020).

Physisorption involves electrostatic interaction and surface adsorption. Electrostatic interaction occurs between the negative and positive charges of adsorbate and adsorbent (Yang et al., 2019). As this process involves charges on the surface of AC, pH and ionization on the surface of AC play a significant role in its operation. Physical adsorption is based on intermolecular forces or Van Der Waals force that is driven by the affinity of adsorbate towards the surface of AC (Yunus et al., 2020; Zhou et al., 2015). This type of absorbance is also caused by hydrophobicity, π interactions (in $\pi - \pi$ bonding), steric interaction, hydrogen bonding, dipole interactions, polarity attractions or a combination of these interactions (Zhou et al., 2015). No chemical bonding is formed in physical absorbance. In brief, physical adsorption occurs by adsorbate accumulating on the AC surface. The physisorption is therefore highly dependent on the pore structure and the AC surface area (Yang et al., 2019). A combination of micropores and mesopores is crucial to enhance this type of adsorption. This is due to micropores increase the AC surface area whereas mesopores accelerate adsorption kinetics (Yang et al., 2019). Additionally, the heterogeneity and polarity associated with functional AC surface groups will also cause physical movements to promote adsorption.

This study hypothesizes that the adsorption of AC soot is facilitated by the physical adsorption of AC pore particles. This is because the black carbon produced during combustion has a range of properties. According to Shrestha *et al.* (2010), the size of

black carbon soot produced by plant material combustion is within the range between nanometers and a few centimeters. The same study discovered that black carbon contains aromatic rings and a few other functional groups. Furthermore, the study examined the physical adsorption of these soot particles by analyzing the FESEM images due to the physical visibility of black carbon.

CHAPTER 3: METHODOLOGY

3.1 Materials and Chemicals

Agricultural wastes studied in this research were palm kernel shells (PKS) and coconut shells (CS). PKS (Figure 3.1) was collected from Sime Darby Plantation, Pulau Carey, Selangor and CS (Figure 3.2) was collected from the coconut milk industry in Kampung Telaga Air, Kuching Sarawak. For application of activated carbon prepared in this study, paddy straw (Figure 3.3) which was used to provide soot from the combustion process, was collected from a paddy field in Kangar, Perlis. All chemicals and reagents used in this study were of analytical grades.



Figure 3.1: Palm kernel shells



Figure 3.2: Coconut shells



Figure 3.3: Paddy straws used for combustion to produce soot

3.2 Pre-treatment of agriculture biomass waste

The biomass was crushed to sizes between 0.15 mm to 2 mm. Then, it was rinsed thoroughly using tap water and the rinsing was repeated several times until the decanted water was colourless. The clean biomass was dried in an oven at 110°C for 24 h or until a constant mass was obtained. The dried starting materials were placed in an airtight container until further use.

3.3 Proximal analysis

For proximate analysis, the American Society for Testing and Materials (ASTM) methods D4442 and E1775 were used to determine the moisture and ash content, respectively. Briefly, to determine the moisture content, an approximate2 g (m₁) of sample was weighed. Then, it was placed in an oven at 102°C until a constant mass was obtained. The mass of the dried sample was recorded (m₂). Moisture content was calculated by using Eq 3.1:

Moisture (%) =
$$\frac{m_1 - m_2}{m_1} \times 100 (3.1)$$

The ash content was determined by weighing 2 g of dried sample (m₃) and placed in an electrical furnace at 650°C for 3 hours. Residual solid or ash was cooled in a desiccator and the final mass, m₄, was recorded. Ash content was calculated using Eq 3.2:

Ash (%) =
$$\frac{m_4}{m_3} \times 100 (3.2)$$

The fixed carbon was calculated from the moisture value, ash content and volatile matter composition using Eq 3.3 (Liew *et al.*, 2018). The volatile matter composition of biomass was determined by TGA analysis as described in Section 3.5.

Fixed carbon = 100% weight – moisture – ash – volatile matter (3.3)

3.4 Ultimate analysis

Ultimate analysis, which is also commonly known as CHNS analysis, is the quantification of elements such as carbon (C), hydrogen (H), nitrogen (N), sulfur (S) and oxygen (O) content in a sample. The analysis was conducted to study the CHNS/O content in the raw materials. In this study, the instrument PE 2400 Series II CHN/S Elemental Analyzer was used. An approximate 2 g of sample was placed in a capsule. The capsule was inserted into the instrument and the analysis was carried out. Oxygen content was calculated by using Eq 3.4:

Oxygen content (%) =
$$100\%$$
 - (C + H + N + S) (3.4)

3.5 Thermogravimetric analysis (TGA)

Thermogravimetric analysis (TGA) was conducted to study the mass change of a sample over time as temperature increases. This analysis was carried out to study the thermal stability of starting materials and to compare the decomposition pattern characteristic between different biomasses. TGA also provide information on the volatile matter of the starting material. DTG or derivative thermogravimetric data were also collected during TGA. DTG provides the rate of material changes overheating. An approximate 20 mg of sample was placed in the centre of the weighing balance inside the Perkin Elmer TGA400 instrument, the temperature was set from 30°C to 1000°C and sample heating was conducted until the final temperature was reached.

3.6 Determination of lignocellulosic content

The lignocellulosic content was determined by identifying the extractive contents, hemicellulose, lignin, and cellulose contents. The methodology was adapted from Li *et al.* (2004).

3.6.1 Determination of extractive content

Mass of biomass was determined and recorded (m_0 , g). Biomass was leached with a mixture of benzene and ethanol (2:1 v/v) at room temperature for 3 h. After that, it was dried at 110°C until a constant mass was achieved. The mass was recorded (m_1 , g). The mass difference was identified, and extractive contents were calculated using Eq 3.5. The mass difference between before and after leaching is the number of extractives.

Extractive amount (%) =
$$\frac{m_0 - m_1}{m_0} \times 100\%$$
 (3.5)

3.6.2 Determination of hemicellulose content

An approximate 1 g (m_2) of extractive-free biomass (from Section 3.6.1) was placed in a conical flask and 150 mL NaOH solution (20 g/L) was added. The mixture was boiled for 3.5 h, followed by filtration, and rinsing with distilled water until the pH of the filtrate was 7. Finally, the sample was oven-dried at 110°C until a constant mass was achieved. The sample was weighed again (m_3 , g). The difference in mass was recorded as hemicellulose content as shown in Eq 3.6:

Hemicellulose (%) =
$$\frac{m_2 - m_3}{m_2} \times 100\%$$
 (3.6)

3.6.3 Determination of lignin content

An approximate 5 g (m_4) of extractive-free biomass (from 3.6.1) was soaked in 72% sulfuric acid at room temperature for 2 hours. Then, the mixture was refluxed at 100°C for 2 hours followed by filtration and rinsing with distilled water until pH 7 was achieved. The residue was dried in an oven at 105°C until a constant mass was achieved. The mass was recorded as m_5 . Lignin content was calculated using the formula below.

Lignin =
$$\frac{m_4 - m_5}{m_4} \times 100\%$$
 (3.7)

3.6.4 Determination of cellulose content

Cellulose content was calculated by the difference of extractives, hemicellulose, lignin and cellulose, assuming only these components exist in the biomass. Cellulose content was calculated according to Eq 3.8.

Cellulose (%) = 100 - (contents of extractives + hemicellulose + lignin) (3.8)

3.7 Optimization study

An optimization study was carried out to determine the most suitable conditions in preparing AC. As discussed in Section 2.1, the size of soot produced by combustion is between 10 µm to less than 1 µm. According to the size of the AC pores described in Section 2.3, the best pore opening for capturing soot particles is an AC with a micropore and macropore surface. The desired conditions are the most feasible method that emphasizes green method approaches in AC production. The targeted greener approaches in the present study are the reduction in reaction temperature and a shorter preparation time. High carbonization temperature requires higher energy while less time consumption for the carbonization step in preparing AC will also save time and energy.

The optimized carbonization temperature was first determined. The furnace was heated up to the desired temperature of 400°C to 700°C with an interval temperature of 50°C. To collect data on optimum carbonization temperature, the heating time is set to 30 min each. After the desired temperature data was obtained, the temperature heating time was varied from 15 min to 1 h with a 15 min interval to obtain the optimum heating time. FTIR data on carbonized biomass was carried out to obtain the best temperature and heating time. The raw material FTIR spectrum was determined first. By comparing the FTIR spectral between the raw materials and the carbonized samples, the largest reduction

of the entire FTIR peaks before and after carbonization process was concluded as the optimized temperature and time.

In carbon activation, KOH was the activation agent used to determine the optimum parameters conditions. For H₃PO₄ and ZnCl₂, the same optimum parameter conditions were used as previously applied for KOH. This was to ensure that the other parameters remained constant while the activating agent was the only the variable.

The parameters that were optimized includes impregnation ratio and impregnation time. Impregnation ratio has been set to 1:1, 1:2, 1:3 and 1:4 w/w for 24 hours. FTIR analysis was also conducted for each ratio to investigate the changes in the functional group when a higher activation ratio was implemented. The microwave radiation time was set at 700 W for 4 minutes. This parameter was based on reviews conducted by Kumar *et al.* (2020) and it was used without prior optimization study.

3.8 Carbonization

After the pre-treatment process, the biomass was carbonized in an electrical furnace Carbolite Gero HTF 17/5. The optimized conditions, namely, heating for 30 minutes and temperature of 600°C for coconut shell and 650°C for palm kernel shell were applied to produce biochar. The biochar was placed in an airtight jar until the activation process. The mass before and after the carbonization process was recorded to determine the percentage of yield.

3.9 Activation of Carbon

The ultimate step of producing AC was activation process. Activation was carried out through two pathways; physical and chemical activation. Activation of carbon was conducted *via* chemical activation using phosphoric acid (H₃PO₄), potassium hydroxide (KOH), and zinc chloride (ZnCl₂). Physical activation used microwave radiation.

The activating agent was incorporated directly into the charred starting material in the ratio of activating agent to carbon mass (mass of activating agent/ mass of carbon) of 1:1 (w/w). A small amount of distilled water was added to the mixture to ensure better contact between biochar and the activating agent. The impregnation time was 2 hours at room temperature. After that, the mixture was placed in a microwave for 4 minutes. Panasonic microwave with a capacity of 42 L model NN – CD997S was used for the radiation process.

The resulting product was washed with hydrochloric acid (HCl) or sodium hydroxide (NaOH) and distilled water until the pH of 6-7 was attained. pH was determined using pH paper. Finally, the AC was dried in an oven at 110° C overnight until a constant mass was obtained.

3.10 Percentage yield

The percentage yield of the carbonization process was calculated using Eq. 3.9:

Percentage of carbonization yield (%) =
$$\frac{Mass\ after\ carbonisation\ (g)}{Original\ mass\ (g)} \times 100\%\ (3.9)$$

The percentage yield of AC was calculated to indicate the process efficiency using the formula below:

Percentage of AC yield after activation (%) =
$$\frac{Mass\ after\ activation\ (g)}{Original\ mass\ (g)} \times 100\%$$
 (3.10)

3.11 Fourier transform infrared (FTIR)

Fourier transform infrared (FTIR) is infrared spectroscopy that uses infrared radiation energy to excite molecules to a higher energy state. This analysis was carried out to observe the changes that occur in all functional groups that existed in the starting materials after the carbonization and activation process are conducted. FTIR analysis was carried out using Perkin Elmer FTIR Spectrum 400 with Attenuated Total Reflection (ATR) extension. A few samples were placed on the sample stage, tighten the knob for better contact between stage and sample and the scanning was conducted.

3.12 Boehm titration

Boehm titration was conducted to study the surface functional group of activated carbon using the method that has been described by Boehm (1994). In this method, an approximate 1.0 g of AC was added to four reagents, namely, 0.1 M of sodium hydroxide (NaOH), sodium carbonate (Na₂CO₃), sodium bicarbonate (NaHCO₃) and hydrochloric acid (HCl) for 48 hours while stirring in a sealed flask at room temperature. The resultant products were then filtered, and 10 ml of the filtrate was pipetted into a conical flask. It was back titrated with 0.1 M HCl for acidic and NaOH 0.1 M for basic groups. NaOH neutralized carboxylic, lactonic and phenolic groups, Na₂CO₃ neutralized carboxylic and lactonic groups and carboxylic groups were neutralized by NaHCO₃. Basic sites were neutralized by HCl and can also be determined by Eq 3.11 as described by Schonherr *et al.* (2018):

$$n_{functional\ group}\ \left(\frac{mmol}{g_{AC}}\right) = \frac{V_{sample} - V_{reference\ (mL)\ \times\ titer\ (ml)\ \times\ M_{titrator}}}{mass\ of\ AC\ \times\frac{1}{3}}\ \left(3.11\right)$$

 V_{sample} = spent titrator volume for titration of carbon treated reaction base

 $V_{reference}$ = spent titration volume during titration of untreated reaction base

3.13 Brunauer-Emmett-Teller (BET) Surface Area

The BET surface area was analyzed using Advance Surface Area and Porosity Analyzer Micromeritics TriStar II Plus using nitrogen (N₂) gas as the carrier gas. BET analysis was conducted to further verify the surface area and adsorption ability of the produced AC. An approximate 5 mg of sample was weighed and placed in the degassing chamber. The degassing process was conducted overnight. Then, the sample was placed in a test tube and placed in the instrument for analysis.

3.14 Field Emission Scanning Electron Microscope (FESEM) and Energy Dispersive X-ray Analysis (EDX)

Field Emission Scanning Electron Microscope (FESEM) and Energy Dispersive X-ray Analysis (EDX) model SU8220, Hitachi Brand was used to study the surface morphology and element identification. Images of sample surface area were generated by scanning the surface using electron beams. The interaction of atoms will produce signals and give information on the topography of AC. Element identification was carried out by X-ray emitted by instrument and comparing it with an elemental fingerprint. Some samples were placed on a holder and placed in the chamber of the instrument. The chamber was tightly closed for a vacuum environment and the images can be seen on the computer screen. Adjustment on the targeted surface was made manually using the software on the computer. The filter paper was used as a control to study the adsorption of smoke on its surface. The blank filter paper was scanned first followed by filter paper that has undergone the same combustion condition as AC.

3.15 Evaluation of activated carbon produced as soot adsorbent

A custom-made smoke muffler (Figures 3.4 to 3.8) with a maximum capacity of 5 kg per feeding was used to adsorb soot obtained from combustion of paddy straws (in a laboratory scale) to test the ability of the prepared AC in the present study. It consists of a burning chamber (Figure 3.4 and 3.5) for the burning process and an AC holder (Figure 3.6) to place AC. Maximum amount of AC that could be filled in the AC holder is 1.05 g. The particle size of AC was varied to ensure that smoke would be able to pass through the AC efficiently. If the AC particle size is too small (<0.15 mm), smoke would not be able to go through the muffler but instead, pressure would build up inside the chamber. Meanwhile, if the particle size is too huge (>5.0 mm) the adsorption would not be able to take place efficiently as smoke might escape through the gaps in AC. By varying the sizes of AC, it would ensure a better chance for soot to adsorb on the surface of the AC and fits tightly in the AC holder.

Soot produced from smoke during combustion will exit through the AC holder. Paddy straw was used as burning material to produce soot was placed on the bottom part of the smoke muffler (Figure 3.7). The fire was introduced through an additional inlet located on the side of the smoke muffler. The muffler was tightly closed (Figure 3.8) to ensure smoke exited only through the AC holder located on top of the muffler.

To test the smoke muffler, maximum contact time between soot generated and AC was investigated. A 0.1 g of AC (with particle size from 0.15 mm to 2 mm) was placed in the AC holder (Figure 3.6). Although the AC can hold up to 10-fold of the mass used, a minimal amount of AC was used as this is more feasible to study the surface morphology.

The combustion time was set to 30 minutes then increased to 60 minutes. The initial mass of paddy straw was recorded. Mass of unburnt paddy straw was recorded as well. Mass of paddy straw burned was calculated using equation (3.12). This step was repeated

several times to obtain a consistent result. FESEM and EDX analysis were performed after combustion proses was conducted to observe the soot adsorption on AC surface.

Mass of paddy straw combusted = Initial mass of paddy straw - mass of paddy straw unburnt (3.12)

To study the adsorption of smoke on different surfaces, the filter paper was used as a comparison. Whatman filter paper with a diameter of 125 mm was used for this purpose. The filter was subjected to the same conditions as AC.

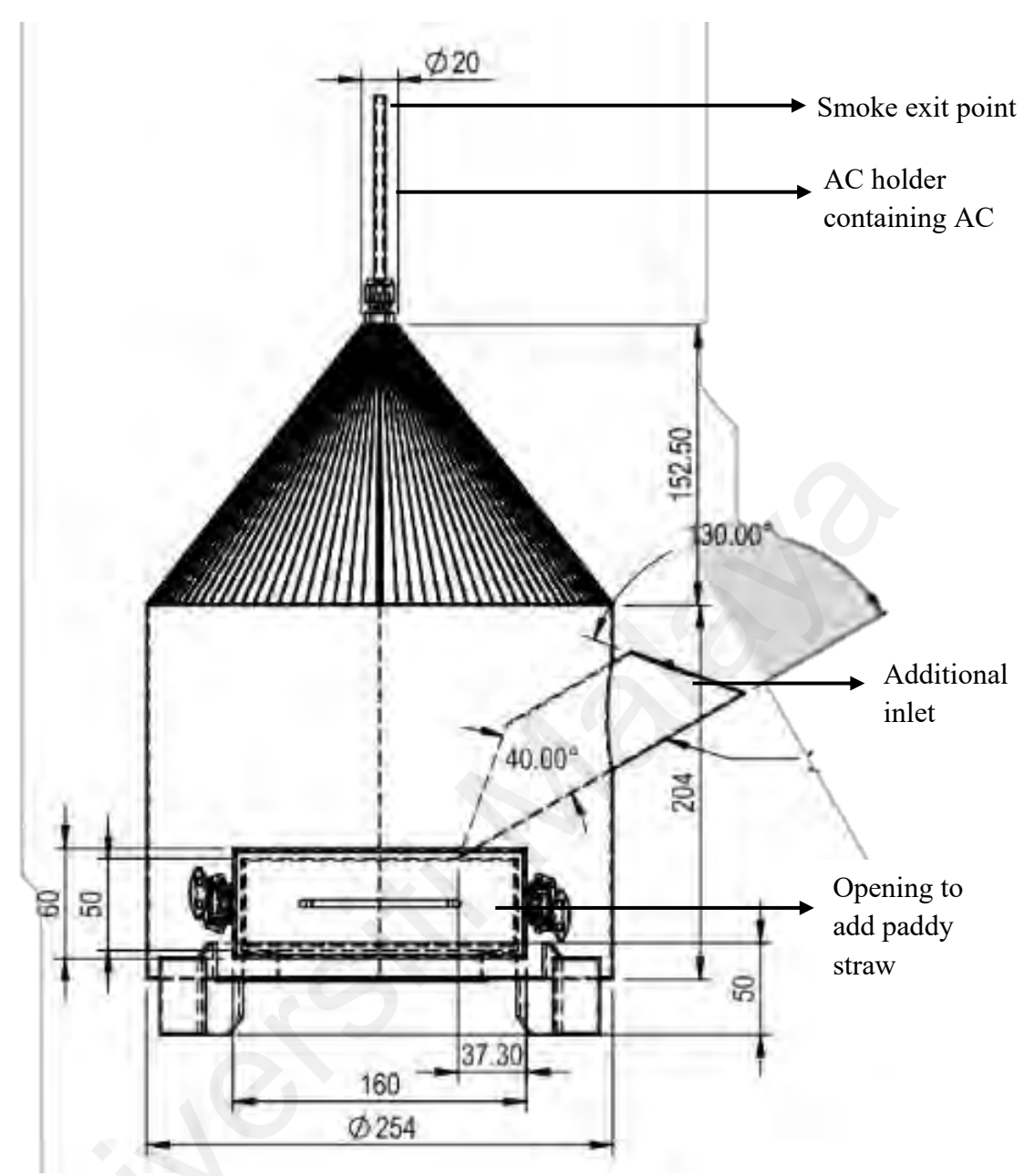


Figure 3.4: Schematic design of the smoke muffler

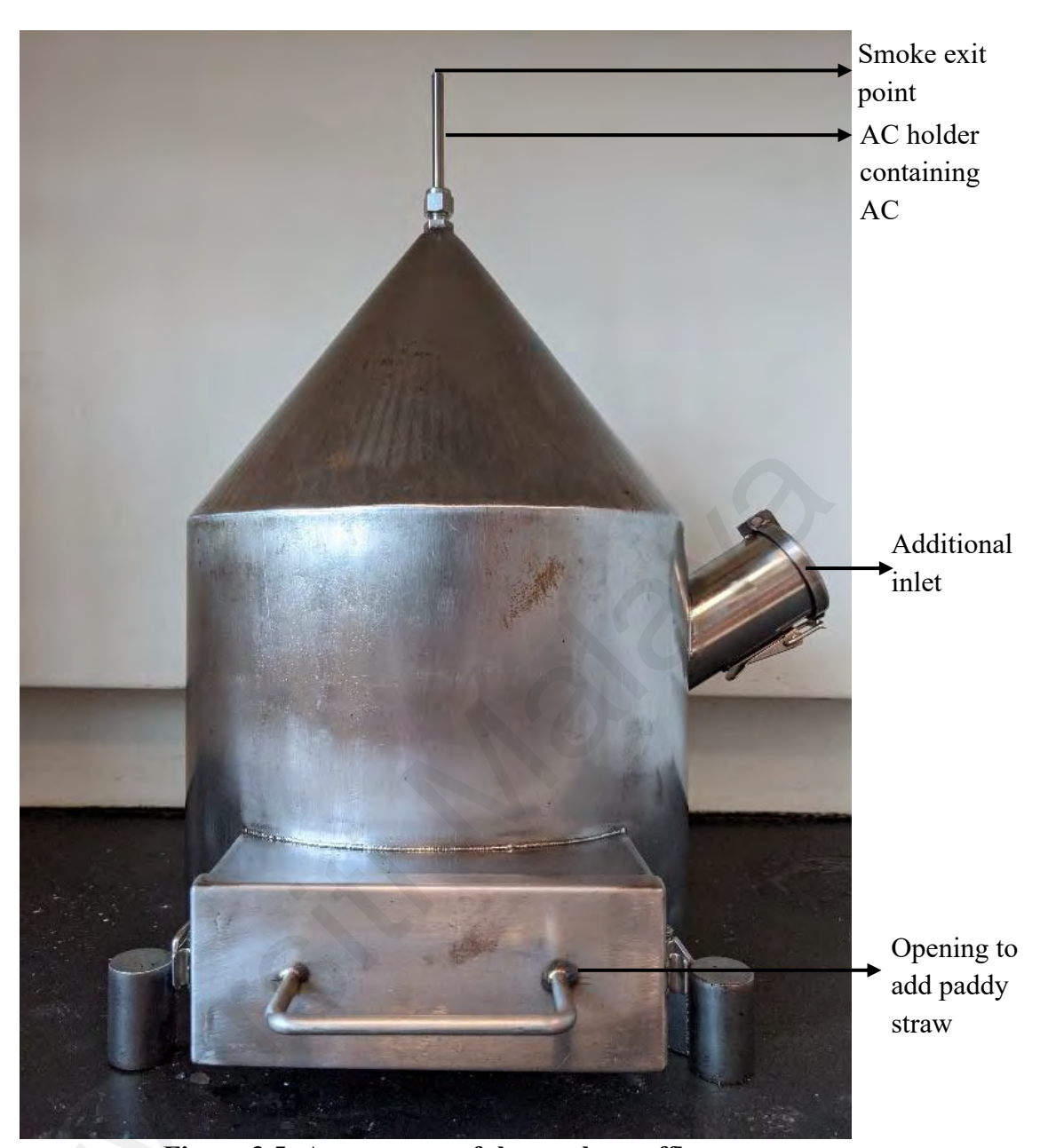


Figure 3.5: Appearance of the smoke muffler



Figure 3.6: AC holder (left). AC inserted into AC holder (right)



Figure 3.7: Paddy straw placed at the bottom of combustion chamber before combustion started



Figure 3.8: The opening of the muffler that was tightly secured to ensure no smoke escaped during combustion

CHAPTER 4: RESULTS AND DISCUSSION

4.1 Background study of starting materials

The study begins with the background study of biomasses as the raw materials; palm kernel shell (PKS) and coconut shell (CS). The proximal analysis provides information on the moisture content, fixed carbon content, volatile matter content, and ash content of the starting material. Following that was the CHNS/O content, also known as ultimate analysis. The lignocellulosic background was then determined using a variety of techniques. Thermogravimetric analysis (TGA) was used to study the lignocellulosic background content. Additionally, TGA analysis was performed to determine the mass loss as the temperature increased. FTIR was also conducted on the biomass to obtain its functional group profile.

4.2 Proximal analysis

Proximal analysis in this research includes the moisture, ash content, volatile matter and fixed carbon content. The proximate analysis provides information about the energy-conversion capacity of biomass (Sanchez – Silva *et al.*, 2012).

Moisture is the quantity of water in the biomass. High moisture content tends to lower the gasifier temperature and, as a result, the rate of carbon conversion (Pisupati & Krishnamoorthy, 2017). Pisupati & Krishnamoorthy (2017) recommend that moisture levels should be less than 2% to ensure finer char particles formation. To ensure a better char is produced, the raw materials are heated until a constant mass is achieved before the carbonization process takes place. As tabulated in Table 4.1, moisture content for PKS and CS was 6.47% and 5.64% respectively. Findings from other studies showed that moisture content varied from one study to the other as tabulated in Table 2.1 and Table

2.2. The moisture level of a starting material can easily be affected by several factors such as method of handling and weather. Hence, the moisture value for biomass differs in each study. Since moisture is easily removed by heating, this parameter is considered insignificant but provides a background understanding of the starting materials to increase the efficiency of subsequent steps.

Ash value is the amount of inorganic residue left after the combustion process. Silica, aluminum, iron, and calcium are the primary components measured in ash content. Other than that, trace amounts of magnesium, sodium, and potassium may also be present (Basu, 2018). Ash acts as a heat resistant component, potentially protecting organic compounds from degradation (Enders et al., 2012). High ash content may contribute to an increase in carbonization temperature. As shown in Table 4.1, the ash content was found to be slightly higher in PKS (2.16%) than that of CS (0.24%). Furthermore, the present study revealed that PKS required a higher carbonization temperature (650°C) compared to that of CS (600°C). Hence, it is concluded that high ash content contributes to the high heating value in a carbonization process. By referring to previous research findings, (Section 2.2.1, Table 2.1), the ash contents obtained from PKS varied within the range between 2.80 - 9.30% which may be due to the different biomass source. The ash content (2.16%) obtained in this study was slightly lower than the values reported in the literature. This explains why the optimum carbonization temperature optimized in this work is significantly lower than that of previous findings. Meanwhile, for CS, the ash content obtained in other researches (Table 2.2, Section 2.2.2) also recorded a higher value than that of this study. Therefore, the carbonization temperature of PKS is slightly lower in this study compared to other studies. However, by comparing the ash content between the studied starting materials, PKS has a slightly higher heating value. On that account, it is further agreed that findings in this study are constant with other discoveries as tabulated in Table 2.1, Section 2.2.1 and Table 2.2, Section 2.2.2.

Volatile matter is the mass percent of gas emission after the sample was heated at an elevated temperature. High volatile matter value will decrease the yield due to high gas production required during the carbonization process. As reported in Section 4.9, PKS with less volatile matter (72.13%) has a higher yield at 27.37% while CS with volatile matter at 79.63% yielded 24.87% products. This result is also consistent with the findings of Liew *et al.* (2018) which reported that PKS with a lower volatile matter of 53% (refer to Table 2.1), yielded high AC up to 89%. For CS, there is no data from other research to compare with current findings.

Fixed carbon content is the residue that remains after volatile content is released from the sample following combustion at high temperatures. Fixed carbon value is primarily carbon, but contains trace amounts of hydrogen, oxygen, nitrogen and sulphur that are not carried away by the gases. Higher fixed carbon content means higher char formation and char yield. For example, woody biomass has a higher fixed carbon value compared to fibrous raw materials. Fixed carbon data aids in the selection of combustion equipment in a large-scale AC production as its hardness provides information about biomass caking properties (Sarkar, 2015). By measuring the proportion of fixed carbon and volatile matter, the chemical energy of biomass can be calculated and gives information on the ability of biomass to be converted into energy (Sanchez – Silva et al., 2012). A high value of volatile matter over fixed carbon means that the biomass can release high energy and leads to high operational costs (Sanchez – Silva et al., 2012). According to Table 4.1, it can be observed that the fixed carbon content of CS (14.49%) is lower than PKS (19.24%) but CS has a higher volatile matter (79.63%) than PKS (72.13%). Since CS has a higher volatile matter with lower fixed carbon, CS was estimated to outperform PKS in terms of low operational costs and energy consumption.

Table 4.1: Proximal analysis of starting materials

Content (% w/w)	PKS	CS
Moisture	6.47	5.64
Ash	2.16	0.24
Volatile matter	72.13	79.63
Fixed carbon	19.24	14.49

4.3 Ultimate analysis

CHNS/O content of a starting material was conducted to study the carbon, hydrogen, nitrogen, sulphur and oxygen content of the biomasses. Table 4.2 summarizes the CHNS/O content for both starting materials. From the values reported, the H/C ratio of PKS and CS are 0.29 and 0.28 meanwhile the O/C ratio are 0.95 and 0.80, respectively. Low H/C and O/C ratio values are preferred as these will result in a lower heating value during carbonization process (Sami *et al.*, 2001; Soh *et al.*, 2019). The present results indicate that CS has a lower heating value than that of PKS. Therefore, it is expected that CS has a lower carbonization temperature than PKS based on the ultimate analysis results obtained in this work.

Apart from this, it is also found that the N and S content are relatively low for both starting materials as shown in Table 4.2. Low N and S contents are desirable as these will reduce the emission of SO_x and NO_x during pyrolysis. Emission of SO_x and NO_x gas are known to cause harmful effects on the human respiratory system and the earth atmosphere. The advantage of lower N and S content ensures that these biomasses are environmentally sustainable to be utilized as AC feedstock. In comparison of both starting materials, the content of N and S is much lower in CS than that of PKS. Other research findings also reported that low N content for both starting materials as presented in Table 2.1 and Table 2.2. Meanwhile, the present study found CS, to contain sulphur which was

not reported by other studies as tabulated in Table 2.2. Hence, both PKS and CS have potential as sustainable starting material for the production of AC.

Table 4.2: CHNS/O content of starting materials

Content (% w/w)	PKS	CS
Carbon	43.37	47.07
Hydrogen	12.69	13.16
Nitrogen	0.90	0.36
Sulphur	1.69	1.68
Oxygen	41.35	37.73

4.4 Lignocellulosic content

The lignocellulosic content of both starting materials was studied to get a broader view of the biomass's characteristics. The main lignocellulosic content in both materials includes hemicellulose, cellulose and lignin. The results of lignocellulosic content for PKS and CS are shown in Table 4.3. The percentage values of lignocellulosic content obtained in this study for both materials fall within the range of biopolymer components found in reported literature as shown in Table 2.3. From data tabulated in Table 2.1, Table 2.2 and Table 2.3, it is noted that, the lignin content is always dominant in PKS. Meanwhile, for CS, the lignocellulosic content varies between studies. However, the lignin content is always lower than hemicellulose and cellulose contents in literatures.

In the present study, it can be observed that CS contains more hemicellulose than PKS at 38.89% and 29.80%, respectively. In the meantime, PKS (40.67%) has higher lignin content than CS (33.07%). Since the lignin structure is dominant, a higher temperature is required for carbonization of PKS. This is in line with the findings of Liew *et al.* (2018) which reported that the complex structure of lignin contributes to its high chemical stability. As mentioned in Section 2.2.3, lignin is rigid and requires high energy to break the structure down. The presence of lignin structure in PKS means there are more acetyl

groups in the structure as depicted in Figure 2.6. Meanwhile, for hemicellulose in CS, hydroxyl is dominant in its structure (Figure 2.5). The acetyl and hydroxyl groups will degrade and vaporize as the carbonization process proceeds. The release of these small compounds will cause the major biopolymer to be fragmented and causes activation of the surface. The fragmentation of starting materials will be discussed further in Section 4.7, meanwhile, activation on the surface will be explained in Section 4.8. In this work, TGA has also been performed to validate the values of the lignocellulosic biomass content that has been carried out experimentally. In the next section (Section 4.5), more discussion on TGA and its relation to the lignocellulosic content is reported and discussed.

Table 4.3: Lignocellulosic content of starting materials

Content (% w/w)	PKS	CS
Hemicellulose	29.80	38.89
Lignin	40.67	33.07
Cellulose	13.68	16.00
Extractives	5.53	5.14

4.5 Thermogravimetric Analyses (TGA) and Differential Thermogravimetric Analyses (DTG)

TGA was conducted on CS and PKS (Figure 4.1 and 4.2) to study the effect of elevated temperature on mass of biomass and verification of lignocellulosic content. Mass loss at temperature of less than 110°C denotes the removal of water and volatile matter during lignocellulosic biomass decomposition. While degradation of hemicellulose occurs between 220°C and 315°C, followed by decomposition of cellulose at 315°C to 400°C. Degradation of lignin occurs at a temperature above 450°C (Nizamuddin *et al.*, 2016; Sanchez – Silva *et al.*, 2012).

According to the DTG and TGA curves of both biomasses, the release of moisture and small volatile matter occurs between 29°C and 110°C. As the temperature increases, the percentage weight of each sample decreases tremendously. This occurs at 294°C until 410°C for both biomasses due to hemicellulose and cellulose degradation. Cellulose begins to decompose at 351°C. The weight percentage continues to decrease at 410°C, indicating lignin degradation.

From the results obtained from lignocellulosic content analysis in Section 4.4, it is known that hemicellulose and cellulose content from PKS is 40.67%. According to DTG curves, two distinct drops in derivative weight occurs at 294°C until 410°C. Between these temperatures, the derivative weight loss is recorded at 41% that indicates the percentage of hemicellulose and cellulose content. This value agrees with the experimental value collected from Section 4.4. The same findings can be seen in CS whereby experimentally, hemicellulose and cellulose percentage content in CS is 54.89%. Meanwhile, DTG data recorded that the hemicellulose and cellulose content in CS is 51%. Hence, the data collected experimentally and through DTG analysis is consistent.

Lignin degrades at a higher temperature than hemicellulose and cellulose. A rigid structure of lignin is a result of its function as cellular glue, which significantly contributes to maintaining the stiffness of the biomass cell wall (Isikgor & Becer, 2015). In CS and PKS, the degradation of lignin starts at a temperature of 410°C. The weight loss continues to increase until the maximum temperature was reached.

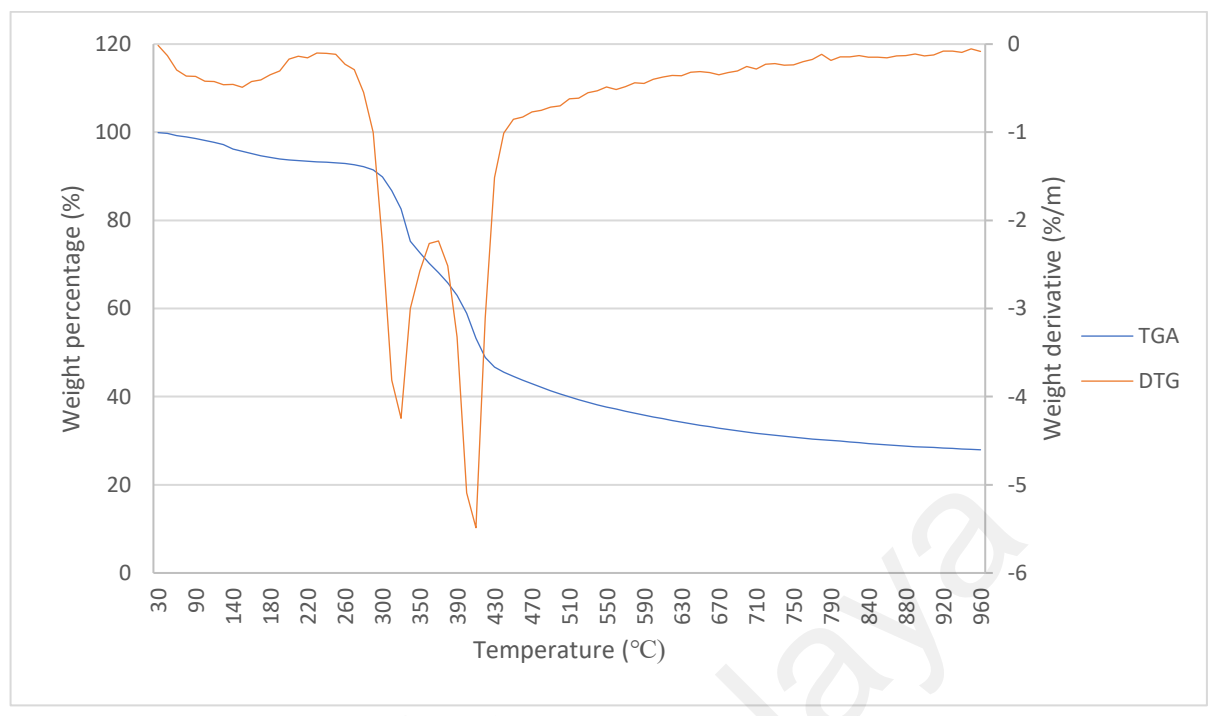


Figure 4.1: TGA and DTG curves of PKS

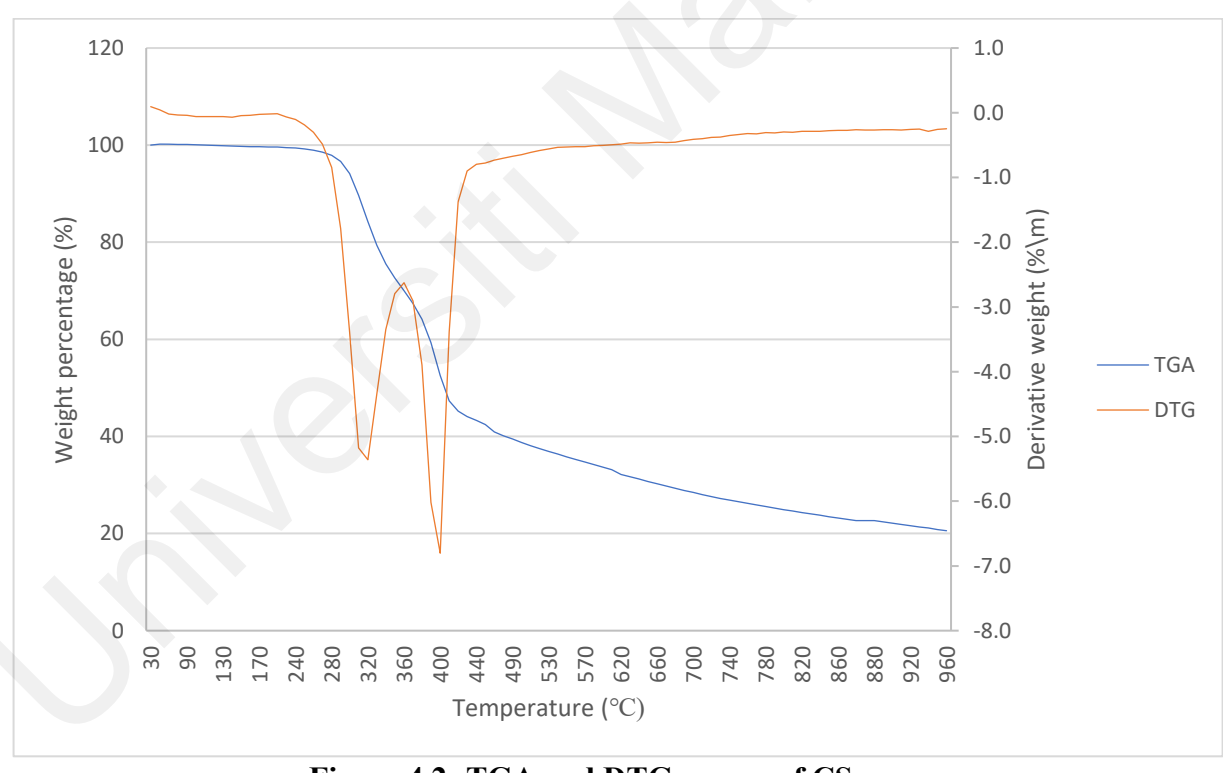


Figure 4.2: TGA and DTG curves of CS

4.6 FTIR of starting materials

As mentioned in Section 3.7, FTIR analysis plays a significant role in the optimization of AC production. Figures 4.3 and 4.4 show the FTIR spectra for both starting materials. Generally, bands observed are dominated by the functional groups in their respective major component, namely, hemicellulose for CS and lignin for PKS (Table 4.3, Figures 2.5 and 2.6). Briefly, the peaks observed from 2500 to 4000 cm⁻¹ represent O — H, C — H and N — H. The peaks obtained at 1800 – 1550 cm⁻¹ represent C = O bonding. In addition, the peaks observed at 1650 to 1550 cm⁻¹ correspond to the functional group of C = N and C = C while the peaks below 1550 cm⁻¹ represent C — C, C — O and other carbon single bonds. From the CHNS results, the presence of N in each biomass is below 1%. Hence, the presence of nitrogen bonded peaks was negligible in both spectrums.

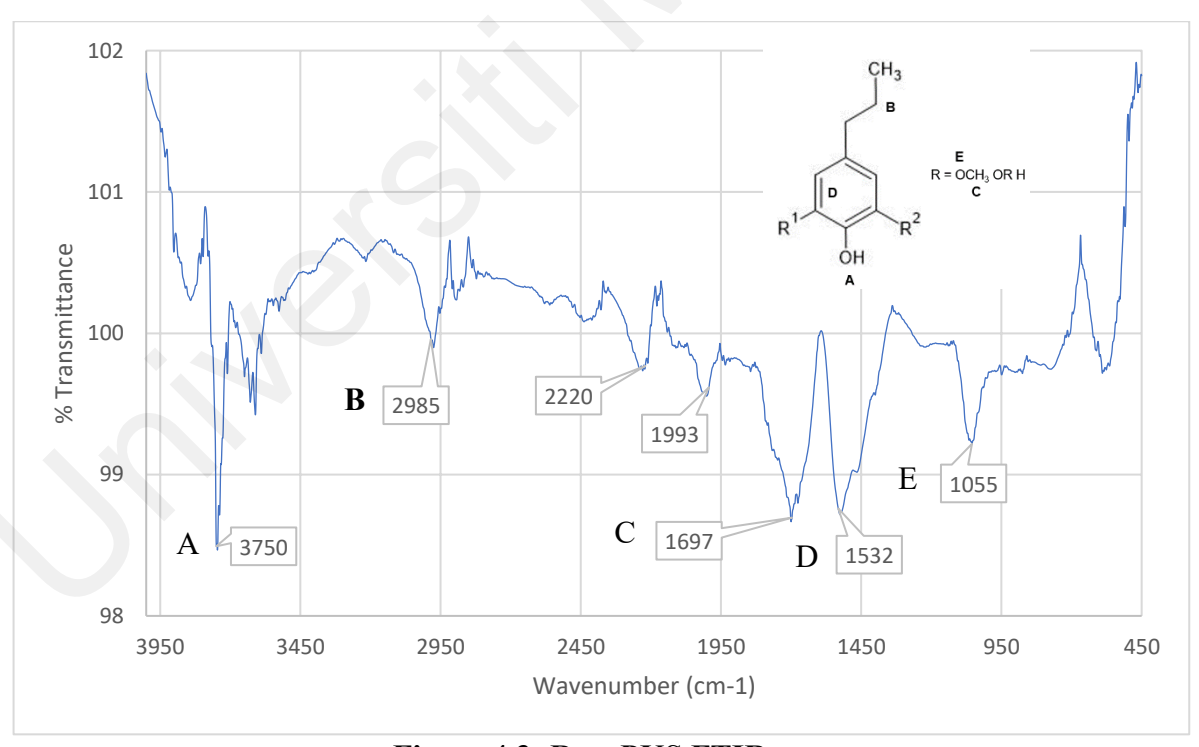


Figure 4.3: Raw PKS FTIR spectra

Figure 4.3 shows the spectra of raw PKS which contains lignin mainly. The medium broad band at 3750 cm^{-1} corresponds to the stretching vibration of the hydroxyl group in the alkyl chain substitutions at the aromatic ring. The band at 2985 cm^{-1} is the aldehyde aliphatic CH— stretching vibration meanwhile peak at 1697 cm^{-1} is the C = O of an acetyl group. The peak at 1532 cm^{-1} represents C = C stretching vibration in the aromatic ring in the main monomer of lignin whereas the peaks obtained at 1055 cm^{-1} is associated with carbonyl group C - O and C - O - C stretching. Adsorption below 1300 cm^{-1} represents a mixture of alkane and alkene bending.

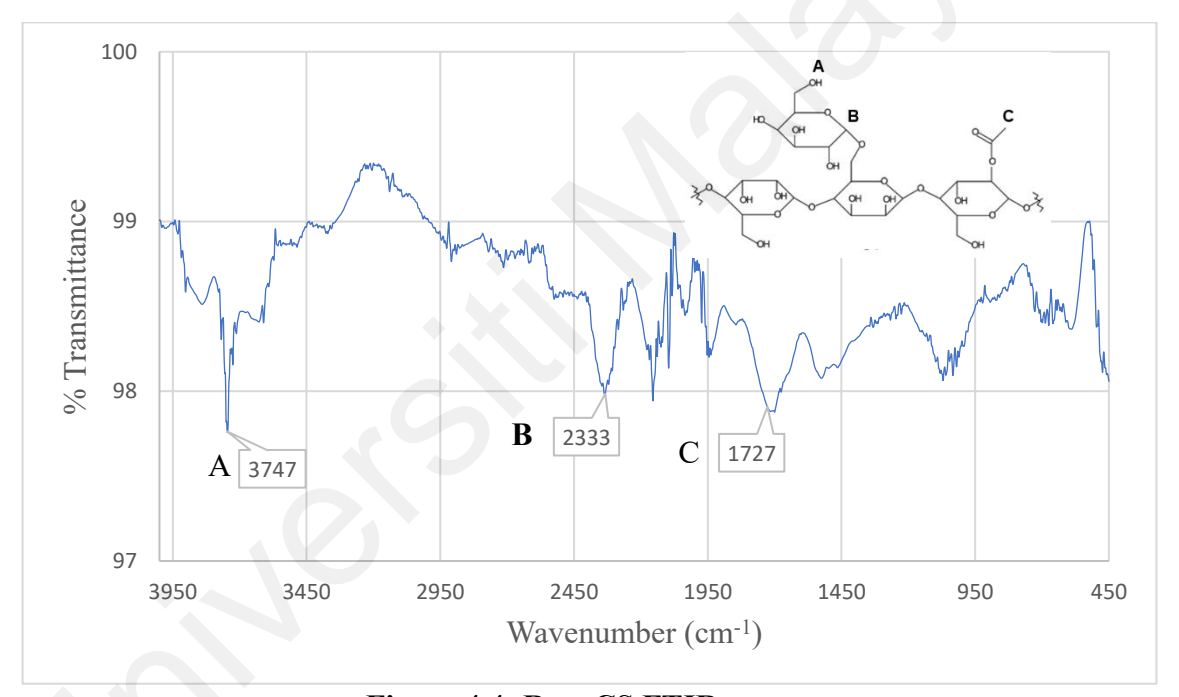


Figure 4.4: Raw CS FTIR spectra

Figure 4.4 depicts the FTIR spectra of raw CS. The peaks observed at 2333 cm⁻¹ represent the C - O - C stretching vibration in aryl – alkyl linkages in hemicellulose polymer (Figure 2.5). The medium bands at 3950 - 3500 cm⁻¹ corresponds to the hydroxyl – OH group stretching vibration that is present in raw CS. The peak at 1727 cm⁻¹ is associated with stretching of carbonyl C = O of the acetyl group in the CS chemical structure.

4.7 Carbonization of biomass

4.7.1 Optimization carbonization temperature and duration

Carbonized biomasses are abbreviated as "C". For example, CCS stands for carbonized coconut shell and CPKS means carbonized palm kernel shell.

The determination of the optimum carbonization temperature was studied by measuring the FTIR spectra before and after carbonization processes. Raw biomass FTIR spectrum was first determined (Figures 4.3 and 4.4). After carbonization, FTIR analysis was conducted again (Figures 4.5 and 4.6). Carbonized spectra should have substantial signal loss as this indicates the original functional group has fragmented and degraded to form a carbon skeleton (Wang *et al.*, 2019). Carbonization temperature lower than optimized temperature gives no changes in their FTIR spectra. An ideal carbonization temperature ensures an increase in the degradation of biomass (Wang *et al.*, 2019; Ahmed & Hameed, 2020). In this work, temperatures of 650°C for PKS and 600°C for CS were found to be the optimal for carbonization.

Figures 4.5 and 4.6 shows the signal loss of raw PKS and raw CS at the optimized temperature. Upon carbonization of PKS, the peaks at 1993 cm⁻¹ and 1532 cm⁻¹ are still present (Figure 4.6). The band at 1993 cm⁻¹ represents para substituent in the aromatic ring of lignin monomer, whereas the band at 1532 cm⁻¹ corresponds to the C = C in the aromatic ring that does not undergo fragmentation. Meanwhile, in the carbonization of CS, signal loss occurs at peaks around 3950 cm⁻¹ to 3500 cm⁻¹ and 1711cm⁻¹ (Figure 4.6) which can be associated with the defragmentation of C = C in the acetyl group and the release of the hydroxyl group from the main structure. Meanwhile, the rigid C - C - C bond was not affected at optimized carbonization temperature and can still be seen at 2339 cm⁻¹ both raw CS and CCS (Figure 2.7).

The above explanation is consistent with the discussion in Section 2.3.2. From Figure 2.9, smaller moieties such as hydroxyl and acetyl bonded to the main polymer structure

of biomass undergone fragmentation at a temperature higher than 500°C (Prauchner *et al.*, 2016). FTIR spectra show that most acetyl and OH substituents experience signal loss. The resultant carbon skeleton remains as the main body framework of the biopolymer itself which is left after the carbonization process. For example, in CPKS, the aromatic double bond in the aromatic ring is still present after the carbonization process. This forms the carbon skeleton of carbonized biomass.

As mentioned under Sections 4.1 and 4.3, the PKS carbonization temperature is expected to be higher than that of CS due to their lignocellulosic composition. As mentioned in Section 4.4, lignin content in PKS is higher compared to CS. It is well known that lignin is a rigid structure that is stable at high temperatures. Since the lignin content of PKS is comparatively higher than CS, PKS has a higher carbonization temperature than CS.

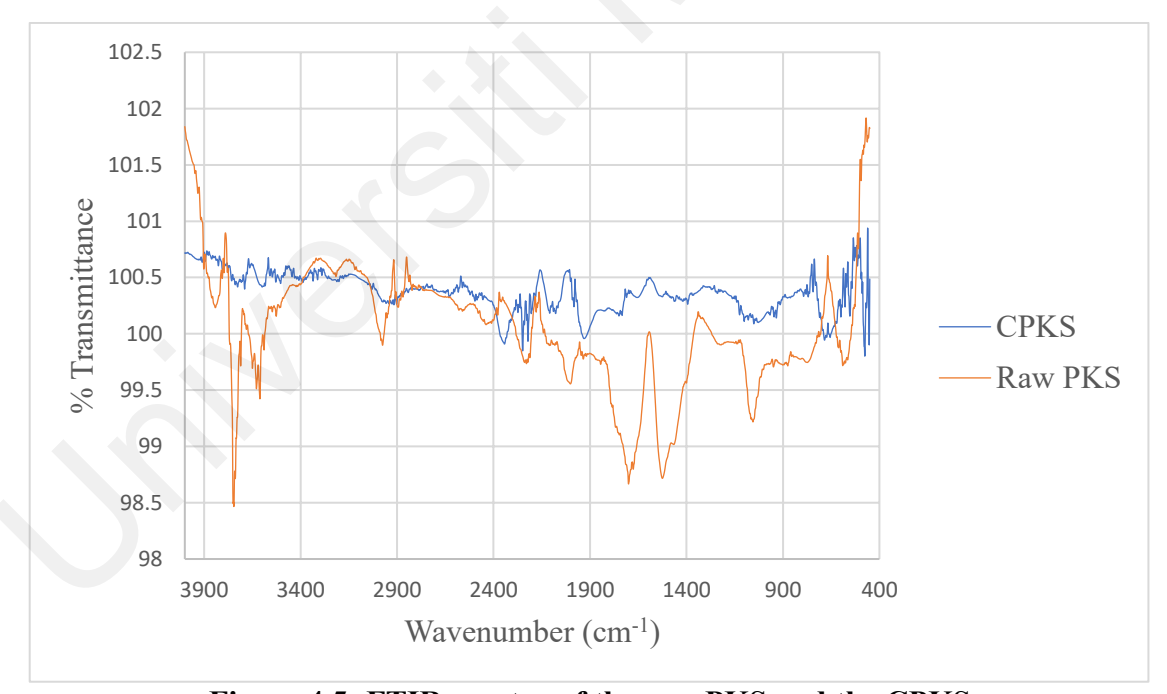


Figure 4.5: FTIR spectra of the raw PKS and the CPKS



Figure 4.6: FTIR spectra of the raw CS and the CCS

The carbonization duration was studied after the optimum carbonization temperature was determined in this work. By using optimized carbonization temperature of CS at 600°C, the carbonization time increased to 60 mins. However, there was no more signal loss after 60 minutes of carbonization (Figure 4.7). This indicates that no further fragmentation takes place after 30 minutes. The percentage yield was also reduced when the carbonization time was increased. Since there was negligible signal loss with the drawback of decreasing percentage yield, the carbonization temperature is therefore held at 30 minutes.

The present work aims to ensure a low energy method is applied to maintain the green technology approach. Therefore, a comparison of carbonization temperature used in some recent studies conducted in AC production was studied (Table 4.4). It can be observed that high temperature is applied in the production of PKS and CS based AC. CS carbonization carried out by Nasri *et al.* (2019) is at 700°C and 45 minutes. Li *et al.* (2020) recorded a carbonization temperature of 650°C for an hour meanwhile Andrade *et al.* (2018) have a lower carbonization temperature at 500°C but the carbonization duration

spikes for 2 hours. The same pattern can be seen in PKS carbonization in other recent studies. For example, Ma *et al.* (2020) manages to carbonize PKS at 500°C but the carbonization duration is twice that in this study. Sahri *et al.* (2020) and Lee *et al.* (2019) both recorded the optimum temperature to be above 700°C at a duration twice than this research. The present study has successfully produced AC at an optimum condition for PKS and CS, respectively, by taking into consideration of both temperature and time factors as presented in Table 4.4.

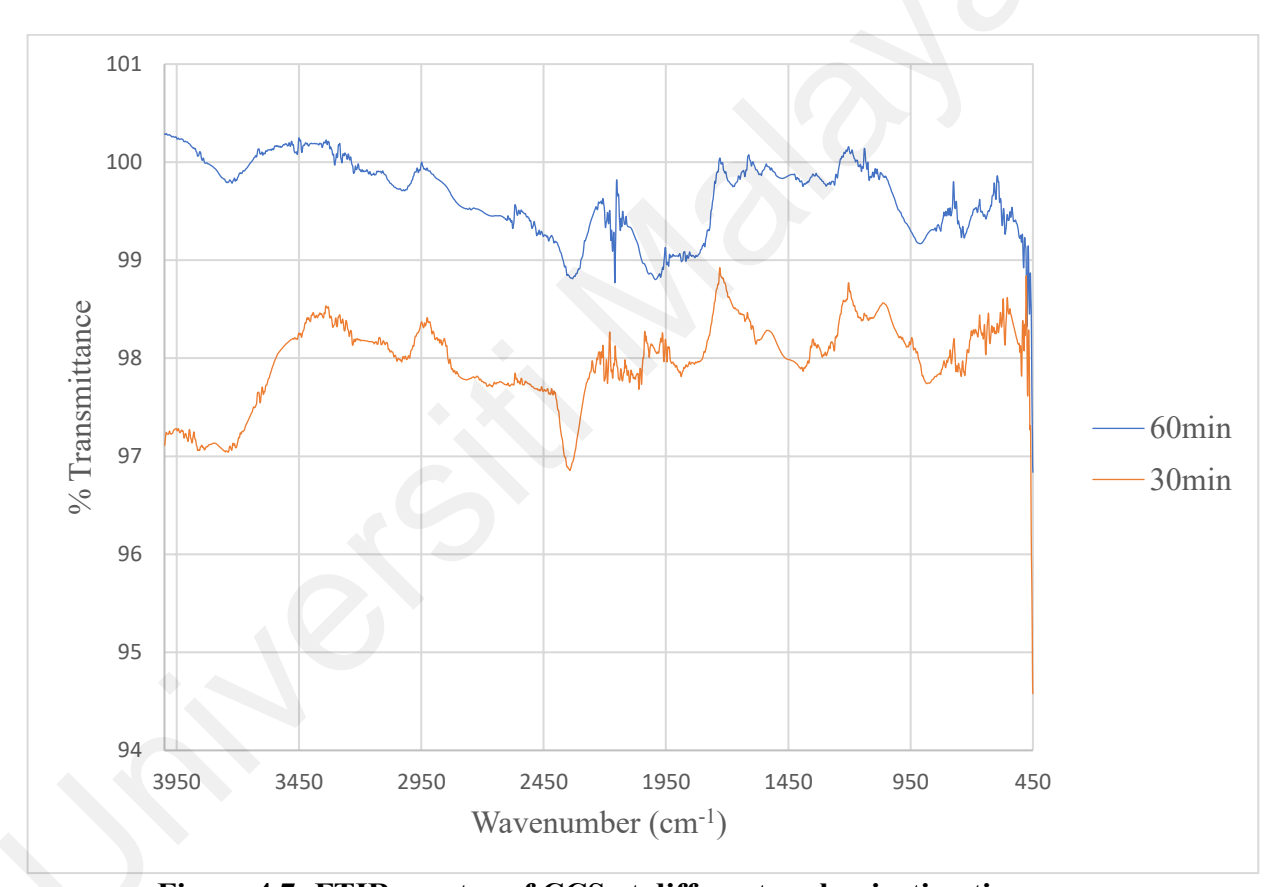


Figure 4.7: FTIR spectra of CCS at different carbonization time

Table 4.4: Comparison of conditions used for carbonization process of palm kernel shell and coconut shell

Author	thor Biomass Carbon temperat		Carbonization duration (min)
Present study	PKS	650	30
Sahri <i>et al.</i> (2020)	PKS	700	120
Ma et al. (2020)	PKS	500	60
Lee et al. (2019)	PKS	715	75
Present study	CS	600	30
Li et al. (2020)	CS	650	60
Nasri <i>et al.</i> (2019)	CS	700	45
Andrade et al. (2018)	CS	500	120

4.8 Activation of carbonized biomass

In this study, physicochemical activation method was studied. Chemical activation was conducted first followed by physical activation using a microwave. KOH has been used to study the most optimized activating condition. H₃PO₄ and ZnCl₂ will follow the same parameter used by KOH. Two optimized main parameters were the activating ratio of carbonized biomass to activating agent and duration of impregnation.

4.8.1 Activation optimization (impregnation ratio and duration)

The present results indicated that there are no significant changes in the FTIR spectra as the chemical ratio increases, as depicted in Figure 4.8. Hence, the impregnation ratio of the carbonized biomass to activating agent is fixed at 1:1 ratio throughout this study based on the results obtained for KOH as the activating agent. A minimal ratio is preferred since an increase in the impregnation ratio does not provide any improvement in terms of efficiency. Furthermore, several studies have also shown that the 1:1 ratio is the most

suitable parameter for the production of AC (Tounsadi *et al.*, 2019; Tounsadi *et al.*, 2016; Lewicka, 2017; Teimouri *et al.*, 2019; Ahmed & Theydan, 2014; Mohd Din *et al.*, 2009).

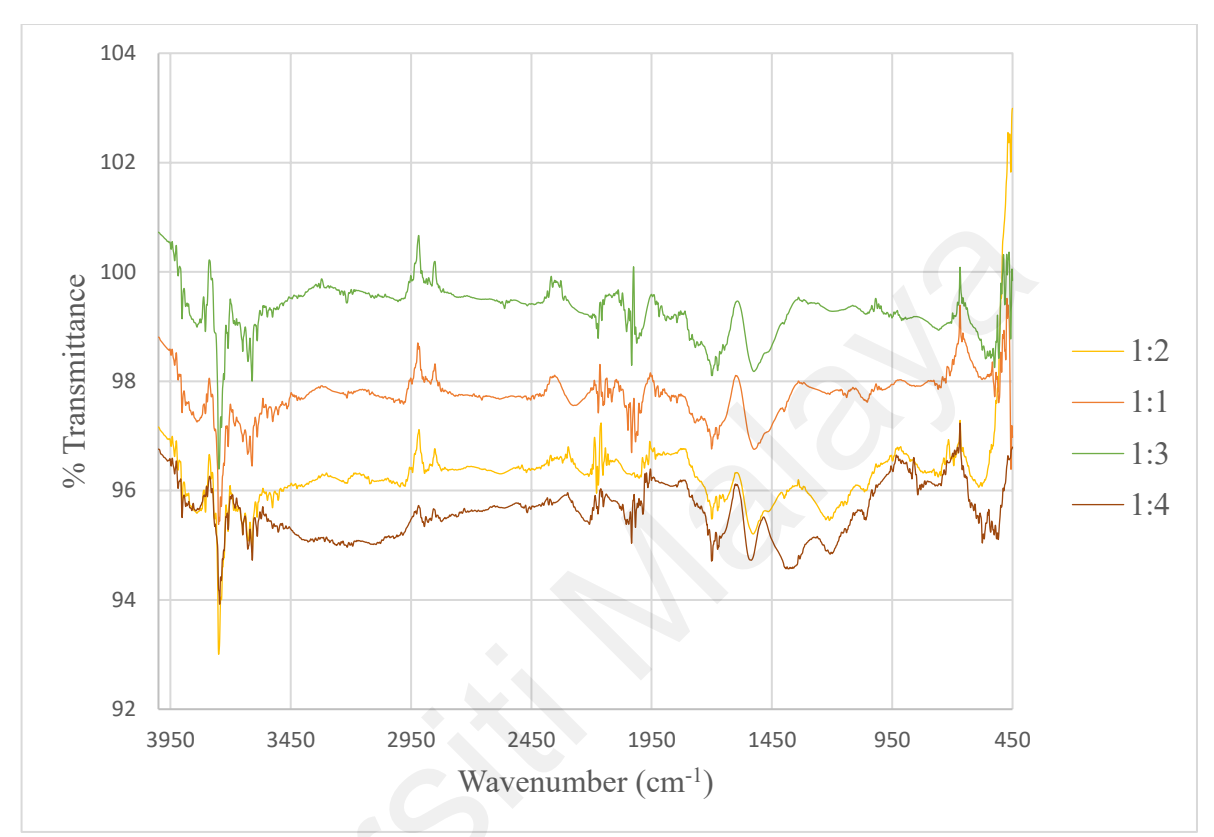


Figure 4.8: FTIR spectra of different impregnation ratio of CCS to the activating agent (g/g) (KOH) in the activation process

Apart from the impregnation ratio, the impregnation time for each activation process was also studied. Activation time was studied from 2 hours to 24 hours at 4 hours interval. However, as depicted in Figure 4.9, there was no distinct difference when the impregnation time was increased to 24 hours. The shortest impregnation time was therefore optimized at 2 hours.

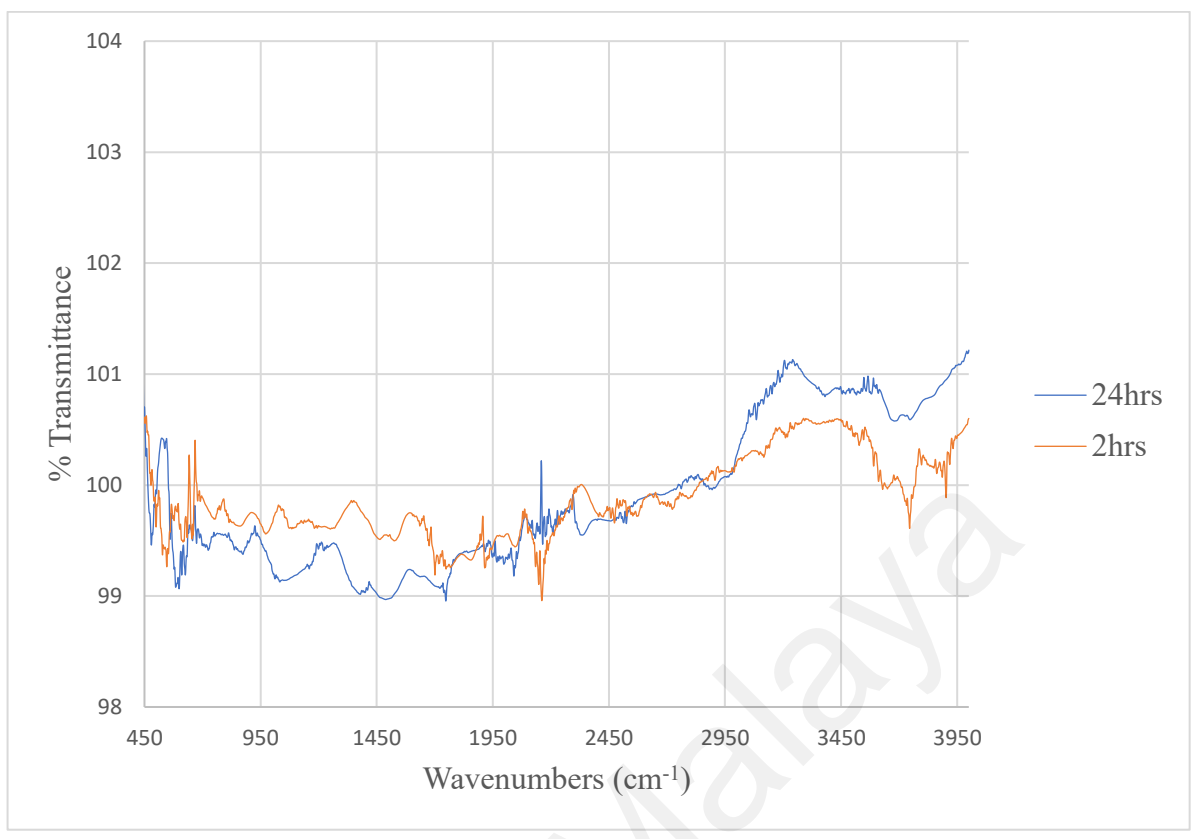


Figure 4.9: FTIR spectra of different impregnation duration

4.8.2 Base activation of carbonized biomass

Base activation utilised KOH as an activating agent. Base activated carbon is abbreviated as "B". For example, BCS refers to the base activated coconut shell and BPKS denoted the base activated palm kernel shell.

As mentioned in Section 4.6, peaks above 3400 cm⁻¹ are related to a carbonyl group. For both PKS and CS, peaks above 3400 cm⁻¹ disappeared upon carbonization, but reappeared after activation. This is due to the activation process that used KOH and oxygen is reintroduced back into the biomass. This is in parallel with the discussion in Section 2.3.3.1 whereby equation (2.5) to (2.11) shows that activation reaction that causes the formation of new carbon – oxygen bond between activating agent and carbon in the starting material. This event occurs during activation with PKS and CS.

Peaks at 2165 cm⁻¹ for PKS in Figure 4.10 and peaks 2032 cm⁻¹ for CS in Figure 4.11 intensifies after being activated prove the reformation of C - O - C bond due to the

formation of K₂CO₃ as equation (2.5) to (2.11) in Section 2.3.3.1. The formation of oxygen containing carbon is crucial as this provides the activate site for adsorption to take place as discussed in Section 2.4. The presence of signals at peak 1536 cm⁻¹ Figure 4.11 spectra indicates the presence of oxygen after the activation process. Both activations of PKS and CS, show indistinguishable results.

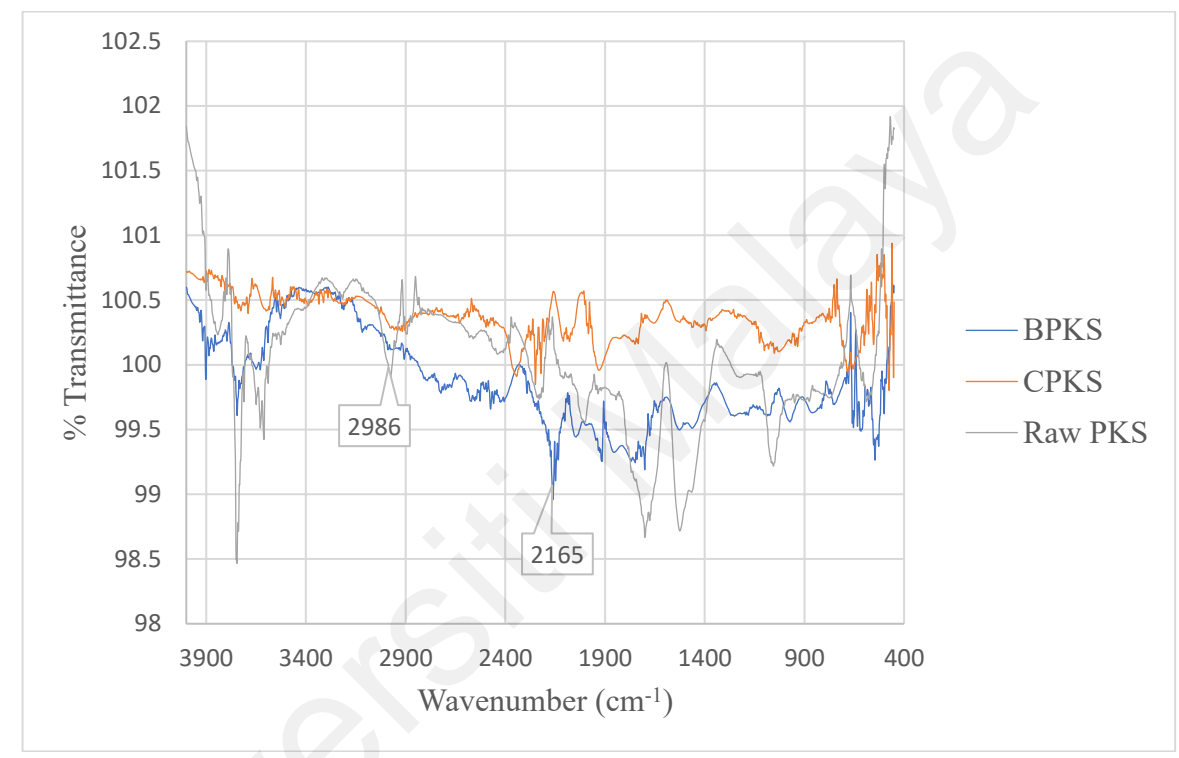


Figure 4.10: FTIR spectra of CPKS, BPKS and raw PKS

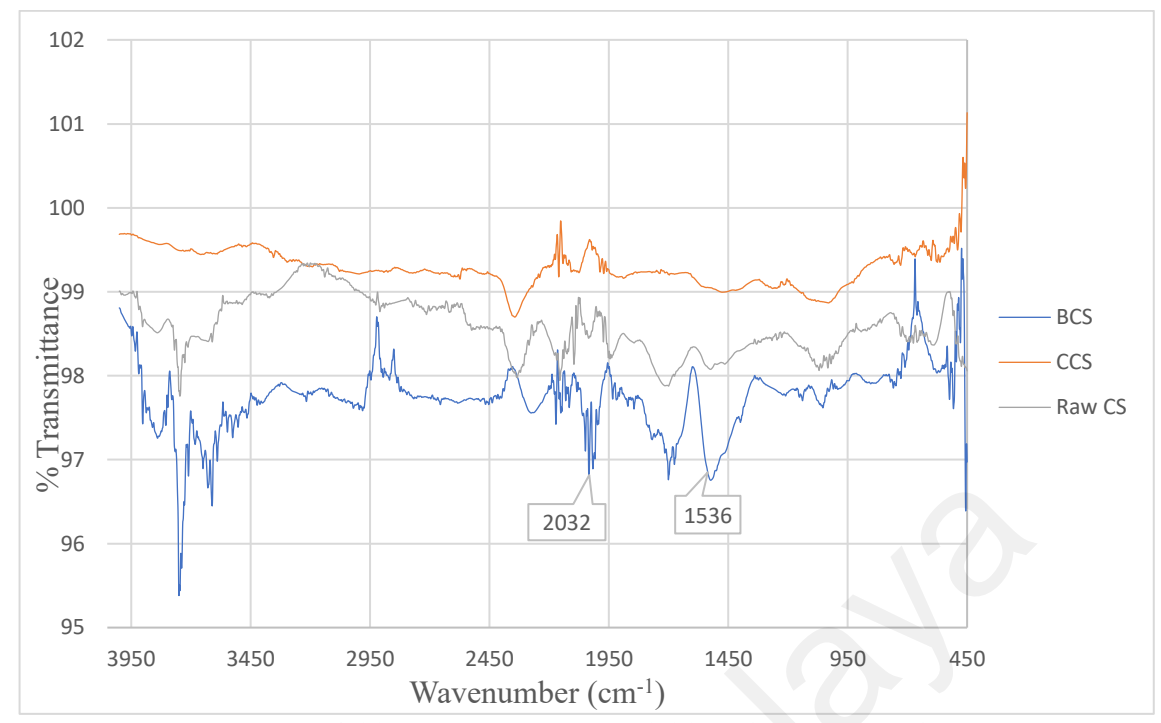


Figure 4.11: FTIR spectra of CCS, BCS and raw CS

4.8.3 Acid activation of carbonized biomass

In the present study, acid activation was studied using H₃PO₄ as the activating agent. Acid activated carbon is abbreviated as "A". For example, ACS denoted acid activated coconut shell and APKS refers to acid activated palm kernel shell.

In activation of PKS using acid, the OH peaks are absent in the FTIR spectra (Figure 4.12). This means that no formation of hydroxyl containing compounds takes place in the biomass which is contrary to results reported by Foo & Hameed (2012) as shown by equation (2.4). However, the C = O bond from the aromatic compound in PKS at 1532 cm⁻¹ is still present that agrees with Prauchner & Reinoso (2012) who observed occurrence of aromatic rearrangement during acid activation.

CS shows the same trend as PKS, no hydroxyl containing compound is present upon acid activation as depicted in Figure 4.13. A complete loss in the signal was seen in the spectra with the only peak at 992 cm⁻¹ indicating the presence of C – H bonding. The research findings can be related to the discussion in Section 2.3.3.1 reported by Sanni *et*

al. (2017) cellulose fiber splitting and depolymerization of hemicellulose by acid might occur during acid activation. In addition, acid attack on hemicellulose as studied by Jadhav & Mohanraj (2016) most probably takes place which causes most bonding in the biopolymer structure destroyed.

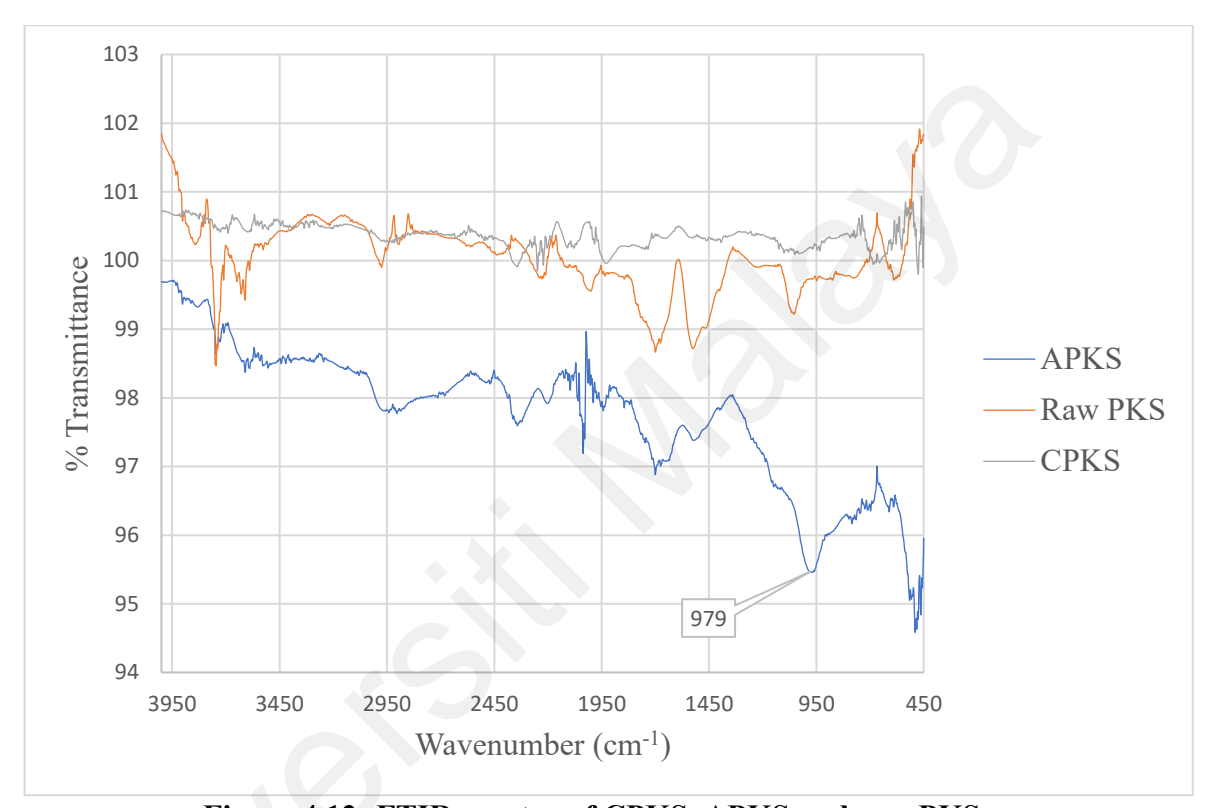


Figure 4.12: FTIR spectra of CPKS, APKS and raw PKS



Figure 4.13: FTIR spectra of ACS

4.8.4 Metal salt activation of carbonized biomass

Metal salt activation using ZnCl₂ as an activating agent was investigated in the present study. Metal salt activated carbon is abbreviated as "Z". For example, ZCS refers to metal salt activated coconut shell and ZPKS refers to metal salt activated palm kernel shell.

While base activated carbon from each starting material is quite similar, metal salt activated carbon shows distinguishable results between CS and PKS. During activation with ZnCl₂ as a metal salt, both starting materials show a huge difference between the FTIR peaks. In PKS activation, it is shown in Figure 4.14 that the oxygen containing peaks at around 3450 cm⁻¹ to 2943 cm⁻¹ intensify after being activated compared to raw PKS and carbonized PKS. As depicted in Figure 2.11, oxygen ions are present throughout the surface of zinc chloride activated carbon. Meanwhile, the C = O aromatic bonding that is represented in peak 1532 cm⁻¹ at raw PKS is still present even after activation which shows that the aromatic ring in starting material is still undisturbed. However, the

C = O bonding of the acetyl group as shown at 1697 cm⁻¹ in raw PKS is still absent after carbonization and activation. The activation process for metal salt activation shows a similar result as reported by Saka (2012) and Ma (2017) in Section 2.3.3.1.

While oxygen containing peaks intensify in ZPKS, CS shows the contrary result. The CCS and ZCS show similar FTIR signals whereby the peak above 3450 cm⁻¹ has completely vanished (Figure 4.15). C – O – C peaks that are present in the main polymer compound in CS represented by signal at 2333 cm⁻¹ is still present in all FTIR spectra. This indicates that despite the high carbonization temperature and activation process conducted, the main biopolymer in the CS structure is undisturbed. The acetyl group or the C = O bonding is still absent in ZCS and CCS. The reaction that might occur during metal salt activation in CS is a reaction that can be related to dehydration reaction as agreed by Jain *et al.* (2014), Andrade *et al.* (2018), Prauchner & Reinoso (2012) and Prauchner *et al.* (2016). This is due to no new formation of bonding and the similar signals shown after the activation process has been carried out.

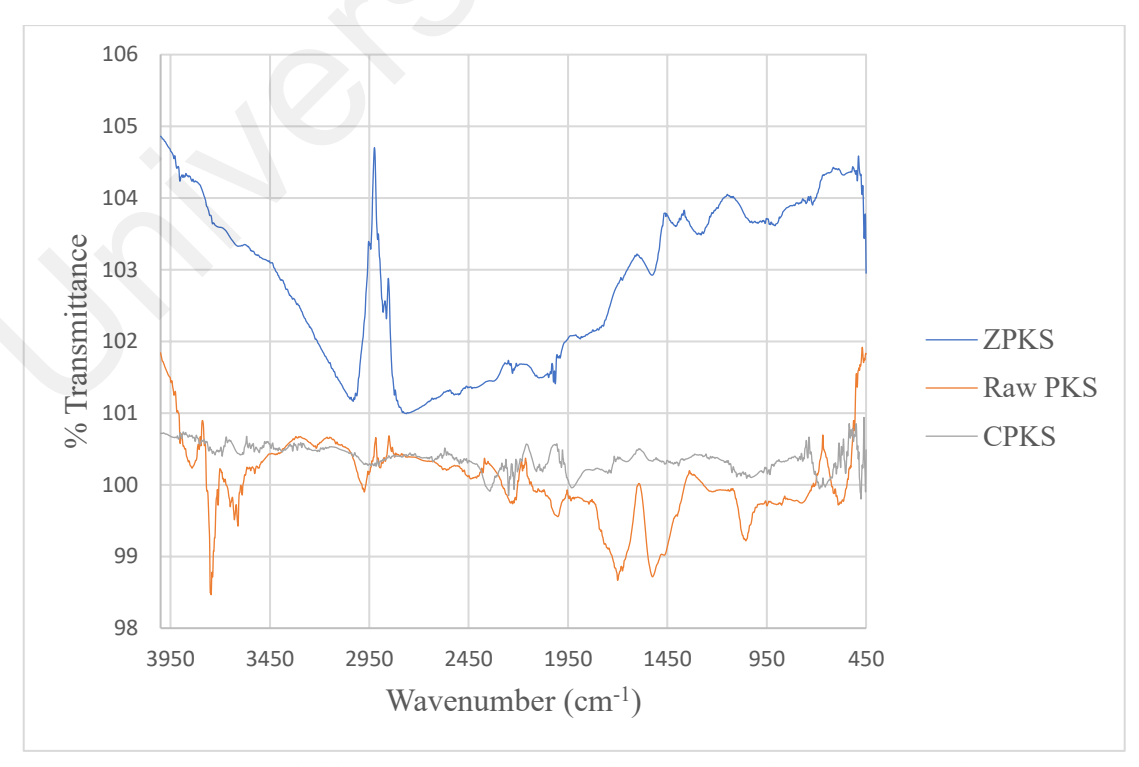


Figure 4.14: FTIR spectra of CPKS, ZPKS and raw PKS

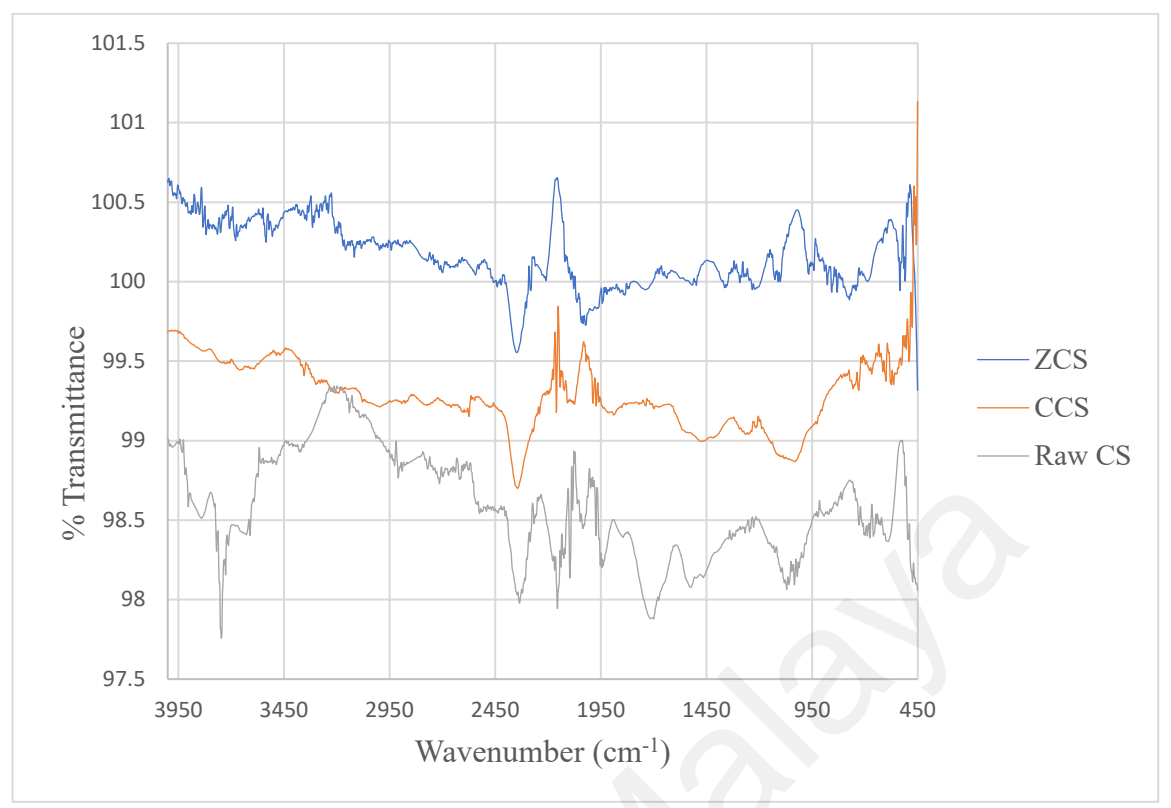


Figure 4.15: FTIR spectra of CS, ZCS and raw CS

4.8.5 Microwave activation (physical activation)

In the present study, microwave activated carbon is produced using microwave radiation as an additional physical activation after chemical activation. Microwave activated carbon is abbreviated as "M" after chemical activation. For example, MZCS means microwave zinc activated coconut shell and MZPKS is microwave zinc activated palm kernel shell.

Figures 4.16 to 4.21 show the comparison of peaks from the FTIR spectrum after chemical activation and microwave radiation. All signals depict that there are no significant changes when the carbonized sample has undergone radiation treatment. This finding occurs for all samples. From Section 2.3.3.2, it is known that microwave radiation causes inner pore formation from heating from the inner to the outer part of the sample. The reaction that occurs during the heating process is as reflected in Equation (2.12) where carbon acted with water inside the sample and causes the formation of carbon dioxide. Hence, no new functional group or bonding formed during microwave radiation.

Since no new functional group were formed, the FTIR spectra remains the same as spectra after chemical activation. Meanwhile, chemical activating agent causes the formation of new bonding. Therefore, formation of new bond can be seen as shown in Figures 4.16 to 4.21.

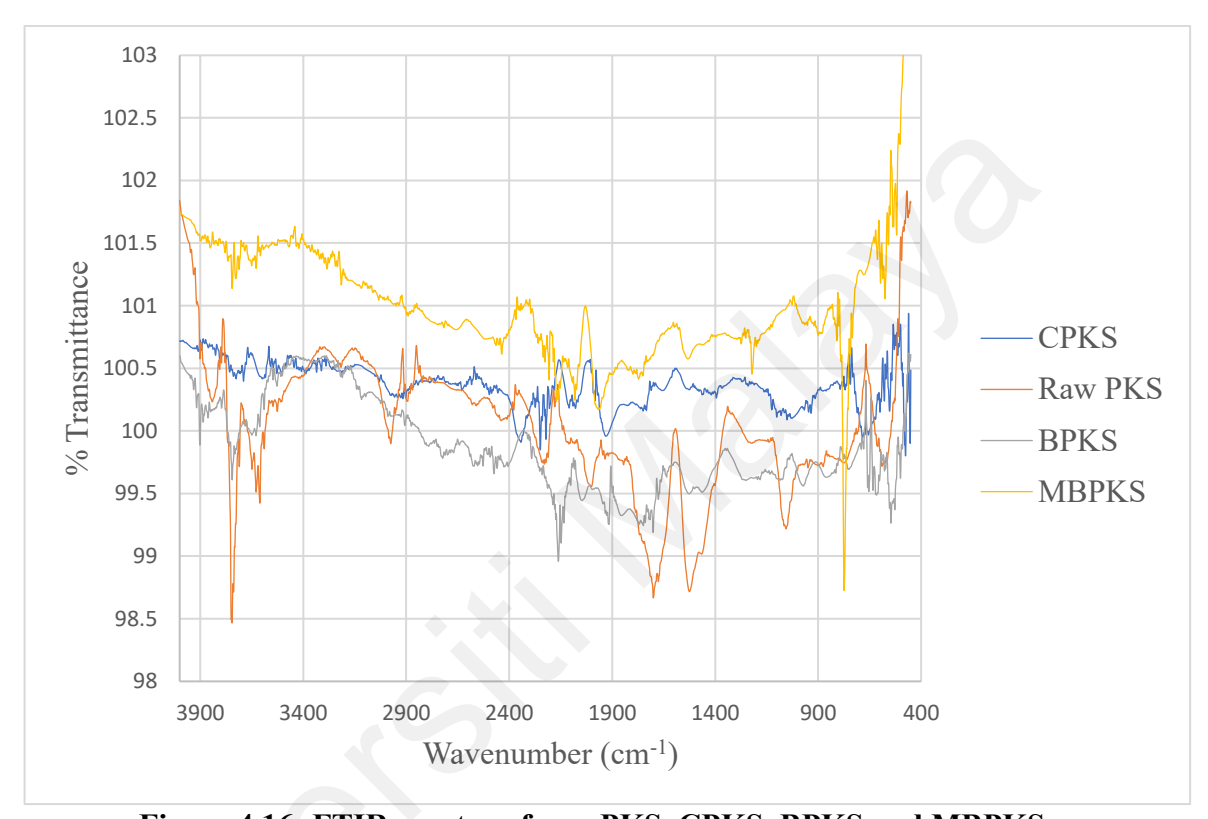


Figure 4.16: FTIR spectra of raw PKS, CPKS, BPKS and MBPKS

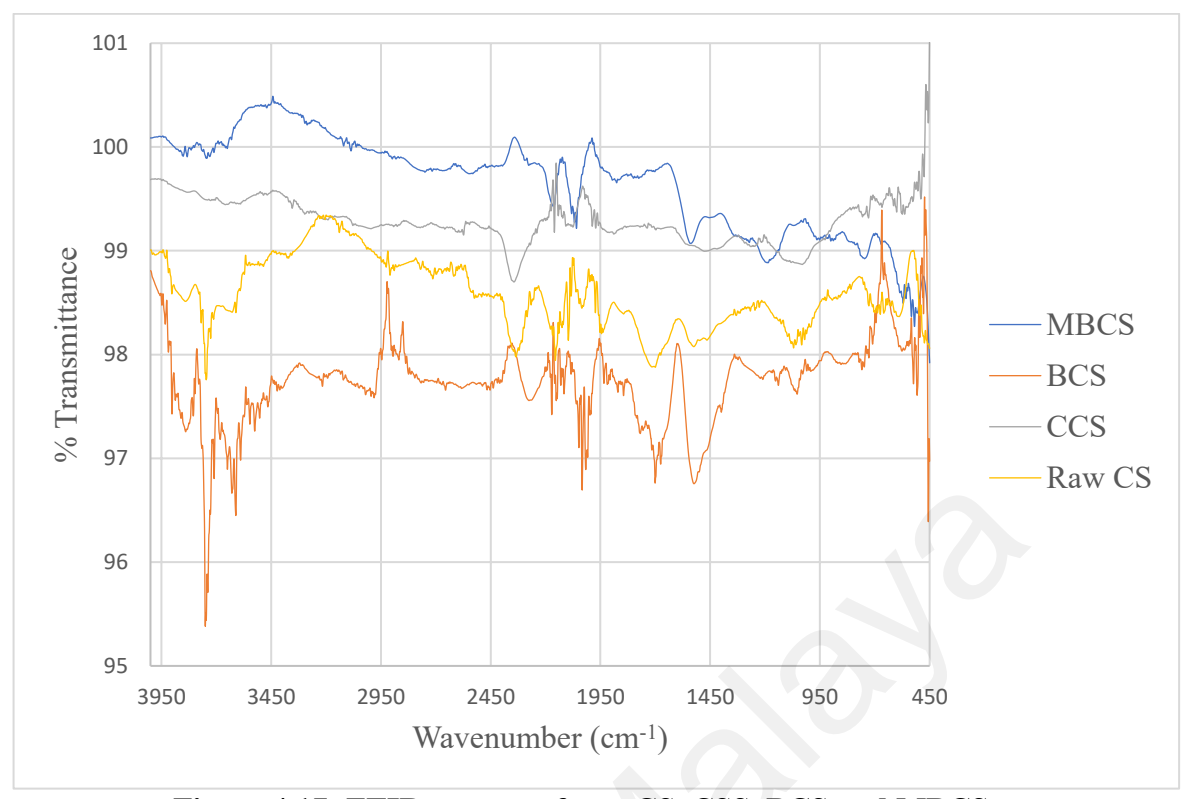


Figure 4.17: FTIR spectra of raw CS, CSS, BCS and MBCS



Figure 4.18: FTIR spectra of raw PKS, CPKS, APKS and MAPKS

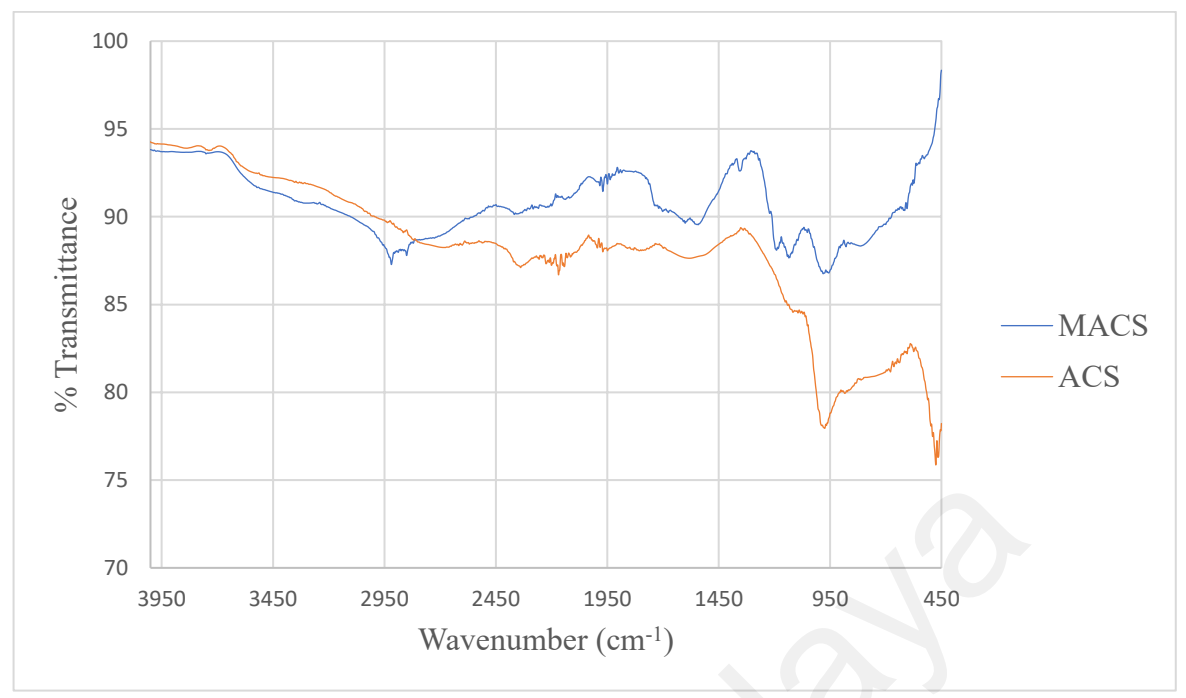


Figure 4.19: FTIR spectra of ACS and MACS

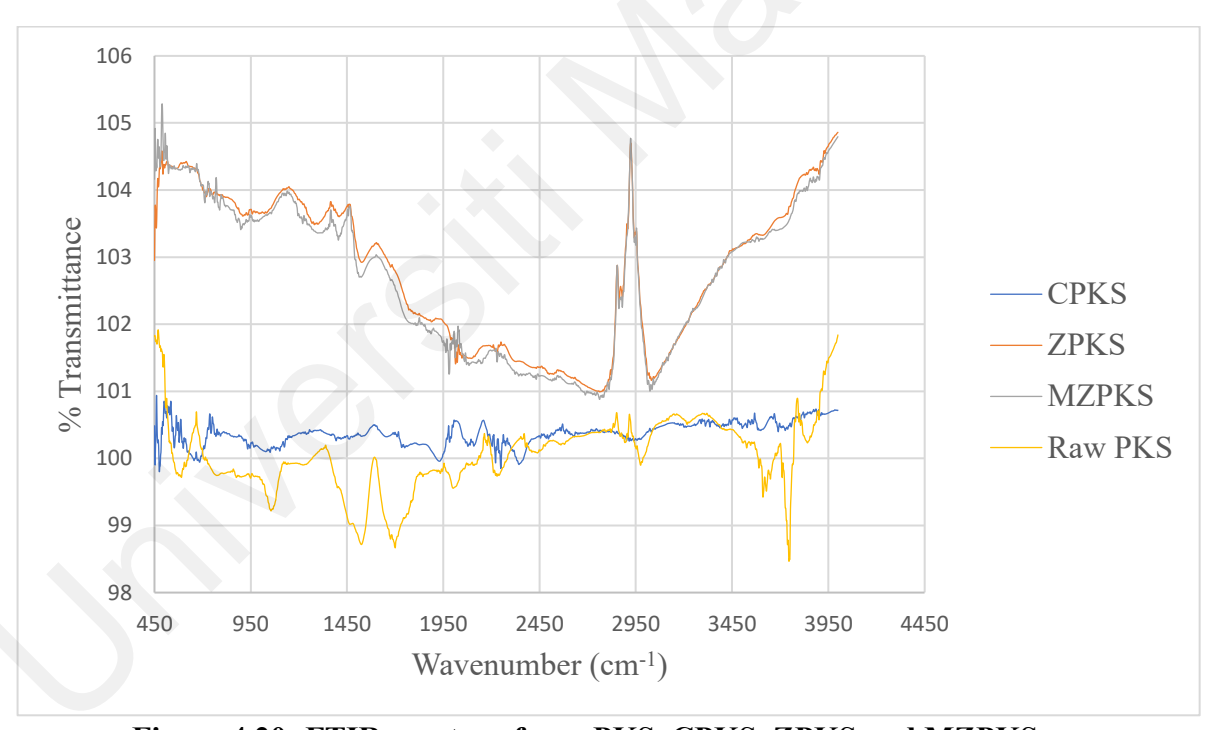


Figure 4.20: FTIR spectra of raw PKS, CPKS, ZPKS and MZPKS

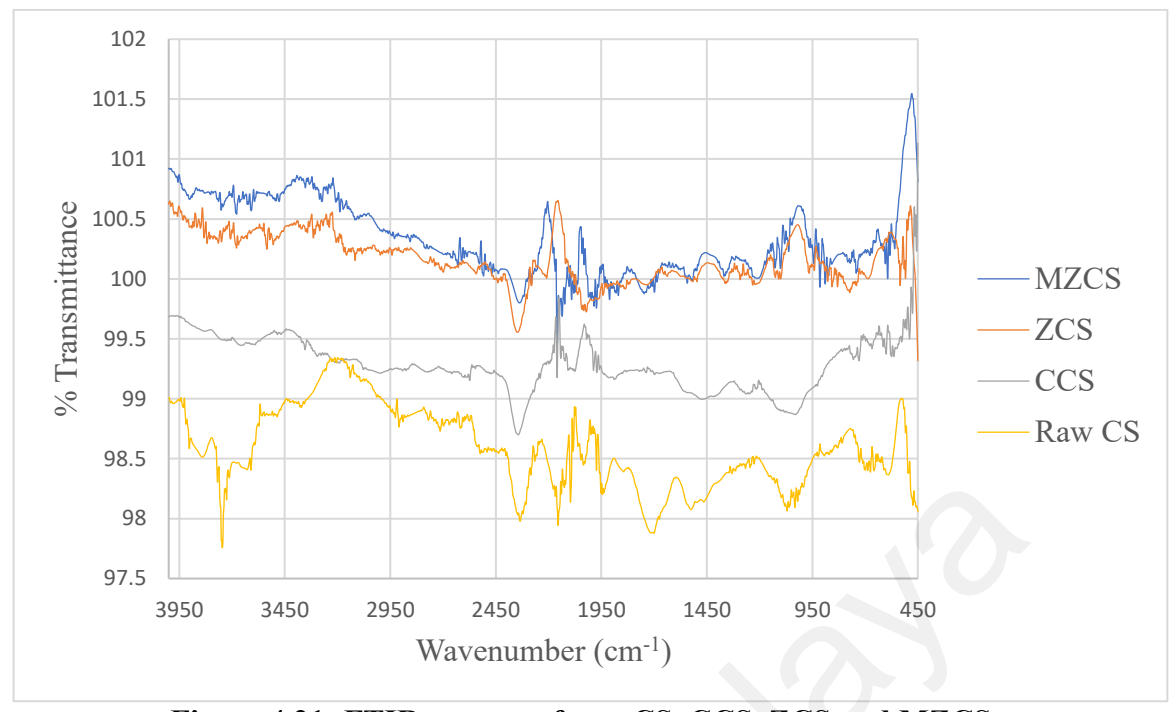


Figure 4.21: FTIR spectra of raw CS, CCS, ZCS and MZCS

4.9 The percentage yield of carbonization and activation

The percentage yield of the raw material carbonization process is tabulated in Table 4.5. It can be observed from the graph shown in Figure 4.22, the higher temperatures will result in a lower percentage yield. Higher temperature results in rapid bond breaking and release of volatile materials. Hence, decreasing the percentage yield (Rahman *et al.*, 2012).

Table 4.5: Percentage yield after carbonization process

Temperature	Percentage yield (%)		
(°C)	CCS	CPKS	
400	35.17	49.98	
450	29.65	37.26	
500	26.77	34.45	
550	26.66	31.95	
600	24.87	28.73	
650	N/A	27.37	

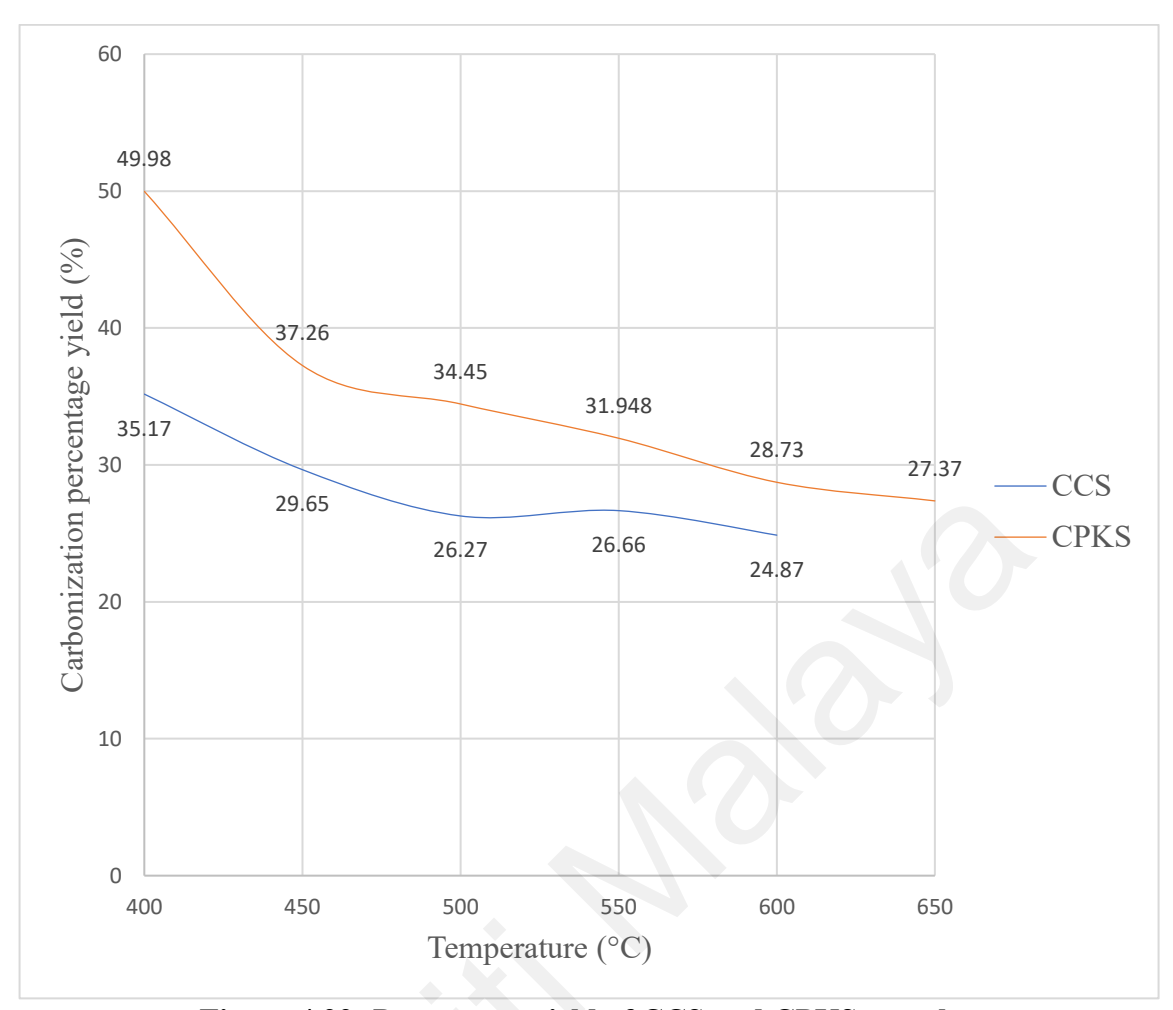


Figure 4.22: Percentage yield of CCS and CPKS samples

Carbonization of CS took place until temperature reached 600°C and no observable changes thereafter until 650°C since, at the former temperature, the carbon skeletal had successfully been formed as proved by FTIR results shown in Figure 4.6, Section 4.7.1. Therefore, there is no need to continue the carbonization process at a higher temperature than 600°C. Meanwhile for PKS, at temperature 650°C, FTIR results show loss of most peaks compared to raw PKS. Hence, the optimal temperature for carbonization for PKS carbonization is determined at 650°C in the present study. No further study on carbonization percentage yield was done beyond its optimum temperature.

Meanwhile, Table 4.6 shows the percentage yield after the activation process. Generally, PKS have a higher percentage yield compared to CS. Due to presence of lignin as the main component of PKS, the rigid structure makes the biomass hard and resistant

to reaction as discussed in Section 4.4. Hence, the percentage yield of PKS is slightly higher compared to CS.

Table 4.6: Percentage yield of activation process

Percentage yield (%)	MA	MB	MZ
PKS	17.6%	27.3%	25.0%
CS	15.5%	20.5%	21.4%

*MA = microwave acid activated, MB = microwave base activated, MZ = microwave zinc chloride activated

In this study, H₃PO₄ activation results in the lowest yield for both biomasses. Due to the aggressive reaction of PKS and CS with H₃PO₄ as mentioned in Section 4.8.3. This may contribute to the low percentage yield of acid-activated AC. To compare with other studies, the percentage yield of AC production at 22 – 25% is considered common as recorded by Yang *et al.* (2010), Ghazali and Abdullah (2012), Zailani *et al.* (2013) and Hidayu & Muda (2016).

4.10 BET value of activated carbon

Table 4.7 presents the surface area, pore volume and pore diameter of prepared AC in the present study. For both starting materials, the highest surface area of AC is obtained through ZnCl₂ activation. Followed by activation by KOH and activation using H₃PO₄.

By comparing all AC prepared in this study, MZCS registered the highest surface area and pore volume. The pore diameter, however, is significantly smaller than that of MZPKS. MZPKS has a high surface area of 367.12 m²/g indicating that ZnCl₂ used as an activating agent produces AC with a high surface area.

KOH activation shows some interesting results for both starting materials. KOH activation on PKS creates a high surface area of 348.19 m²/g, whereas CS activation on

the same activating agent generates a substantially lower surface area (77.45 m²/g). Although the surface area value of both PKS and CS is quite different, the pore diameter is almost same (2.2 nm). This finding is also in contrast to the FTIR analysis in Section 4.8.2. The FTIR results showed that the peaks between the two initial materials are indistinguishable. This indicates that the same reaction might occur between the two biomasses.

Some AC surfaces form a hallow AC when looking at the FESEM images of MBPKS and MBCS (Figures 4.25 and 4.26). Since MBCS pores form very quickly, the current pores perforate through the structure of biomass. The surface area is therefore small, but the pore diameter remains the same. The pore volume of MBCS (0.04 m³/g) is also quite low since the volume cannot be measured due to the hallow structure of AC. Although the same base activation is imposed on the biomass, the MBPKS (348.19 m²/g) still recorded a high surface area. This is related to the lignin content of the MBPKS itself. The lignin structure itself is rigid as discussed in Section 4.4. The activation process that occurs between carbonized biomass and KOH is described in Section 2.3.3.1 and equations (2.5) to (2.11). Due to the stiffness of the lignin system, KOH attacks are more vulnerable to CS rather than PKS. This is because of high hemicellulose and cellulose content in CS.

For both biomasses, acid activation reported the worst BET value in all activation methods. FESEM images shown in Figures 4.27 and 4.28 reveal that, the pores have somehow shaped into tunnels, penetrating the entire biomass from the upper surface. Physically, there are a lot of pores formed throughout the surface. Nevertheless, the pores continue to form which breaks the structure of AC due to the aggressive nature of acid activation. Hence, the surface area of acid prepared AC is small because of the formation of the pore perforated through the biomass. Ilomuanya *et al.* (2016) and Tounsadi *et al.* (2016) have reported that acid activation will lead to the formation of mesopores. By

introducing physical activation after acid activation in preparation of AC will cause micropores to become mesopores and with radiation treatment, the pores experience rapid expansion that causes wall disruption (Kumar *et al.*, 2020). Therefore, acid activation followed by radiation decreases the surface area of the AC formed.

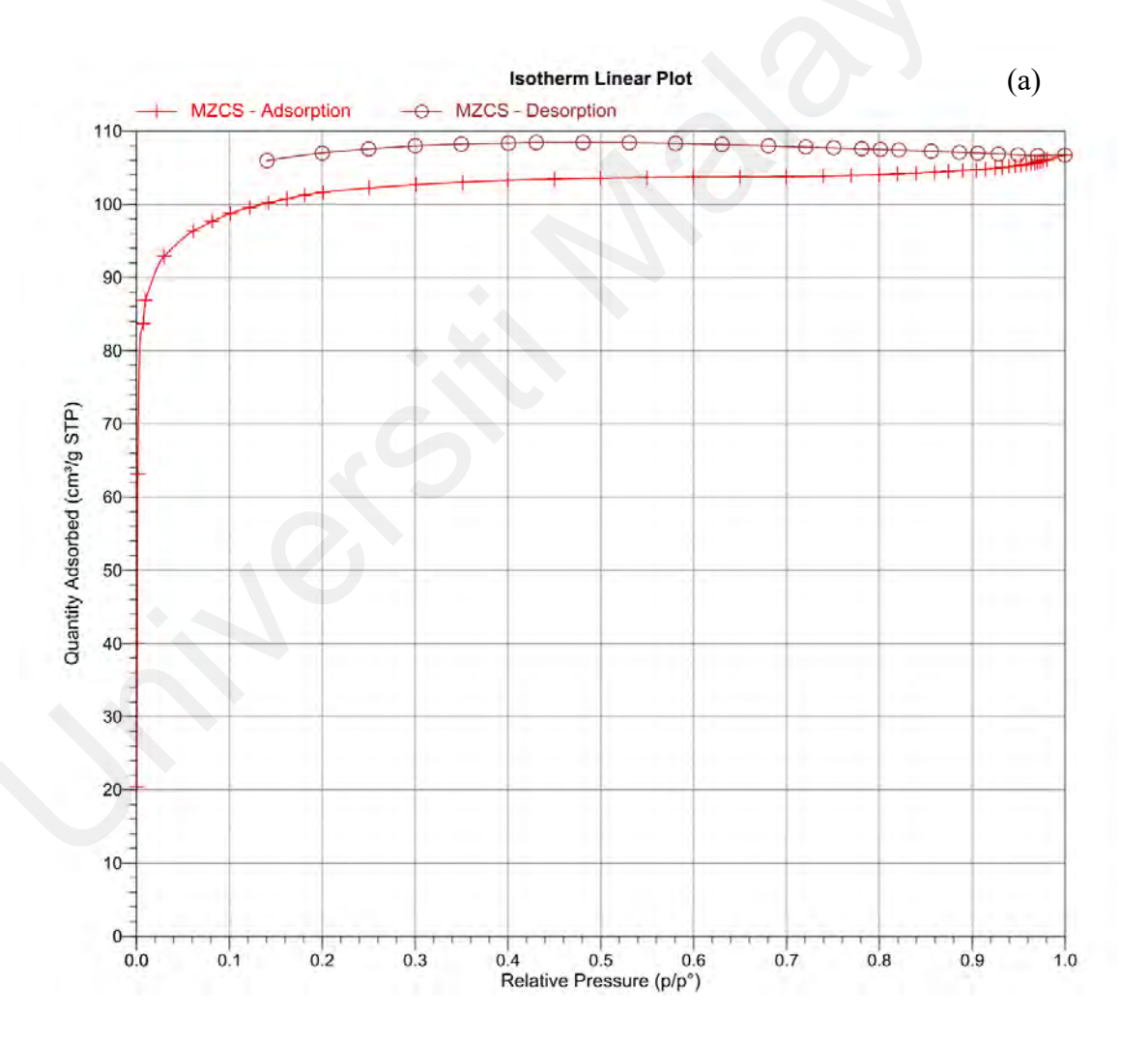
It is noted that the BET values obtained in this study are within $367.12 \text{ m}^2/\text{g}$ to $391.26 \text{ m}^2/\text{g}$ which are considered on the lower end. This is due to the size of AC used in this study. A smaller AC particles size will ensure that a higher surface area is obtained. Nevertheless, in this work (as mentioned in Section 3.15), the size of AC particles is preferred between 0.15 - 0.5 mm which is not too small to make it more feasible to trap soot particles during combustion. Therefore, the larger particle size of AC prepared is preferred in this study. Consequently, the BET surface area is low. In terms of pore diameter and width, all of the AC prepared shows mesopores properties.

As defined by IUPAC, adsorption isotherm that involves physisorption can be classified into six types measured by the graph pattern of quantity adsorb against relative pressure. As shown in Figure 4.23 (a) and (b), both MZCS and MZPKS has shown Type I isotherm, which is in line with activated carbon's properties. In Type I isotherms, single monolayer of adsorbate forms on the adsorbent surface. The filling of the pores marks the completion of a molecular monolayer. In addition, the hysteresis loop shape shows Type H4 hysteresis that indicates slip type micropores.

Table 4.7: BET value of prepared AC

Details / AC	MACS	MBCS	MZCS	MAPKS	MBPKS	MZPKS
BET surface area (m²/g)	3.93	77.45	391.26	2.88	348.19	367.12
Pore volume (m ³ /g)	0.001	0.04	0.17	0.0002	0.12	0.16
Pore diameter (nm)	1.50	2.20	1.69	0.38	0.38	1.72
Pore width (nm)	2.93	0.07	4.03	0.03	3.89	6.94

^{*}MACS = microwave acid activated coconut shell, MBCS = microwave base activated coconut shell, MZCS = microwave metal salt activated coconut shell, MAPKS = microwave acid activated palm kernel shell, MBPKS = microwave base activated palm kernel shell, MZPKS = microwave metal salt activated palm kernel shell



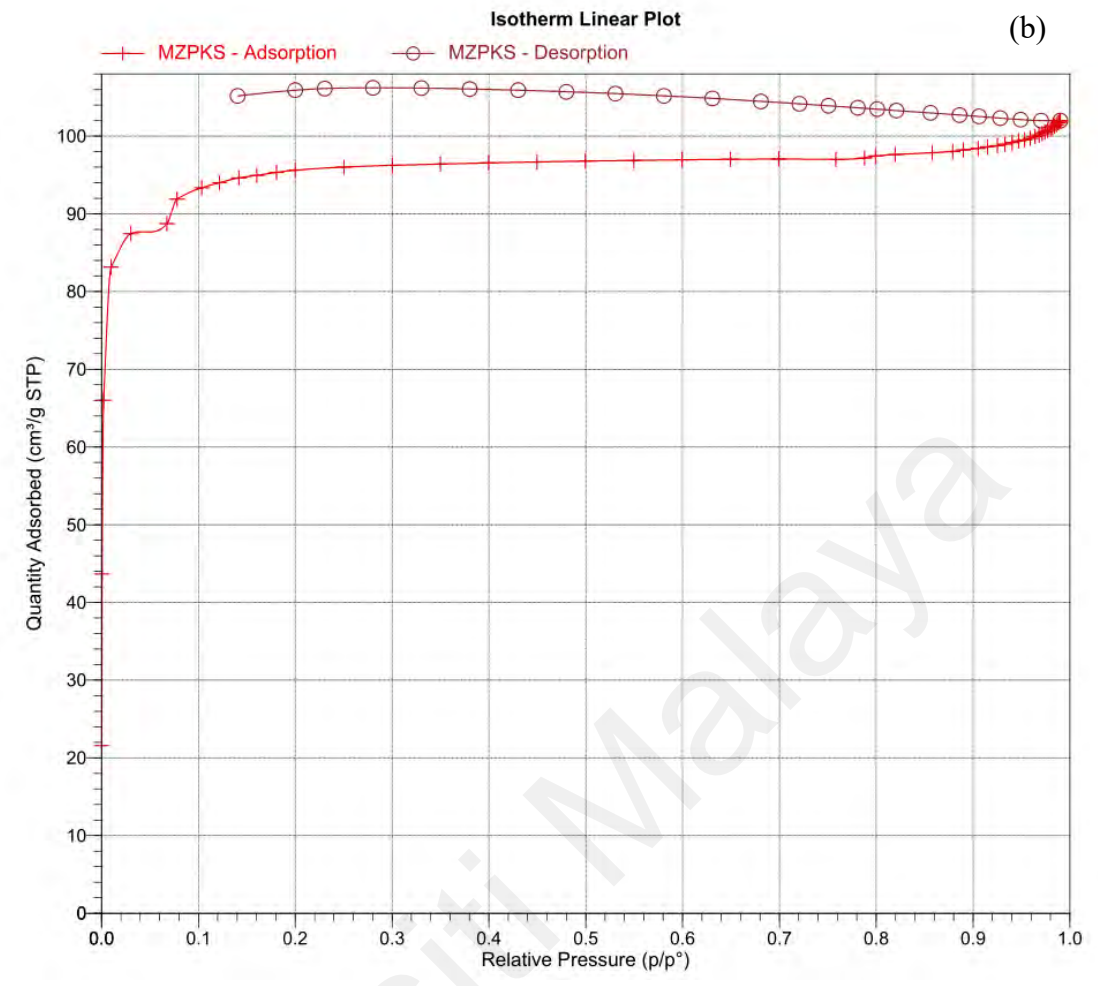


Figure 4.23: Isotherm linear plot of MZCS (a) and MZPKS (b)

4.11 Boehm titration of activated carbon

Boehm titration was conducted to study the surface functional group of AC. Anubriya *et al.* (2020) mentioned that identification of the surface functional group of AC surface provides information on the cation exchange capacity. This contributed to the understanding of the adsorption mechanism. The surface functional group of CS obtained in this study and other researches with similar preparation methods is shown in Table 4.8. However, there were no recorded surface functional groups for PKS.

From Table 4.8, the surface of both AC is mainly acidic. Guo & Rockstraw (2007) reported that the acidic value increases when biomass is subjected to high heating conditions. Since this study practices low-temperature carbonization and activation,

therefore, the total acid value is lower than the results obtained in other studies. The carboxyl content of MZCS is much higher than MZPKS. By referring to Figure 2.5 (structure of hemicellulose, the main component of CS), carboxyl moiety can be seen hence contributing to the high carboxyl content in MZCS.

Table 4.8: Different functional groups on the surface of AC

Surface functional group (mmol g ⁻¹) / AC sample	Carboxyl	Lactones	Phenols	Total acid	Base
MZPKS (Present study)	0.22	0.2964	0.2286	0.747	0.4977
MZCS (Present study)	0.3996	0.1998	0.2286	0.828	0.5544
CS (Cazetta et al., 2011)	0.75	0	1.00	1.75	0.75
CS (Liang et al., 2020)	0.99	0.45	0.79	2.23	0.58

4.12 Morphology of activated carbon

The physical surface morphology of each sample was analyzed using FESEM for both carbonized and activated samples. From Figures 4.24 and 4.25, the carbon skeletal formation can be seen for both CPKS and CCS. The fragmentation and degradation of biopolymers form some pores and the simplest form of carbon body as discussed in Section 4.7. The optimized temperature allows the carbon skeleton to shape. Additional pore will be formed during the activation process, allowing for adsorption.

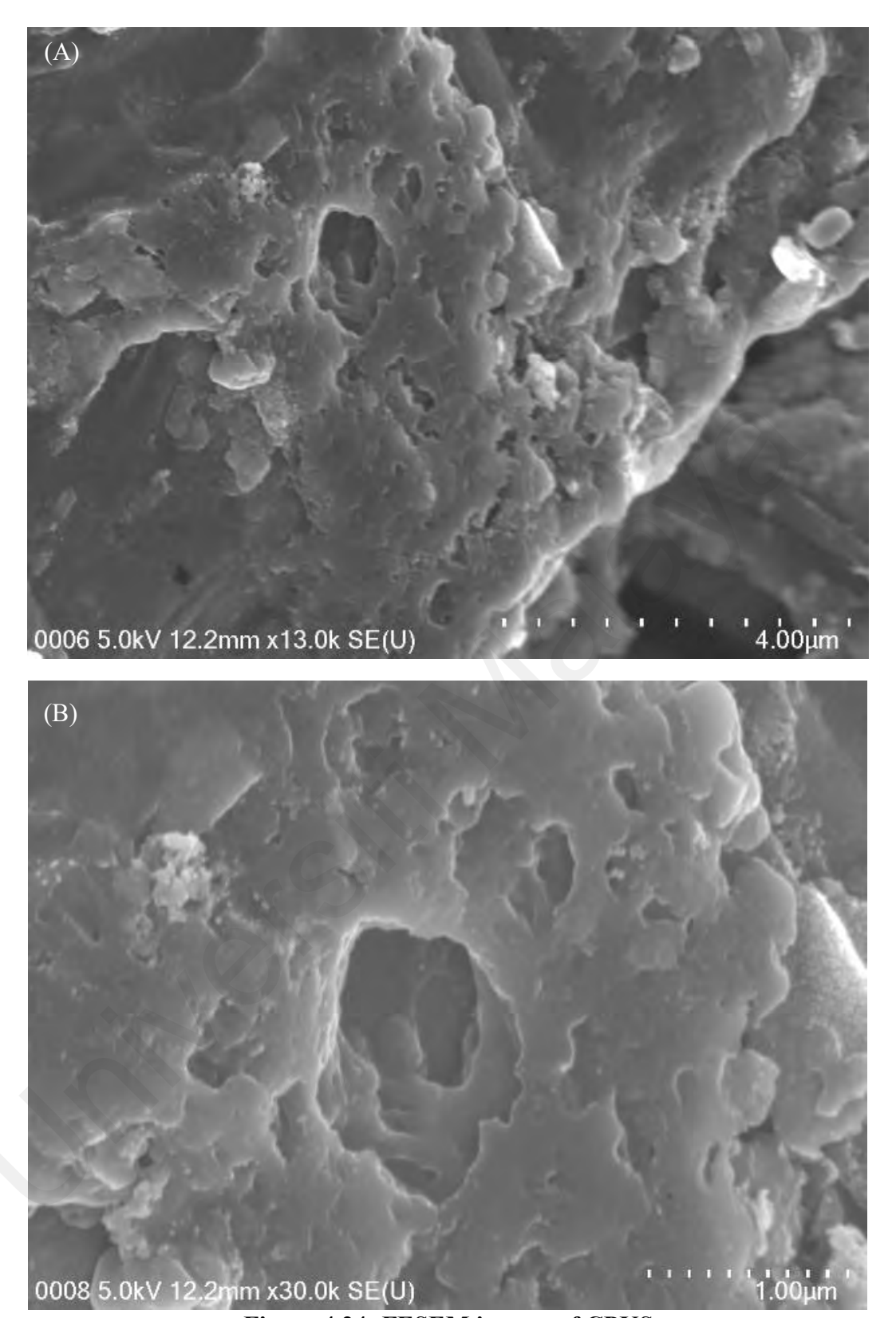


Figure 4.24: FESEM images of CPKS

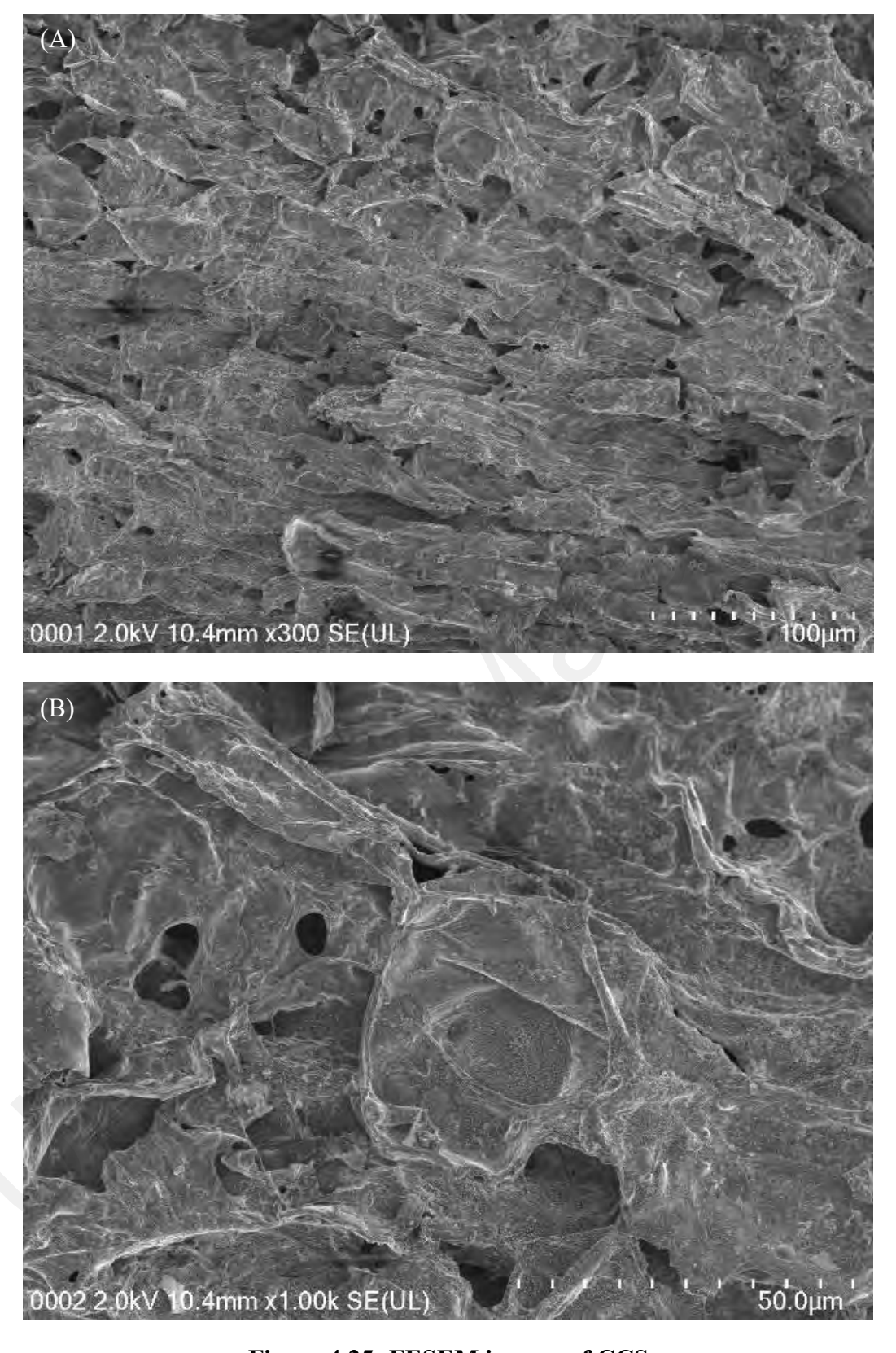
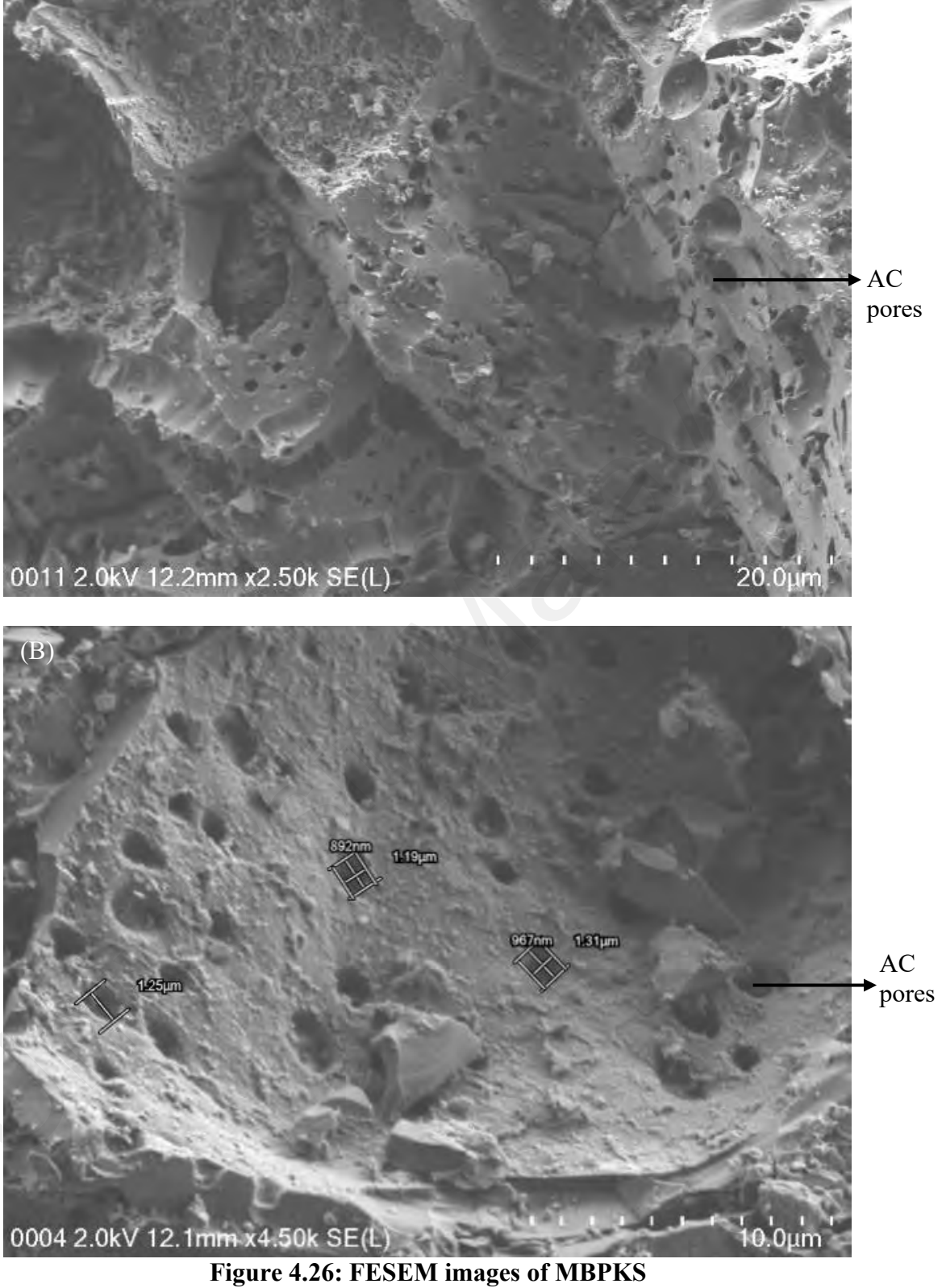
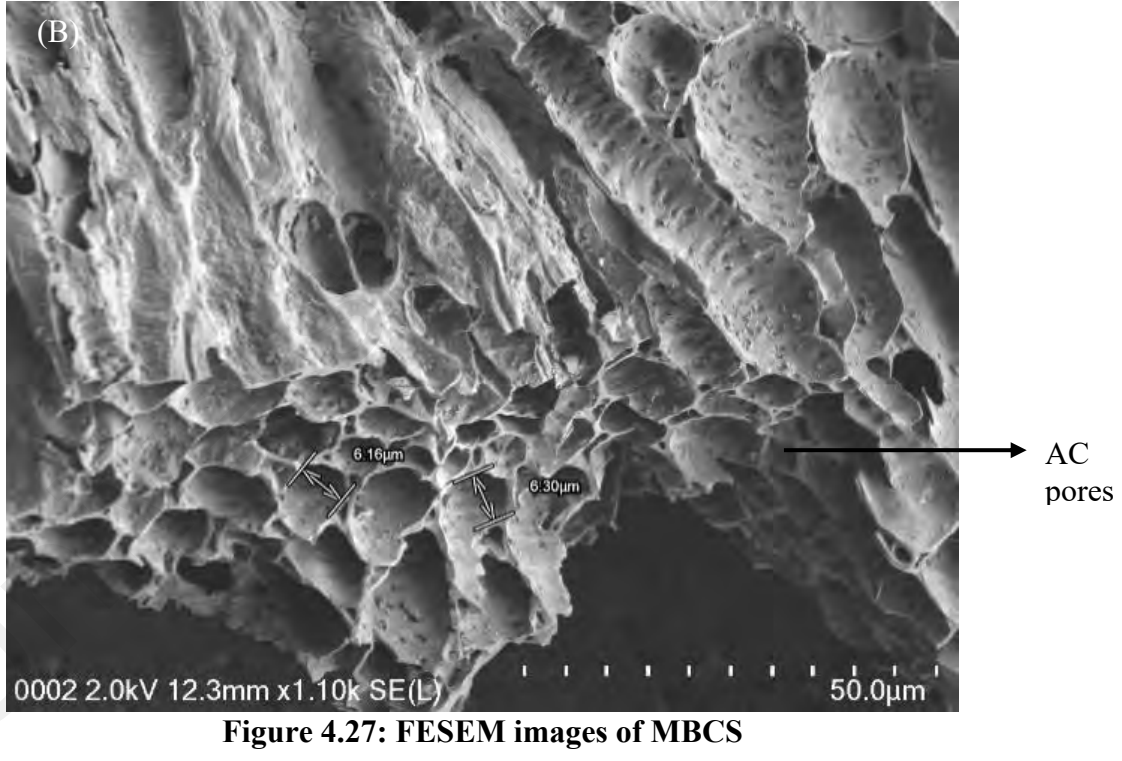


Figure 4.25: FESEM images of CCS

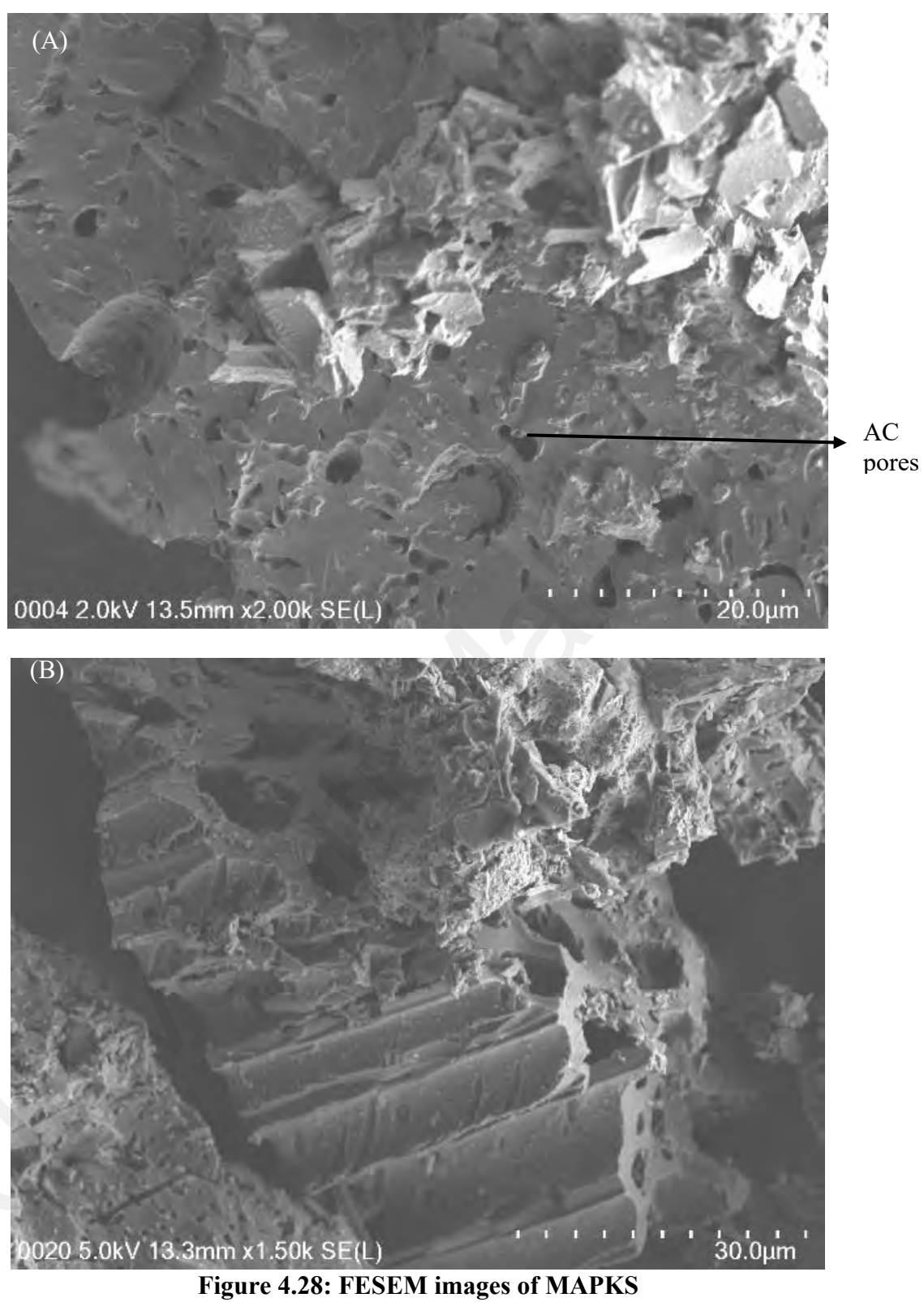
Figures 4.24 and 4.25 shows the FESEM images after AC was activated using base and microwave. Comparing Figures 4.26 and 4.27, it can be seen that pores are formed on the surface of biomass after activation has been successfully done. MBPKS (Figure 4.26 exhibits more pores on the surface meanwhile MBCS (Figure 4.27) shows the formation of hallow and damaged pore walls. Therefore, it is confirmed that MBCS recorded a lower BET value compared with MBPKS due to excessive reaction that destroys pores forming a hollow AC as explained in Section 4.10.







From the images of MAPKS and MACS in Figures 4.28 and 4.29, the wall disruption and the narrowing of pores that penetrate through the whole biomass can be seen. Hollowing of biomass structure occurs in both acids activated biomass. This occurrence causes the AC activated with acid to have the lowest surface area compared to other activation as mentioned in Section 4.10.



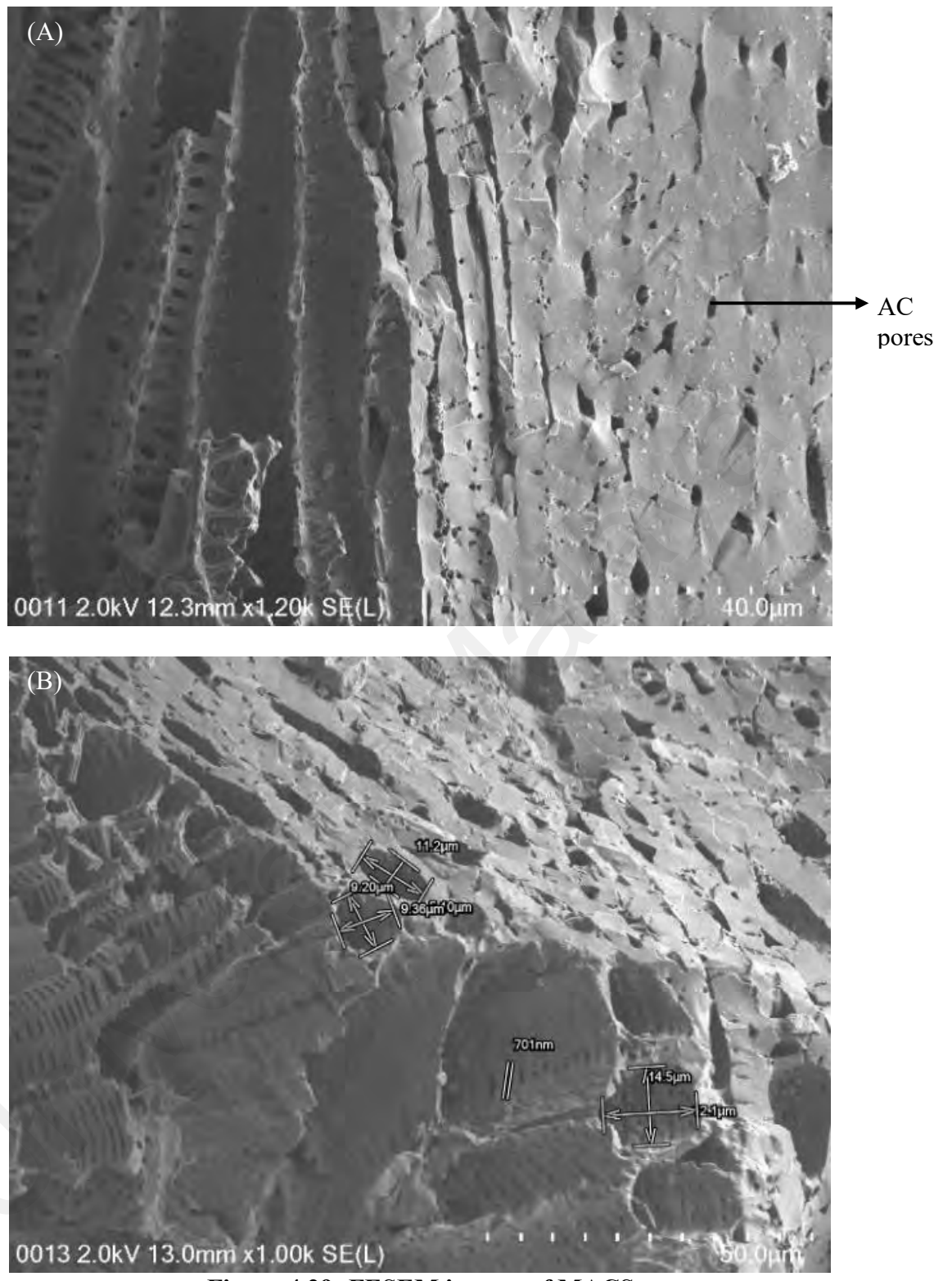
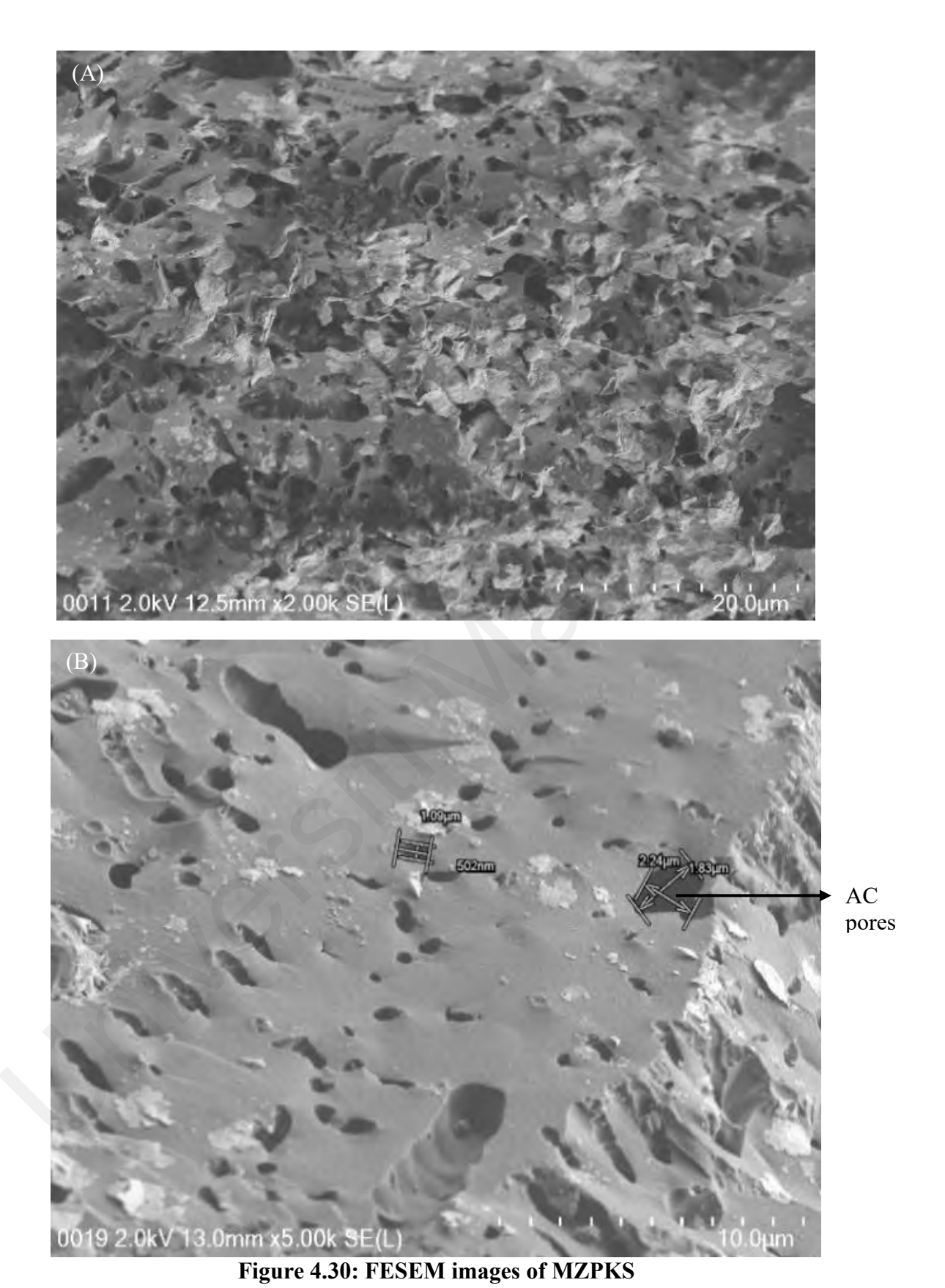


Figure 4.29: FESEM images of MACS

Meanwhile, in metal salt activated carbon shown in Figures 4.30 and 4.31, pores formation is throughout the surface of AC. MZCS (Figure 4.31) has shown more heavily distributed pores throughout the surface of AC. Hence, the MZCS BET value at 391.26 m²/g is the largest among all AC. The hollowing of biomass that can be seen in activation with MB and MA is also absent in the MZ activated AC. In addition, aggression and disruption of pore walls are also absent on the surface.



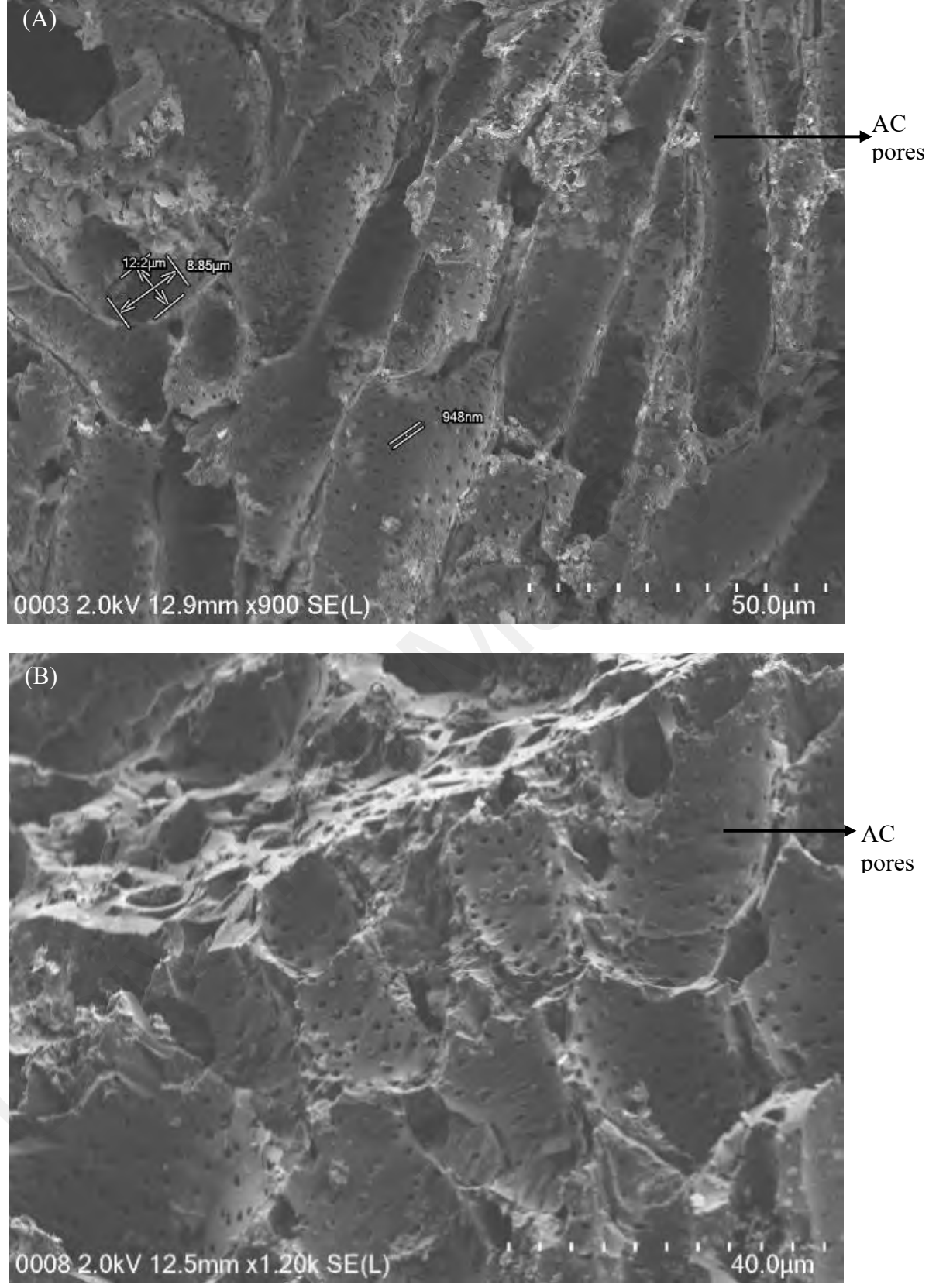


Figure 4.31: FESEM images of MZCS

4.13 Application of activated carbon on the smoke muffler

The AC prepared in this study aims to provide a suitable adsorbent for soot particles adsorption. Factors determining the most suitable AC to be applied include the highest BET surface area value, high percentage yield and pore size that suits the size of soot. Based on those considerations, MZPKS and MZCS are most promising to be applied in the adsorption of soot particles. Both MZPKS and MZCS have high BET surface area at 367.12 and 391.26 m²/g respectively. As mentioned in Section 2.1, studies conducted by Posfai *et al.* (2003) and Phairuang *et al.* (2019) reported that soot emitted from combustion is smaller than 10 μm. With this knowledge, the AC prepared for soot particle adsorption has to be in the size range of 10 μm to less than 1 μm. From the FESEM images (Figure 4.30) the pores opening of MZPKS is between 2 μm to 502 nm. Meanwhile, for MZCS (Figure 4.31) pore opening is 12.2 μm and the smallest pore opening is at 948 nm. Hence, MZPKS and MZCS are suitable for the application of AC as a soot adsorbent.

After the most suited AC has been identified, the application study of AC on the muffler was conducted. Based on the results tabulated in Table 4.9, in 30 minutes, 23.85±4.39 g of paddy straw can be completely burned. Hence, for 30 minutes of burning time, approximately 23 g of paddy straw will be completely burned.

Table 4.9: Study of paddy straw mass that can be combusted within 30 minutes

	Trial 1	Trial 2	Trial 3
Initial mass of paddy straw (g)	65.56	82.38	38.87
Mass of paddy straw unburnt (g)	44.86	53.5	16.96
Mass of paddy straw burnt (g)	20.77	28.88	21.91
The average mass of burnt paddy straw (g)	23.85		
Standard deviation		4.39	

Figures 4.32 and 4.33 show the surface morphology of AC after combustion has been carried out for 30 minutes. As can be seen, soot particles are adsorbed to the surface of both ACs. However, on the surface of MZPKS (Figure 4.21), the soot particles are not evenly adsorbed on the surface of AC. It is scattered throughout its surface and minimal soot particles are seen at the pores opening. Meanwhile, the adsorption of soot is scattered evenly on the surface as well as in the pored of MZCS (Figure 4.33) which indicates a good interaction between AC and soot particles. Hence, from the FESEM images, after the application process has been conducted, it can be concluded that MZCS offers better soot particles adsorption compared with MZPKS.

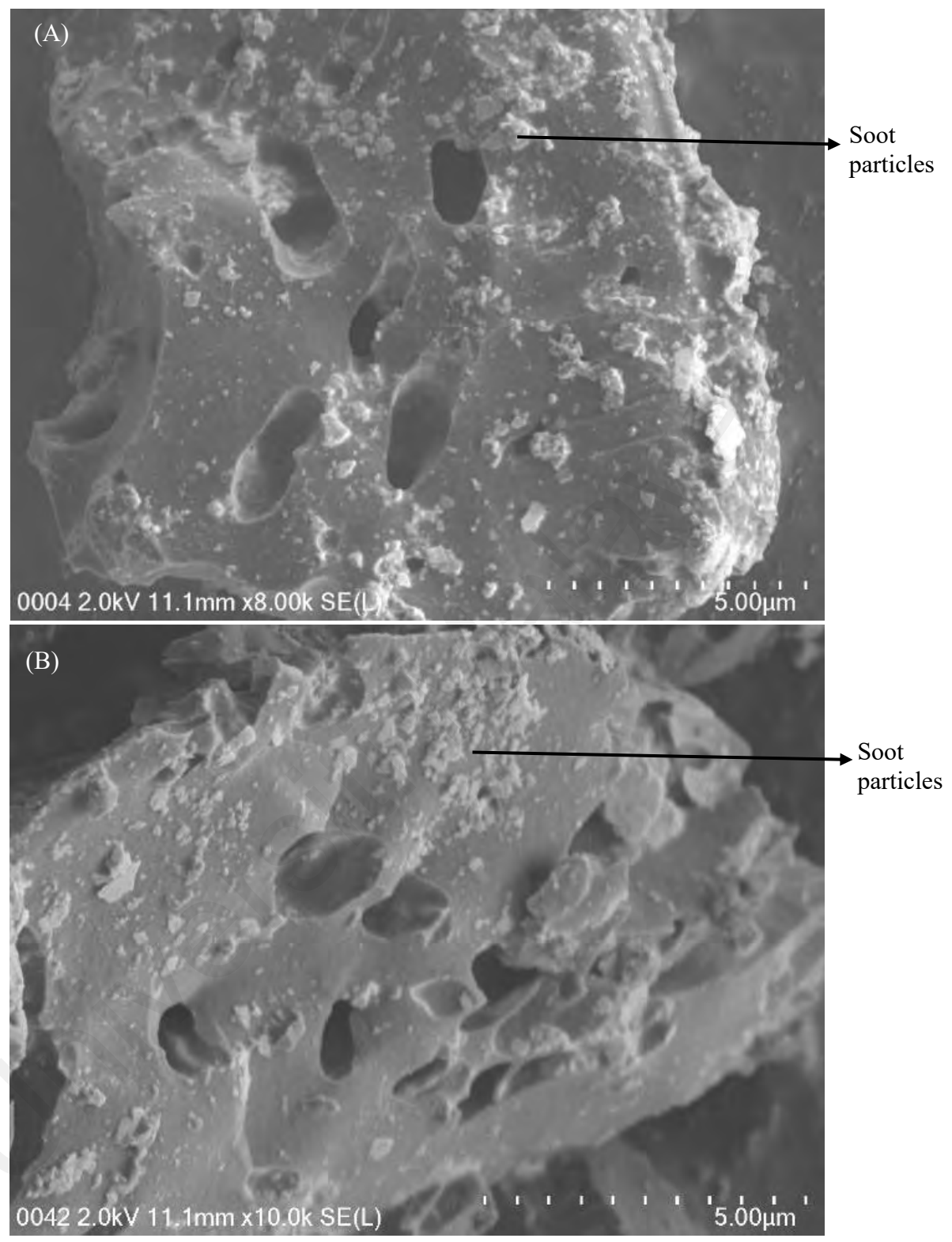


Figure 4.32: FESEM images of MZPKS after 30 minutes of combustion with paddy straw

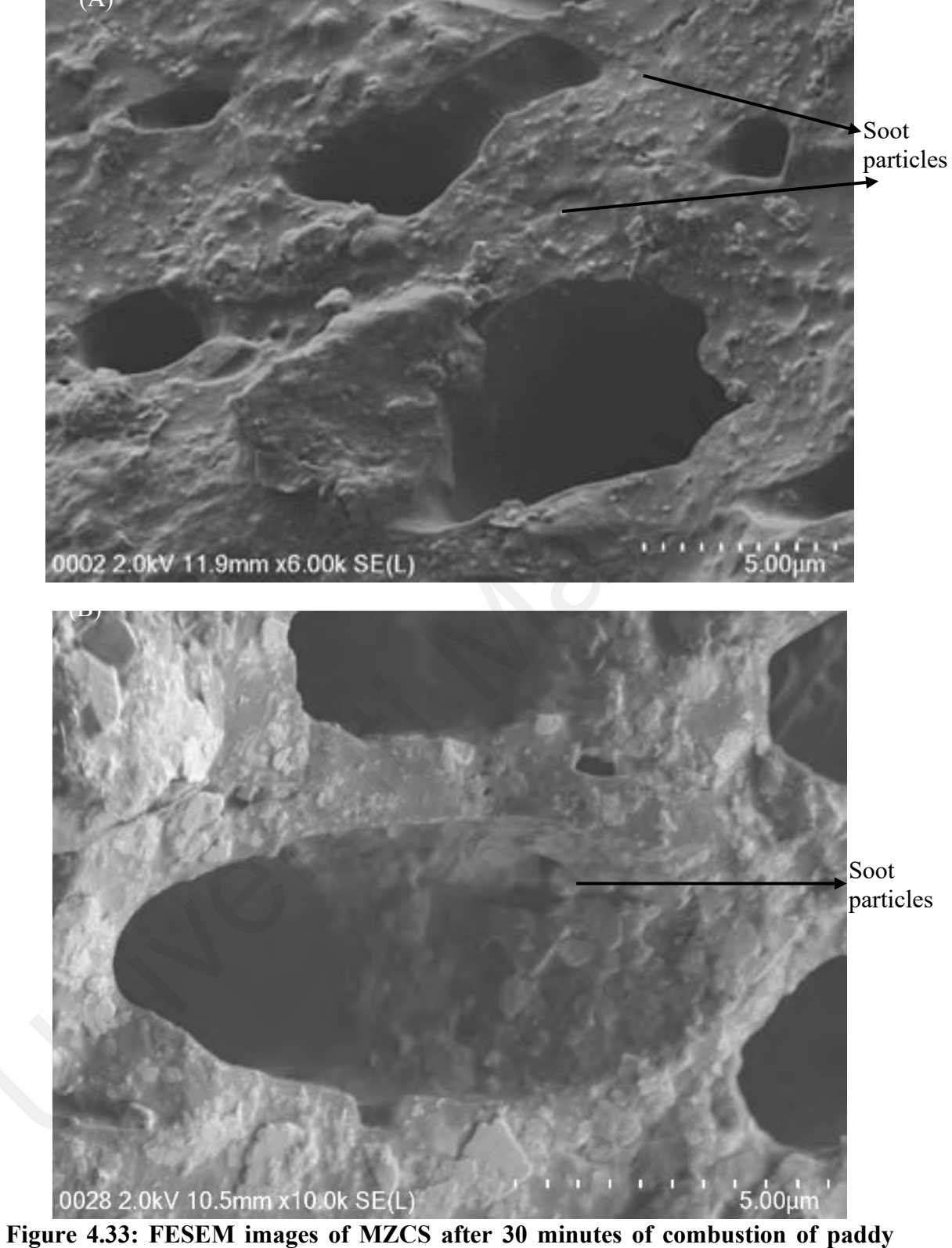


Figure 4.33: FESEM images of MZCS after 30 minutes of combustion of paddy straw

The combustion time was also set at 60 minutes whereby about 40 g of paddy straw was completely burnt. At this duration, the soot particles form clumps on the surface of MZCS. Soot particles are concentrated on the surface (Figure 4.34). Clumps of soot particles formed throughout the surface of MZCS that the original MZCS surface structure was not visible as shown on the FESEM images. This shows that an increase in combustion time and paddy straw mass decreases the adsorption capability. Therefore, the efficiency of produced MZCS is maximum when 0.1 g of AC is used to burn approximately 23 g of paddy straw.

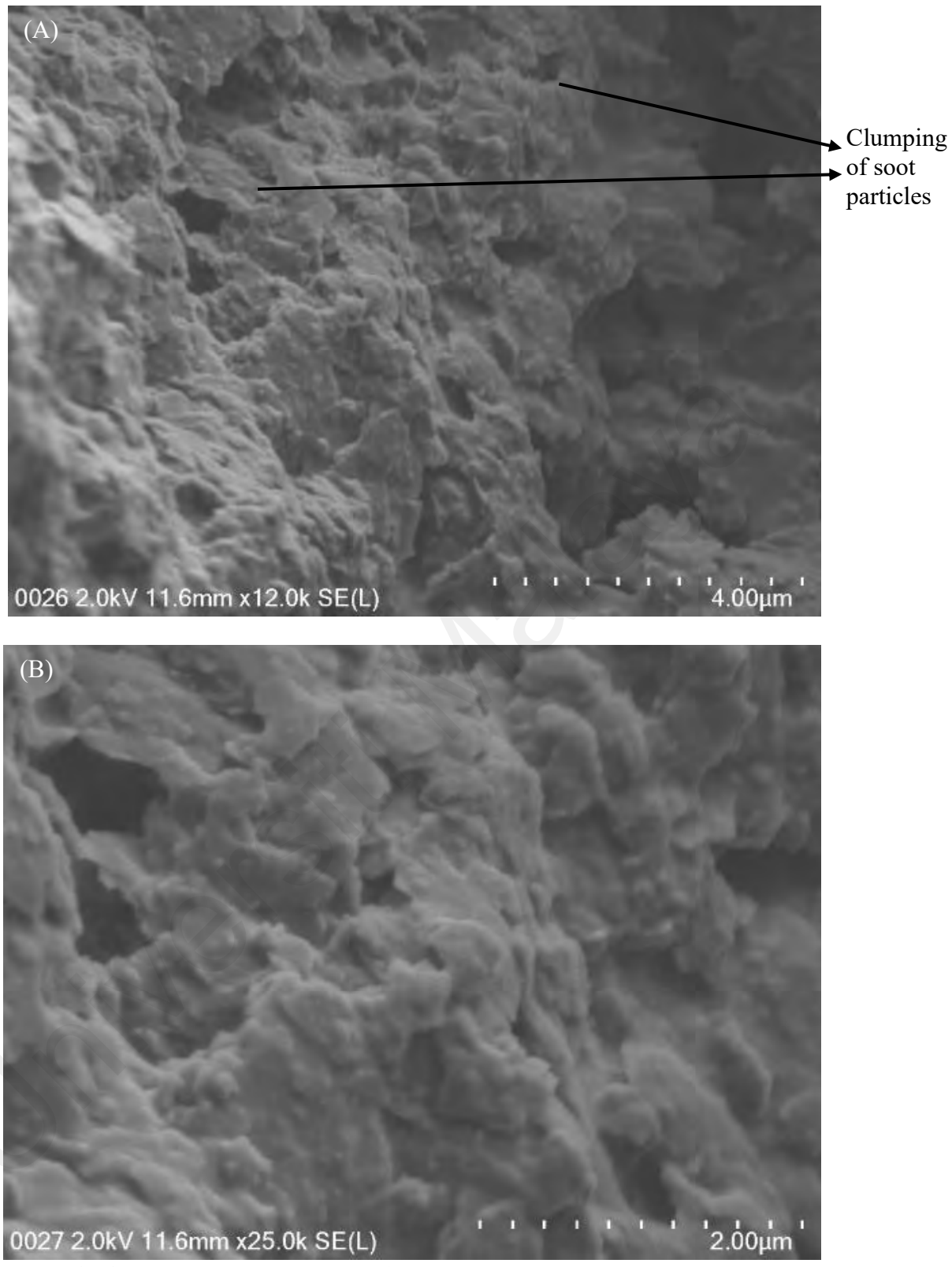


Figure 4.34: FESEM images of MZCS surface after 60 minutes of combustion

Further investigation was conducted to demonstrate the importance of pores openings on AC prepared in the present study by a comparative study using filter paper. Figure 4.34 shows an unused filter paper. The surface of the filter paper is fibrous and clean. After the filter paper was subjected to smoke from the same combustion process as AC, some soot particles can be seen on the surface (Figure 4.36). However, the adsorption of smoke particles on the filter paper surface is very minimal as the filter paper surface does not contain any active sites. This simple experiment has further shown that AC prepared in the present study fits its purpose as an adsorbent.

Since the study of soot particle adsorption of AC surface is new, there is no report on the adsorption type on its surface. As discussed in Section 2.4, the accumulation of adsorbate on the AC surface indicates physical adsorption. Through examination of the FESEM images, it is suggested that the adsorption of soot particles on AC is homogenous physisorption. Additionally, instantaneous adsorption after combustion also suggested physical adsorption. As mentioned in Section 2.1, biomass burning resulted in aerosols with ions such as H⁺ and HCOO⁻. Meanwhile, the AC surface from Boehm titration shows the presence of carboxyl, lactones and phenols that contains oxygen and hydrogen molecules (Table 4.8). Due to these unique components, electrostatic interactions between the ions can also occur as depicted in Figure 2.13. Hence, it can be concluded that the soot particles adsorption on the AC surface experiences physisorption adoptions as hypothesized in Section 2.4.

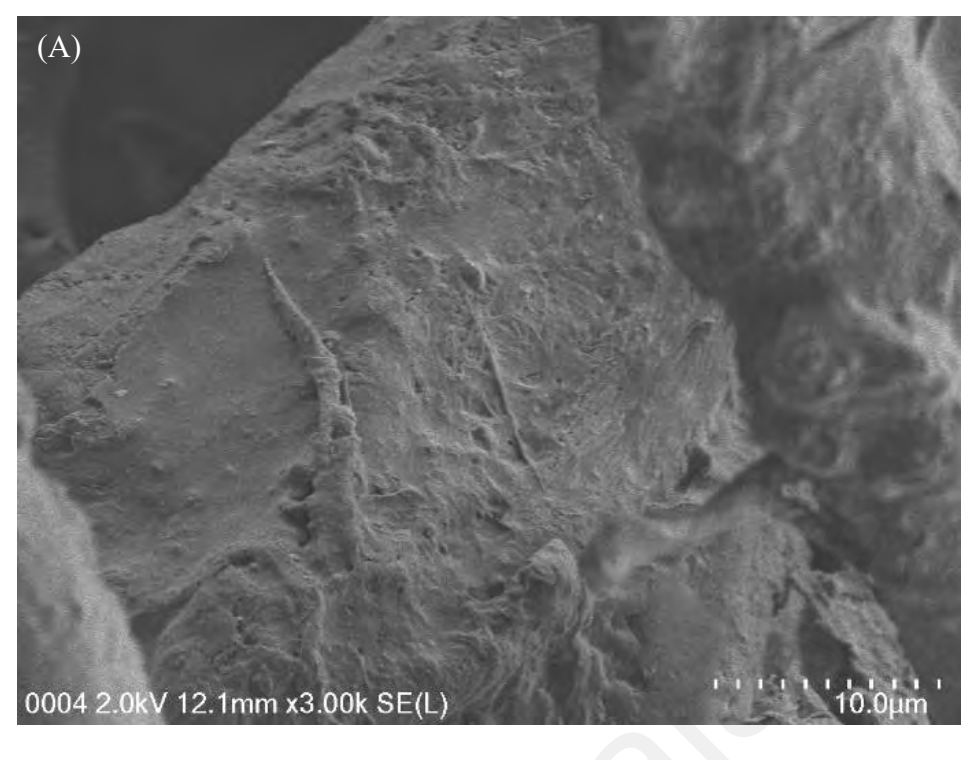
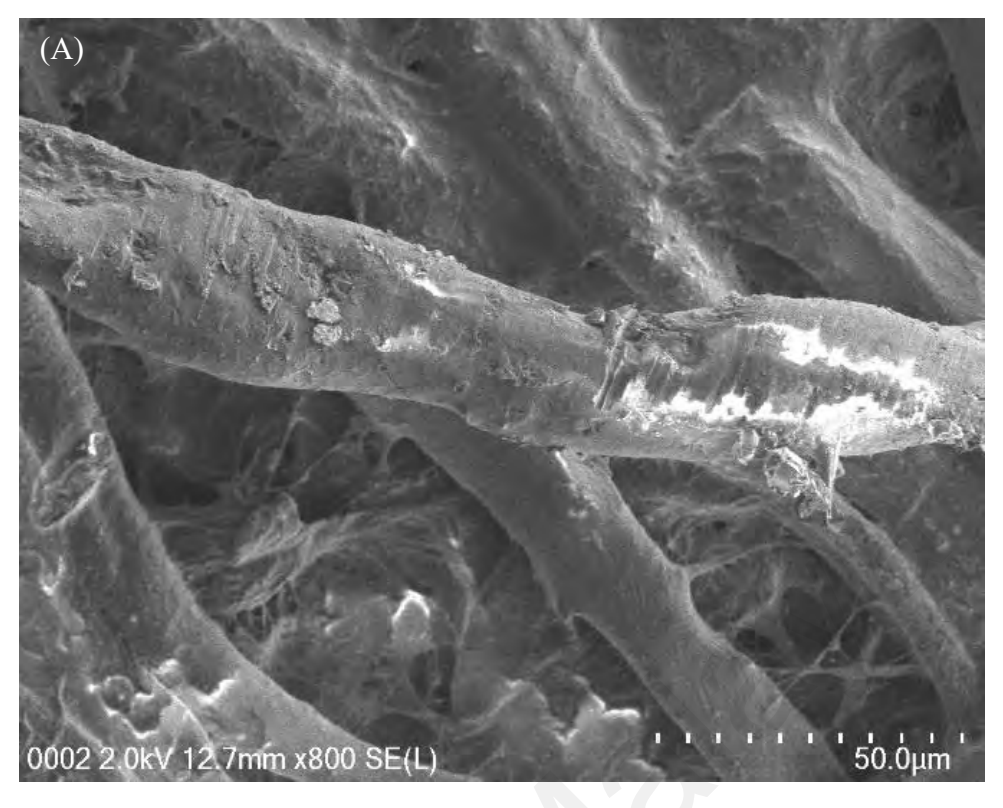




Figure 4.35: FESEM images of blank filter paper before combustion with paddy straw



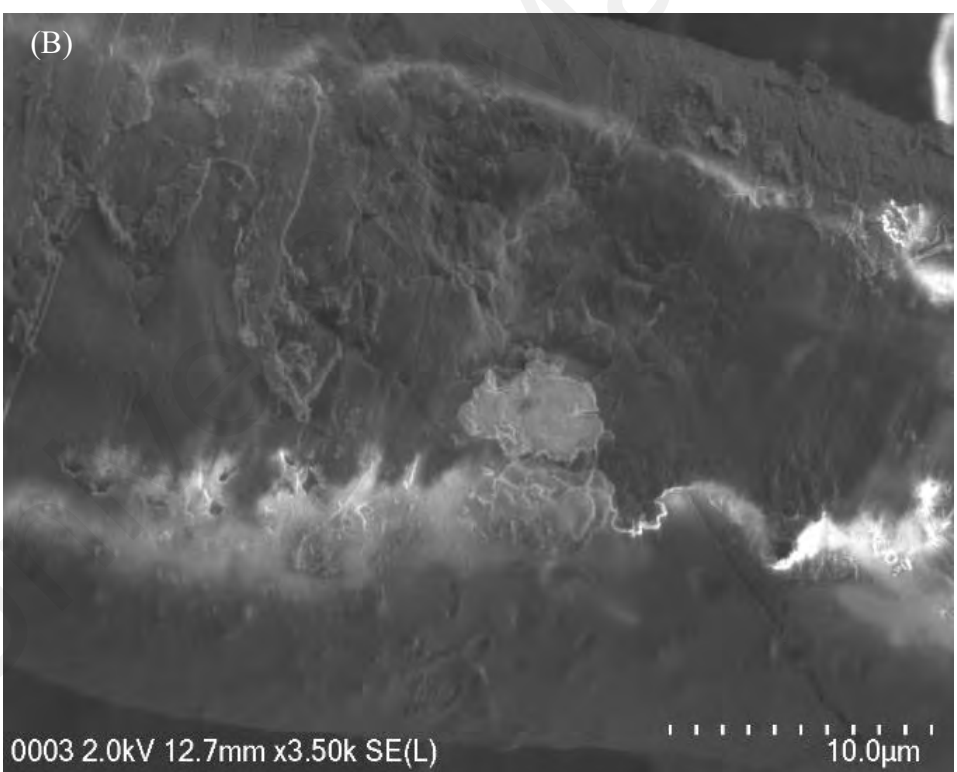


Figure 4.36: FESEM images of filter paper after 30 minutes of paddy straw combustion.

4.14 Energy Dispersive X-ray Analysis (EDX) of activated carbon

EDX was conducted as a qualitative method to identify elements that present in soot particles from the combustion of paddy straw. Soot sediment accumulated on the inner wall of the muffler analyzed using FESEM and EDX. Figure 4.37 shows that the soot has carbonaceous structure.

EDX data of soot sediments were used as a reference to identify soot adsorbed on the surface of MZCS. From the data tabulated in Table 4.10, soot sediments contain more than 20% oxygen content. Blank filter paper shows high oxygen content (42.16%) and low carbon content (57.84%). After the combustion process, soot produced has adhered to the filter paper surface. EDX analysis was carried out on the filter paper fiber at the area where soot particles were visible (Figure 4.38). The data shows an identical content of soot on filter paper surface to soot sediment. The results obtained in this study indicated that soot has indeed adhered to the filter paper surface.

Table 4.10: EDX analysis on filter paper and MZCS before and after combustion

Sample / content percentage (%)	C	0
Filter paper	57.84	42.16
Filter paper after combustion	73.37	26.12
Soot	74.30	22.64
MZCS before combustion	93.67	5.83
MZCS after combustion area 1	89.83	9.67
MZCS after combustion (on soot area 2)	72.49	24.66
MZCS after combustion (on soot area 3)	75.80	21.55

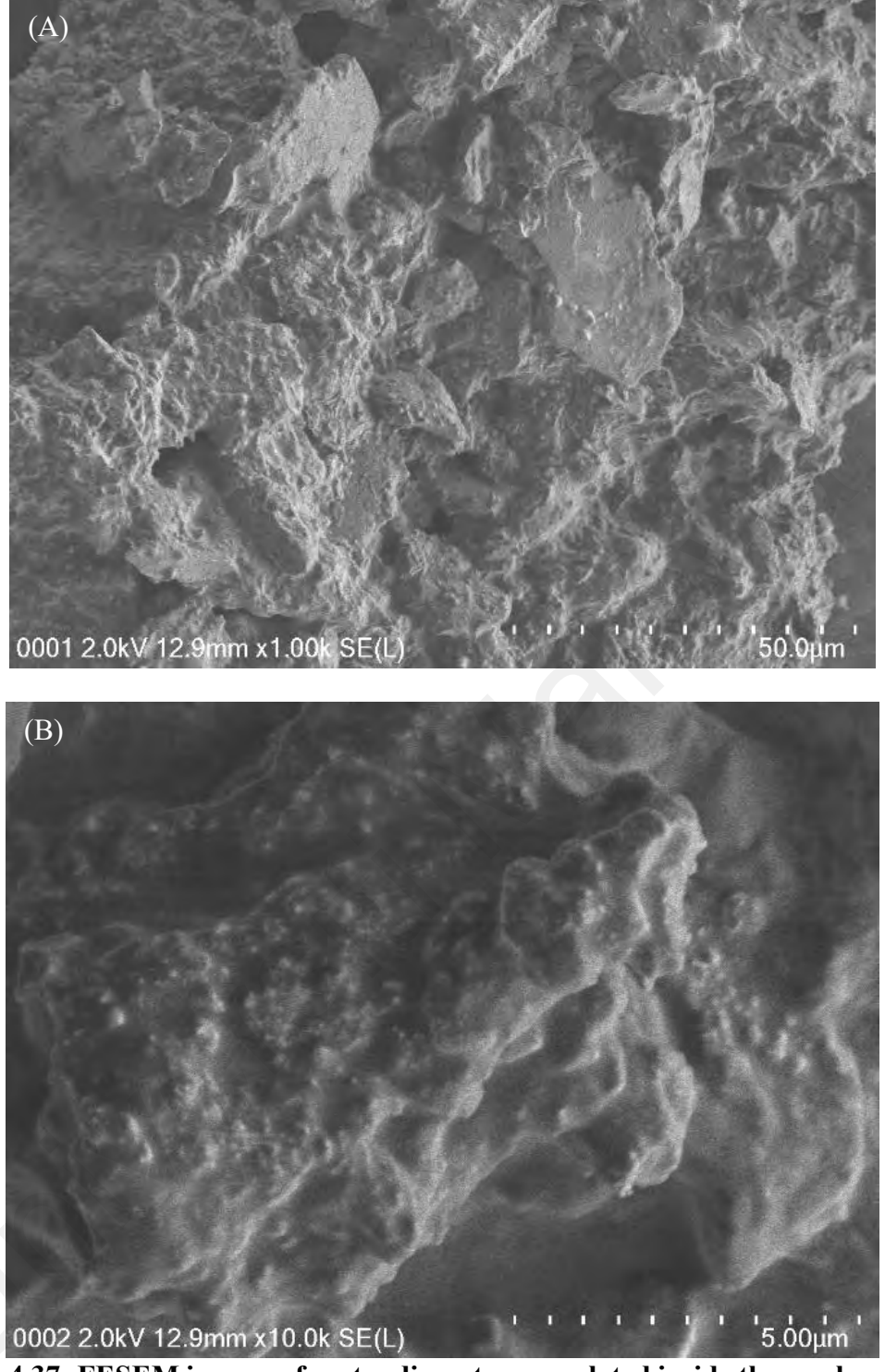


Figure 4.37: FESEM images of soot sediment accumulated inside the smoke muffler

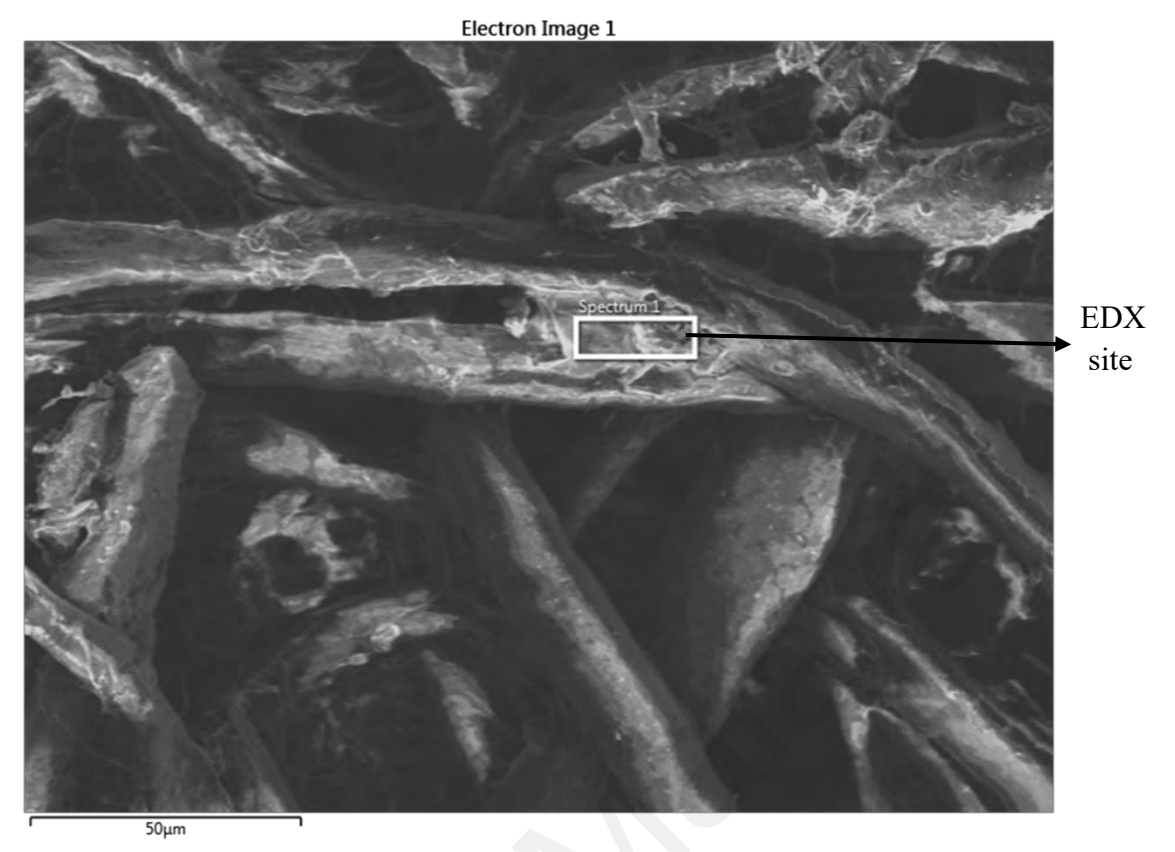


Figure 4.38: EDX site on filter paper after combustion with paddy straw was conducted

Meanwhile, MZCS shows low oxygen content and high carbon content before combustion due to the preparation of AC that produces a fully carbonaceous material. After combustion, EDX data from Table 4.10 on two different soot areas (Figure 4.39) in MZCS shows similar content with soot. Due to the similarities in properties, it is proven that particles adsorbed on the MZCS structure were indeed soot particles. By referring to Figure 4.38, when EDX analysis was conducted on the same MZCS but at a site that does not contain soot particles, the oxygen level dropped (9.67%) and carbon content is higher (89.83%).

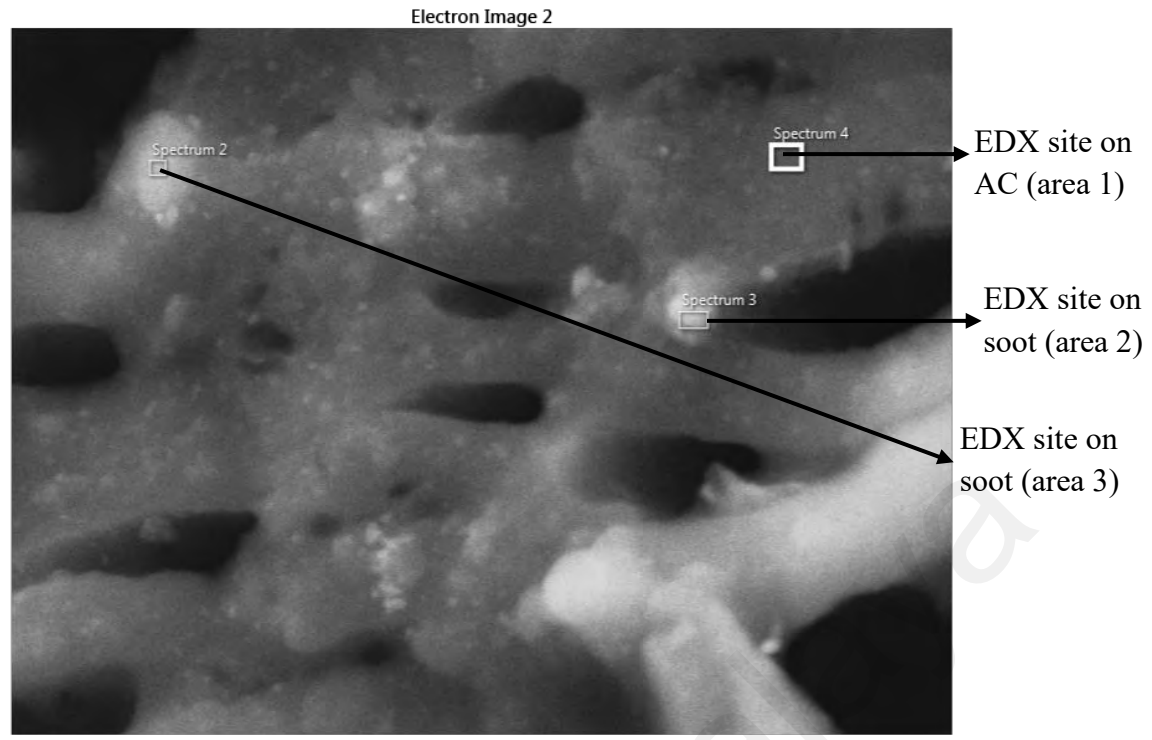


Figure 4.39: EDX analysis on different spots on AC surface

4.15 Economic feasibility of prepared activated carbon

The production cost estimation was based on similar studies conducted by Liew *et al.* (2019). Cost estimations are included in Table 4.11. The total time required for the process includes carbonization and activation. In this study, the capacity and volume for loading feedstock were referred to the current furnace and microwave utilized. The yield of the product is calculated using the data presented in Section 4.9. Feedstock, utility, labor, and depreciation costs were calculated by referring to Liew *et al.* (2019).

This research was able to reduce 46.86% of the lab scale production cost. The cost savings are primarily due to the reduction in chemical costs and the higher feedstock loading capacity. The activation process requires only one low-cost chemical. Additionally, the larger capacity of the furnace (6 L) and microwave (42 L) increases feedstock loading capacity. The furnace and microwave have a combined maximum capacity of 5 kg per batch.

Table 4.11: Estimation cost for lab-scale production compared to Liew *et al.* (2019) using the same starting materials

ısing the same starting materials						
	Present study	Liew <i>et al</i> . 2019				
Production:						
Operating hour	8 h/day	8 h/day				
Total process time	2.5 h/batch	1h/batch				
Feedstock loading capacity	5 kg	1 kg				
Product yield	25 wt% = 1.25 kg/batch	25 wt% = 2.5 kg/batch				
Daily output product	2.5 kg	2 kg				
Annual output product	650 kg	520 kg				
(5 working days/week × 52						
weeks/year = 260 working days						
per year)						
Operating cost (USD):						
Feedstock	0.05 /kg	0.05 /kg				
	$0.05 \times 2600 \text{ kg/year} =$	$0.05 \times 2080 \text{ kg/year} =$				
	130 USD/year	104 USD/year				
Chemical	0.04 USD/kg	0.40 USD/kg				
	$(0.04 \times 2.5 \text{kg char to})$	$(0.4 \times 4 \text{kg feedstock to})$				
	produce 2.5kg product)	produce 1 kg product)				
	\times 650 kg/year =	×				
	65 USD/year	520 kg/year =				
		832 USD/year				
Utilities	0.03 USD/year	0.03 USD/year				
	0.03 x 8 hours/day x	0.03 x 8 hours/day x				
	260 days/year =	260 days/year =				
	62.4 USD	62.4 USD				
Labour	3000 USD/year	3000 USD/year				
Depreciation	1283 USD	1283 USD				
Annual operating cost	4540.4 USD	5281.4 USD				
Annual operating cost / Annual	4.78 USD	10.2 USD				
output (kg/year) =						
Production costing						

4.16 Comparison studies with other findings

Table 4.12 shows a comparison between this study and other related studies that used a similar preparation method and starting materials. Almost all of the listed studies produced higher BET surface area. This is due to their preparation condition under vacuum or inert environment. As mentioned in Section 2.3.2, vacuum environment is preferred although it is not compulsory. While ZnCl₂ is used by three out of the five studies compared, the use of PKS as starting material for AC preparation is scarce. Other than that, none of the studies invested the utilization of AC for the adsorption of soot particles. Hence, proving the novelty of this study.

Table 4.12: A comparison between this study and other findings

Author	Raw material	Preparation method	BET surface area (m²/g)	Application
Vargas- delgadillo, Giraldo, & Moreno- piraján, 2010	CS	ZnCl ₂ , Chemical activation	725	Phenol adsorbents
Wang et al., 2013	CS	H ₃ PO ₄ , Chemical activation	891	Removal/adsorption methylene blue
Hidayu & Muda, 2016)	CS	ZnCl ₂ Chemical activation	953	CO ₂ capture
Hidayu & Muda, 2016)	CS	ZnCl ₂ , Chemical activation	1223	CO ₂ capture
Sahri <i>et al.</i> , 2020	PKS	KOH and microwave, physiochemical activation	322	CO ₂ capture

CHAPTER 5: CONCLUSION

5.1 Conclusion

This research began with a background examination of both biomasses (PKS and CS). Proximal analysis, ultimate analysis, lignocellulosic background, TGA profile, and FTIR analysis were performed on the starting materials. Both starting materials exhibit some similarities, although CS and PKS are derived from distinct species. Moisture, ash, volatile matter, and fixed carbon content of both biomasses are remarkably similar. However, it is found that PKS has slightly higher H/C and O/C ratios than of CS which then renders PKS higher heating value than CS. This is also in agreement with the optimized carbonization temperature for PKS was higher than that for CS. Both starting materials contain negligible amount of nitrogen and sulphur at less than 1% nitrogen and 1.6% sulphur.

Both biomasses have a remarkably similar background in terms of TGA analysis results. The vaporization of two main biopolymers occurs at the same temperature. The greatest percentage of weight loss occurred between 294°C until 410°C with two peaks formed. The first peak indicated hemicellulose and cellulose decomposition, while the second peak indicated lignin decomposition which occurred at a much higher temperature. The percentage weight loss obtained from both peaks is consistent with the amount of lignocellulosic material determined experimentally. Thus, the lignin content of PKS (41%) and the hemicellulose content of CS (38.8%) agree with the TGA results. As a result of this analysis, it is known that PKS contains a high concentration of hemicellulose.

Due to the similarity in the background characteristics of the two biomasses, the preparation conditions for both materials were identical. The primary difference is in the carbonization process, where PKS required a higher temperature (650°C) than CS (600°C), owing to the high concentration of lignin in the PKS structure. Consequently,

the most optimum condition to prepare AC is carbonization temperature of 650°C for PKS and 600°C for CS, 30 minutes carbonization time, a 1:1 activation ratio, and a 2 hours activation time. The percentage yield of AC obtained in this study is 25% and 21.4% for PKS and CS, respectively.

Carbonization success was confirmed by the reduction of peaks in the FTIR analysis for both materials. At the aforementioned optimal carbonization temperature, the loss of FTIR signals is readily apparent. Although the activation process is complete, several significant peaks remain visible. This includes the C = C peaks in the aromatic ring found in the PKS lignin structure. Additionally, C - O - C bonding peaks were observed in the FTIR spectra of CS. These lignocellulosic bonds are rigid and does not break after heating and activation.

In comparison to other activation agents, ZnCl₂ activation had the highest BET surface area value. MZCS was found to have registered the highest surface area value at 391.26 m²/g while MZPKS surface area is at 367.12 m²/g. MZCS and MZPKS have pore diameters of 1.69 nm and 1.72 nm, respectively. The pore opening was sized appropriately for smoke particle adsorption. As a result, MZCS and MZPKS have fulfilled the preparation of AC that suits the objectives of this study. The explanation above answers the second research question in this study.

In terms of application, the FESEM images demonstrate that MZCS is capable of evenly adsorbing soot particles across the surface and inside the pores. Meanwhile, adsorption on the surface of MZPKS is scattered and less dense than on the surface of MZCS. The most optimized condition is for 0.1 g of AC, approximately 23 g of paddy straw could be combusted for 30 minutes. Increasing the mass of paddy straw and increasing duration time will result in the accumulation of smoke particles on the AC surface.

From FESEM images collected after MZCS has been subjected to paddy straw burning, the physical adsorption can be seen on the AC surface. The instantaneous adsorption leads to physisorption interaction of soot with the surface of AC. Hence, the third research question was answered as the produced AC adsorb soot particles from the combustion process through physisorption adsorption.

In conclusion, this research has achieved its objectives. Preparation of AC from PKS and CS has resulted in the production of six AC's namely MACS, MBCS, MZCS, MAPKS, MBPKS and MZPKS. The properties of these AC's have been characterized and the most suited AC to be applied as soot adsorbent was MZCS and MZPKS. After the application of the smoke muffler, it is discovered that the most suitable AC to adsorb soot particles is MZCS.

5.2 Recommendation for future work

Several recommendations for future research have been identified at the end of this study. To begin, it is recommended that the percentage of soot adsorbed by AC be studied. Due to a lack of instrumentation, this parameter was not studied. The percentage of soot adsorbed can be studied using an optical particulate counter that yield result in $\mu g/m^3$ will show the effectiveness of the AC applied.

Next, it is also recommended to increase the surface area of the AC produced by a different preparation method, such as steam or carbon dioxide as an activating agent. Increasing the surface area of the AC may improve its adsorption efficiency.

Additionally, it is recommended that the application of AC in smoke-generating applications be expanded. The AC can serve a dual purpose of adsorbing soot particles and harmful gases released during the combustion process as Boshir *et al.* (2019) and

Chen *et al.* (2019) demonstrated in the adsorption of gases on AC. By allowing this, the AC will be able to further reduce the harmful burning effect.

Lastly, increasing the amount of AC used during the burning process is hypothesized to improve its adsorption capacity. The current study makes use of a single AC filter for each burning. Increasing the amount of AC may affect the capacity of the adsorption process by allowing for the combustion of more biomass.

REFERENCES

- Abioye, A. M., & Ani, F. N. (2017). Advancement in the production of activated carbon from biomass using microwave heating. *Jurnal Teknologi*, 79(3), 79–88.
- Adler, G., Wagner, N. L., Lamb, K. D., Manfred, K. M., Schwarz, J. P., Franchin, A. & Murphy, D. M. (2019). Evidence in biomass burning smoke for a light-absorbing aerosol with properties intermediate between brown and black carbon. *Aerosol Science and Technology*, 53(9), 976–989.
- Agriculture. (2019, November 29). Dosm.gov.my. Retrieve on November 30th 2019 from https://www.dosm.gov.my/v1/index.php?r=column/ctwoByCat&parent_id=45&me nu_id=Z0VTZGU1UHBUT1VJMFlpaXRRR0xpdz09#:~:text=Selected%20Agricu ltural%20Indicators%2C%20Malaysia%2C%202019,contributed%207.3%20per% 20cent%20(RM99.&text=Oil%20palm%20was%20the%20major,%25)%20and%2 0rubber%20(2.8%25).
- Ahmed, M. J., & Hameed, B. H. (2020). Insight into the co-pyrolysis of different blended feedstocks to biochar for the adsorption of organic and inorganic pollutants: A review. *Journal of Cleaner Production*, 265, 121762.
- Ahmed, M. J. (2016). Application of agricultural based activated carbons by microwave and conventional activations for basic dye adsorption: Review. *Journal of Environmental Chemical Engineering*, 4(1), 89–99.
- Ahmed, M. J., & Theydan, S. K. (2014). Optimization of microwave preparation conditions for activated carbon from *Albizia Lebbeck* seed pods for methylene blue dye adsorption. *Journal of Analytical and Applied Pyrolysis*, 105, 199–208.
- Alen, R., Kuoppala, E., & Oesch, P. (1996). Formation of the main degradation compound groups from wood and its components during pyrolysis. *Journal of Analytical and Applied Pyrolysis*, 36(2), 137–148.
- Alonso, D.M., Wettstein, S.G. & Dumesic, J.A. (2012). Bimetallic catalysts for upgrading of biomass to fuels and chemicals. *Chemical Society Reviews*, 41(24), 8075–8098. https://doi.org/10.1039/c2cs35188a.
- Andrade, S. N., Veloso, C. M., Fontan, R. C. I., Bonomo, R. C. F., Santos, L. S., Brito, M. J. P., & State, G. A. D. (2018). Chemical-activated carbon from coconut (*Cocos nucifera*) endocarp waste and its application in the adsorption of β-lactoglobulin protein carbon. *Revista Mexicana de Ingeniería Química*, 463–475.
- Anubriya, D., Mathangi, J. B., & Helen Kalavathy, M. (2020). Performance of nano porous carbon material derived from *Cocos nucifera*: An approach for the recovery of nickel using continuous operation. *Materials Letters*, 262, Article#127101.
- Arami-Niya, A., Daud, W. M. A. W., & Mjalli, F. S. (2011). Comparative study of the textural characteristics of oil palm shell activated carbon produced by chemical and physical activation for methane adsorption. *Chemical Engineering Research and Design*, 89(6), 657–664.

- Bansal, R.C. & Goyal, M. (2005). *Activated Carbon Adsorption*. Florida, USA: CRC Press.
- Basu, P. (2018). Biomass characteristics. In Biomass Gasification, Pyrolysis and Torrefaction: Practical Design and Theory.
- Bedoic, R., Ćosić, B., & Duić, N. (2019). Technical potential and geographic distribution of agricultural residues, co-products and by-products in the European Union. *Science of the Total Environment*, 686, 568–579.
- Bello, O. S., & Ahmad, M. A. (2012). Separation science and technology coconut (*cocos Nucifera*) shell based activated carbon for the removal of malachite green dye from aqueous solutions coconut (*Cocos Nucifera*) shell based activated carbon for the removal of malachite green dye from aqueous solution. *Separation Science and Technology*, 37–41.
- Bernama (2019). Petani Kedah disaran elak bakar jerami. Retrieved on 30 November 2019 from https://selangorkini.my/2019/09/petani-kedah-disaran-elak-bakar-jerami/
- Bhungthong, S., Aussawasathien, D., Hrimchum, K., & Sriphalang, S. N. (2018). Preparation and properties of activated carbon from palm shell by potassium hydroxide impregnation: Effects of processing parameters. *Chiang Mai Journal of Science*, 45(1), 462–473.
- Boehm, H. P. (1994). Some aspects of the surface chemistry of carbon blacks and other carbons. Carbon, 32(5), 759–769.
- Boehm, H.P. (2002). Surface oxides on carbon and their analysis: a critical assessment. *Carbon*, 40, 145.
- Bond, T. C., Doherty, S. J., Fahey, D. W., Forster, P. M., Berntsen, T., Deangelo, B. J. & Zender, C. S. (2013). Bounding the role of black carbon in the climate system: A scientific assessment. *Journal of Geophysical Research Atmospheres*, 118(11), 5380–5552.
- Boshir Ahmed, M., Abu Hasan Johir, M., Zhou, J. L., Hao Ngo, H., Duc Nghiem, L., Richardson, C., & Bryant, M. R. (2019). Activated carbon preparation from biomass feedstock: clean production and carbon dioxide adsorption. *Journal of Cleaner Production*, Article#225.
- California Air Resources Board. (2021). *Agricultural Burning*. California Air Resources Board. Retrieved on 30 December 2021 from https://ww2.arb.ca.gov/ourwork/programs/agricultural-burning/about.
- Cazetta, A. L., Vargas, A. M. M., Nogami, E. M., Kunita, M. H., Guilherme, M. R., Martins, A. C. & Almeida, V. C. (2011). NaOH-activated carbon of high surface area produced from coconut shell: Kinetics and equilibrium studies from the methylene blue adsorption. *Chemical Engineering Journal*, 174, 117–125.

- Chen, Y. T., Huang, Y. P., & Hsi, H. C. (2019). Valorizing Waste Bamboo Tar to Novel Bead Carbonaceous Adsorbent for Volatile Organic Compound Removal. *Journal of Environmental Engineering (United States)*, 145(12), 1–7.
- Collard, F. X., & Blin, J. (2014). A review on pyrolysis of biomass constituents: Mechanisms and composition of the products obtained from the conversion of cellulose, hemicelluloses and lignin. *Renewable and Sustainable Energy Reviews*, 38, 594–608.
- D'Anna, A. (2015). *Kinetics of Soot Formation*., Molecular Sciences and Chemical Engineering. Retrieve on 1st May 2020 from https://doi.org/10.1016/b978-0-12-409547-2.11524-0
- Derbyshire, F., Jagtoyen, M., & Thwaites M. (1995). *Porosity in carbons*. Eduar Arnold.
- Dhyani, V., & Bhaskar, T. (2018). A comprehensive review on the pyrolysis of lignocellulosic biomass. *Renewable Energy*, 129, 695–716.
- European Commission (EC). (2015). EIP-AGRI Workshop "Opportunities for Agriculture and Forestry in the Circular Economy". Retrieve on 1 December 2019 from https://ec.europa.eu/eip/agriculture/sites/agri-eip/files/eipagri_ws_circular_ecomy_final_report_2015_en.pdf
- Enders, A., Hanley, K., Whitman, T., Joseph, S., & Lehmann, J. (2012). Characterization of biochars to evaluate recalcitrance and agronomic performance. *Bioresources Technology*, 114: 644–53.
- Foo, K. Y., & Hameed, B. H. (2012). Coconut husk derived activated carbon via microwave induced activation: Effects of activation agents, preparation parameters and adsorption performance. *Chemical Engineering Journal*, 184, 57–65.
- Food and Agriculture Organization of the United Nations (FAO), 2017. *Strategic Work of FAO for Sustainable Food and Agriculture*. Retrieve on 1 December 2019 from http://www.fao.org/3/a-i6488e.pdf
- Freitas, J. V., Nogueira, F. G. E., & Farinas, C. S. (2019). Coconut shell activated carbon as an alternative adsorbent of inhibitors from lignocellulosic biomass pre-treatment. *Industrial Crops and Products*, 137 (May), 16–23.
- Ganesapillai, M., Simha, P., & Gugalia, A. (2014). Recovering urea from human urine by bio-sorption onto Microwave Activated Carbonized Coconut Shells: Equilibrium, kinetics, optimization and field studies. *Journal of Environmental Chemical Engineering*, 2(1), 46–55.
- Ge, S., Foong, S. Y., Ma, N. L., Liew, R. K., Wan Mahari, W. A., Xia, C., & Lam, S. S. (2020). Vacuum pyrolysis incorporating microwave heating and base mixture modification: An integrated approach to transform biowaste into eco-friendly bioenergy products. *Renewable and Sustainable Energy Reviews*, 127(April), Article#109871.

- Ghazali, Z., & Abdullah, M. P. (2012). Preparation of activated carbon from coconut shell to remove aluminum and manganese in drinking water. *Advances in Natural and Applied Sciences*, 6(8), 1307–1312.
- Gonzalez-Garcia, P. (2018). Activated carbon from lignocellulosic precursors: A review of the synthesis methods, characterization techniques and applications. *Renewable and Sustainable Energy Reviews*, 82, 1393–1414.
- Grondahl, M., Teleman, A., & Gatenholm, P. (2003). Effect of acetylation on the material properties of glucuronoxylan from aspen wood. *Carbohydrate Polymers*, 52(4), 359–366.
- Guo, Y., & Rockstraw, D. A. (2007). Physicochemical properties of carbons prepared from pecan shell by phosphoric acid activation. *Bioresource Technology*, 98(8), 1513–1521.
- Gummert, M., Hung, N. Van, Chivenge, P., & Douthwaite, B. (2020). Sustainable Rice Straw Management. Sustainable Rice Straw Management. Retrieve on 1st January 2021 from https://doi.org/10.1007/978-3-030-32373-8
- Hassan, A. F., Abdel-Mohsen, A. M., & Fouda, M. M. G. (2014). Comparative study of calcium alginate, activated carbon, and their composite beads on methylene blue adsorption. *Carbohydrate Polymers*, 102(1), 192–198.
- He, K., Zhang, J., & Zeng, Y. (2019). Knowledge domain and emerging trends of agricultural waste management in the field of social science: A scientometric review. *Science of the Total Environment*, 670, 236–244.
- Heidarinejad, Z., Dehghani, M. H., Heidari, M., Javedan, G., Ali, I., & Sillanpää, M. (2020). Methods for preparation and activation of activated carbon: A Review. *Environmental Chemistry Letters*.
- Hesas, H. R., Arami-Niya, A., Wan Daud, W. M. A., & Sahu, J. N. (2015). Microwave-assisted production of activated carbons from oil palm shell in the presence of CO₂ or N₂ for CO₂ adsorption. *Journal of Industrial and Engineering Chemistry*, 24, 196–205.
- Hidayu, A. R., & Muda, N. (2016). Preparation and characterisation of impregnated activated carbon from palm kernel shell and coconut shell for CO₂ capture. *Procedia Engineering*, 148, 106–113.
- Huang, P., Cheng, H., & Lin, S. (2015). Adsorption of carbon dioxide onto activated carbon prepared from coconut shells. *Journal of Chemistry*, 1–10.
- Husseinsyah, S., & Zakaria, M. M. (2011). The Effect of Filler Content on Properties of Coconut Shell Filled Polyester Composites. *Polymer*, 6(1), 87–97.
- Ilomuanya, M., Nashiru, B., Ifudu, N., & Igwilo, C. (2016). Effect of pore size and morphology of activated charcoal prepared from midribs of *Elaeis guineensis* on adsorption of poisons using metronidazole and *Escherichia coli* O157:H7 as a case study. *Journal of Microscopy and Ultrastructure*, Article#5(1), 32.

- Ioannidou, O., & Zabaniotou, A. (2007). Agricultural residues as precursors for activated carbon production-A review. *Renewable and Sustainable Energy Reviews*, 11(9), 1966–2005.
- Isikgor, F. H., & Becer, C. R. (2015). Polymer Chemistry The Production Of Bio-Based Chemicals and Polymers. 4497–4559.
- Jain, A., Jayaraman, S., Balasubramanian, R., & Srinivasan, M. P. (2014). Hydrothermal pre-treatment for mesoporous carbon synthesis: enhancement of chemical activation. *Journal of Materials Chemistry*, 2, 520–528.
- Jakab, E., Faix, O., Till, F., & Székely, T. (1995). Thermogravimetry/mass spectrometry study of six lignins within the scope of an international round robin test. *Journal of Analytical and Applied Pyrolysis*, 35(2), 167–179.
- Jadhav, A., & Mohanraj, G. (2016). Synthesis of activated carbon from *Cocos Nucifera* of *Cocos Nucifera* leaves activated carbon nucifera leaves activated carbon. *Chemistry & Chemical Technology*, 10(2), 201–208.
- Jawad, A. H., Sabar, S., Azlan, M., Ishak, M., Wilson, L. D., Solehah, S., & Farhan, A. M. (2017). Microwave-assisted preparation of mesoporous activated carbon from coconut (*Cocos Nucifera*) leaf by H₃PO₄-activation for methylene blue adsorption. *Chemical Engineering Communications*, 6445(July).
- Jones, D.A., Lelyveld, T.P., Mavrofidis, S.D., Kingman, S.W., & Miles, N.J. (2002). Microwave heating applications in environmental engineering: A Review. *Resources, Conservation Recycling*, *34*, 75-90.
- Kamarul Zaman, K., Balasundram, V., Ibrahim, N., Samsudin, M. D. M., Kasmani, R. M., Hamid, M. K. A., & Hasbullah, H. (2018). Effect of particle size and temperature on pyrolysis of palm kernel shell. *International Journal of Engineering and Technology (UAE)*, 7(4), 118–124.
- Kan, T., Strezov, V., & Evans, T. J. (2016). Lignocellulosic biomass pyrolysis: A review of product properties and effects of pyrolysis parameters. *Renewable and Sustainable Energy Reviews*, 57, 1126–1140.
- Koplitz, S.N., Mickley, L.J., Marlier, M.E., Buonocore, J.J., Kim, P.S., & Liu, T. (2016). Public health impacts of the severe haze in Equatorial Asia in September–October 2015: demonstration of a new framework for informing fire management strategies to reduce downwind smoke exposure. *Environmental Research Letters*, 11(9): Article#094023.
- Koyuncu, F., Güzel, F., & Sayğılı, H. (2018). Role of optimization parameters in the production of nanoporous carbon from mandarin shells by microwave-assisted chemical activation and utilization as dye adsorbent. *Advanced Powder Technology*, 29(9), 2108–2118.
- Kumar N, S., Grekov, D., Pré, P., & Alappat, B. J. (2020). Microwave mode of heating in the preparation of porous carbon materials for adsorption and energy storage applications An overview. *Renewable and Sustainable Energy Reviews*, 124(December 2019).

- Lack, D. A., Moosmüller, H., McMeeking, G. R., Chakrabarty, R. K., & Baumgardner, D. (2014). Characterizing elemental, equivalent black, and refractory black carbon aerosol particles: A review of techniques, their limitations and uncertainties. *Analytical and Bioanalytical Chemistry*, 406(1), 99–122.
- Lee, C. L., H'ng, P. S., Chin, K. L., Paridah, M. T., Rashid, U., & Go, W. Z. (2019). Characterization of bioadsorbent produced using incorporated treatment of chemical and carbonization procedures. *Royal Society Open Science*, 6(9), Article#190667.
- Lewicka, K. (2017). Activated carbons prepared from hazelnut shells, walnut shells and peanut shells for high CO2 adsorption. *Polish Journal of Chemical Technology*, 19(2), 38–43.
- Li, D., Wang, Y., Zhang, X., Zhou, J., Yang, Y., Zhang, Z., & Zhao, X. (2020). Effects of compacting activated carbons on their volumetric CO₂ adsorption performance. *Fuel*, 262(November 2019), Article#116540.
- Li, N., Ma, X., Zha, Q., Kim, K., Chen, Y., & Song, C. (2011). Maximizing the number of oxygen-containing functional groups on activated carbon by using ammonium persulfate and improving the temperature-programmed desorption characterization of carbon surface chemistry. *Carbon*, 49(15), 5002–5013.
- Li, S., Xu, S., Liu, S., Yang, C., & Lu, Q. (2004). Fast pyrolysis of biomass in free-fall reactor for hydrogen-rich gas. *Fuel Processing Technology*, 85(8–10), 1201–1211.
- Liang, Q., Liu, Y., Chen, M., Ma, L., Yang, B., Li, L., & Liu, Q. (2020). Optimized preparation of activated carbon from coconut shell and municipal sludge. *Materials Chemistry and Physics*, 241(July 2019), Article#122327.
- Liew, R. K., Chai, C., Yek, P. N. Y., Phang, X. Y., Chong, M. Y., Nam, W. L., & Lam, S. S. (2019). Innovative production of highly porous carbon for industrial effluent remediation via microwave vacuum pyrolysis plus sodium-potassium hydroxide mixture activation. *Journal of Cleaner Production*, 208(2019), 1436–1445.
- Liew, R. K., Chong, M. Y., Osazuwa, O. U., Nam, W. L., Phang, X. Y., Su, M. H. & Lam, S. S. (2018). Production of activated carbon as catalyst support by microwave pyrolysis of palm kernel shell: a comparative study of chemical versus physical activation. *Research on Chemical Intermediates*, 44(6), 3849–3865.
- Liu, L., & Mishchenko, M. I. (2020). Spectrally dependent linear depolarization and lidar ratios for nonspherical smoke aerosols. *Journal of Quantitative Spectroscopy and Radiative Transfer*, 248, Article#106953.
- Liu, Y., Li, K., Ge, B., Pu, L., & Liu, Z. (2016). Influence of Micropore and Mesoporous in Activated Carbon Air-cathode Catalysts on Oxygen Reduction Reaction in Microbial Fuel Cells. *Electrochimica Acta*, 214, 110–118.
- Ma, Y. (2017). Comparison of Activated Carbons Prepared from Wheat Straw via ZnCl₂ and KOH Activation. *Waste and Biomass Valorization*, 8(3), 549–559.
- Ma, R., Hao, J., Chang, G., Wang, Y., & Guo, Q. (2020). Nitrogen-doping microporous adsorbents prepared from palm kernel with excellent CO₂ capture property. *Canadian Journal of Chemical Engineering*, 98(2), 503–512.

- McNaught, A.D. & Wilkinson, A. (1997). *IUPAC. Compendium of Chemical Terminology*. Blackwell, Oxford: Scientific Publications.
- Menendez-Diaz, J.A. & Martin-Gullon, I. (2006). Types of Carbon Adsorbents and Their Production. Act. Carbon Surfaces Environment Remediation. Philadelphia, PA: Elsevier Ltd, p. 1–47.
- Metaxas, A. C. (1991). Microwave Heating. Power Engineering Journal. 5(5): 237-247.
- Mohammed, J., Nasri, N. S., Zaini, M. A. A., Hamza, U. D., & Ahmed, M. M. (2014). Optimization of preparation of microwave irradiated bio-based materials as porous carbons for VOCs removal using response surface methodology. *Applied Mechanics and Materials*, 554, 175–179.
- Mohammed, J., Shawal, N., Abbas, M., Zaini, A., Dadum, U., & Nasir, F. (2015). Adsorption of benzene and toluene onto KOH activated coconut shell-based carbon treated with NH₃. *International Biodeterioration & Biodegradation*, 1–11.
- Mohd Din, A. T., Hameed, B. H., & Ahmad, A. L. (2009). Batch adsorption of phenol onto physiochemical-activated coconut shell. *Journal of Hazardous Materials*, *161*, 1522–1529.
- Nasri, N.S., Umar, H., Abbas, M., Zaini, A., Rashid, N. M., Abdul, Z., & Zaini, N. (2019). Methane and natural gases kinetic and equilibrium adsorption comparison on synthesized porous coconut shell kernel activated carbon. *Chemical Engineering Transactions*, 72, 61–66.
- Nizamuddin, S., Jayakumar, NS., Sahu, JN., Ganesan, P., Bhutto, AW., & Mubarak, NM. (2015) Hydrothermal carbonization of oil palm shell. *Korean Journal of Chemical Engineering*, 32, 1789–1797
- Nizamuddin, S., Shrestha, S., Athar, B., Ali, S., & Siddiqui, M. A. (2016). A critical analysis on palm kernel shell from oil palm industry as a feedstock for solid char production. *Reviews in Chemical Engineering*, 32(5): 489–505.
- Peng, W., Li, H., Liu, Y. & Song, S. (2017). A review on heavy metal ions adsorption from water by graphene oxide and its composites. *Journal of Molecular Liquid*, 230, 496–504.
- Phairuang, W., Suwattiga, P., Chetiyanukornkul, T., Hongtieab, S., Limpaseni, W., Ikemori, F., & Furuuchi, M. (2019). The influence of the open burning of agricultural biomass and forest fires in Thailand on the carbonaceous components in size-fractionated particles. *Environmental Pollution*, 247, 238–247.
- Pisupati. S.V. & Krishnamoorthy, V. (2017). *Utilization of Coal in IGCC Systems*. Woodhead Publishing, 83-120.
- Pósfai, M., Simonics, R., Li, J., Hobbs, P. V., & Buseck, P. R. (2003). Individual aerosol particles from biomass burning in southern Africa: 1. Compositions and size distributions of carbonaceous particles. *Journal of Geophysical Research: Atmospheres*, 108(13), 1–13.

- Prauchner, M. J., & Rodríguez-reinoso, F. (2012). Microporous and mesoporous materials chemical versus physical activation of coconut shell: A comparative study. *Microporous and Mesoporous Materials*, 152, 163–171.
- Prauchner, M. J., Sapag, K., & Rodríguez-reinoso, F. (2016). Tailoring biomass-based activated carbon for CH₄ storage by combining chemical activation with H₃PO₄ or ZnCl₂ and physical activation with CO₂. *Carbon*, 110, 138–147.
- Pye, H. O. T., Nenes, A., Alexander, B., & Zuend, A. (2020). The acidity of atmospheric particles and clouds, *Atmospheric Chemistry and Physics*, 20(8), 4809–4888
- Rahman, M. M., Adil, M., & Yusof, A. M. (2012). Porosity Development in Activated Carbon from Palm Kernel and Coconut Shell by Chemical Activation Method. *Research Journal of Chemistry and Environment*, 16(4), 2010–2012.
- Ramirez-García, R., Gohil, N., & Singh, V. (2019). Recent Advances, Challenges, and Opportunities in Bioremediation of Hazardous Materials. *Phytomanagement of Polluted Sites*, 517 568.
- Rashidi, N. A., Yusup, S., Ahmad, M. M., Mohamed, N. M., & Hameed, B. H. (2012). Activated Carbon from the Renewable Agricultural Residues Using Single Step Physical Activation: A Preliminary Analysis. *APCBEE Procedia*, *3*, 84–92.
- Ritchie, H. & Roser, M. (2020). *Agricultural Production*. Retrieved on 1st December 2020 from https://ourworldindata.org/agricultural-production.
- Rodriguez Reinose, F. (1997). *Introduction to Carbon Technologies*. Publication of University De Alicante.
- Rouzitalab, Z., Maklavany, D. M., Jafarinejad, S., & Rashidi, A. (2020). Lignocellulose-based adsorbents: A spotlight review of the effective parameters on carbon dioxide capture process. *Chemosphere*, 246, Article#125756.
- Saka C. (2012). BET, TG-DTG, FT-IR, SEM, iodine number analysis and preparation of activated carbon from acorn shell by chemical activation with ZnCl₂. *Journal Analysis Applied Pyrolysis*. 95,21–24.
- Sahri, D. M., Zaini, N., Nasri, N. S., Zain, H. M., Rashid, N. M., & Noor Shawal, A. S. (2020). Carbon Dioxide Adsorption Equilibrium Rates Comparative Temperature Study Using Palm Kernel Shell Sorbent. IOP Conference Series: *Earth and Environmental Science*, 479(1), 0–8.
- Sami, M., Annamalai, K. & Wooldridge, M. (2001). Co-firing ofbcoal and biomass fuel blends. *Progress in Energy and Combustion Science*, 27(2):171–214.
- Sanchez-Silva, L., López-González, D., Villaseñor, J., Sánchez, P., & Valverde, J. L. (2012). Thermogravimetric-mass spectrometric analysis of lignocellulosic and marine biomass pyrolysis. *Bioresource Technology*, 109, 163–172.
- Sanni, E. S., Emetere, M. E., Odigure, J. O., Efeovbokhan, V. E., Agboola, O., & Sadiku, E. R. (2017). Determination of optimum conditions for the production of activated carbon derived from separate varieties of coconut shells. *International Journal of Chemical Engineering*.

- Saleem, M., Ali, M., Siddiqi, Z., & Al Qahtani, A. S. (2017). Preparation of Activated Carbon from Acacia (Vachellia seyal) Tree Branches and Application to Treat Wastewater Containing Methylene Blue Dye. *Modern Applied Science*, 11(12)
- Sarkar, D.L. (2015). Thermal Power Plant. Elsevier, 91-137.
- Schönherr, J., Buchheim, J. R., Scholz, P., & Adelhelm, P. (2018). Boehm Titration Revisited (Part I): Practical Aspects for Achieving a High Precision in Quantifying Oxygen-Containing Surface Groups on Carbon Materials. *Journal of Carbon Research*, 4(2), Article#21.
- Selvaraju, G., & Bakar, N. K. A. (2017). Process conditions for the manufacture of highly micro-mesoporous eco-friendly activated carbon from *Artocarpus Integer* bio-waste by steam activation. *Journal of the Taiwan Institute of Chemical Engineers*, 93, 414–426.
- Sharma, Y. C., Uma, & Gode, F. (2010). Engineering data for optimization of preparation of activated carbon from an economically viable material. *Journal of Engineering Data*, 55, 3991–3994.
- Shen, D. K., Gu, S., Luo, K. H., Wang, S. R., & Fang, M. X. (2010). The pyrolytic degradation of wood-derived lignin from pulping process. *Bioresource Technology*, 101(15), 6136–6146.
- Shrestha, G., Traina, S. J., & Swanston, C. W. (2010). Black carbon's properties and role in the environment: A comprehensive review. *Sustainability*, 2(1), 294–320.
- Soh, M., Chew, J. J., Liu, S., & Sunarso, J. (2019). Comprehensive kinetic study on the pyrolysis and combustion behaviors of five oil palm biomass by thermogravimetric-mass spectrometry (TG-MS) Analyses. *Bioenergy Research*, 12(2), 370–387.
- Suhas, Gupta, V. K., Carrott, P. J. M., Singh, R., Chaudhary, M., & Kushwaha, S. (2016). Cellulose: A review as natural, modified and activated carbon adsorbent. *Bioresource Technology*, 216, 1066–1076.
- Sun, K., Huang, Q., Chi, Y., & Yan, J. (2018). Effect of ZnCl₂-activated biochar on catalytic pyrolysis of mixed waste plastics for producing aromatic-enriched oil. *Waste Management*, 81, 128–137.
- Tacconi L. Preventing fires and haze in Southeast Asia. (2016). *Nature Climate Change*, 6(7), Article#640.
- Tan, Y. L., Abdullah, A. Z., & Hameed, B. H. (2017). Fast pyrolysis of durian (*Durio zibethinus L*) shell in a drop-type fixed bed reactor: Pyrolysis behavior and product analyses. *Bioresource Technology*, 243, 85–92.
- Teimouri, Z., Salem, A., & Salem, S. (2019). Clean and new strategy for catalytic impregnation: Applied and eco-friendly aspect for decoloration of industrial corn syrup and process identifications. *Journal of Environmental Chemical Engineering*, 7(3), 2213-3437.

- Tounsadi, H., Khalidi, A., Farnane, M., Abdennouri, M., & Barka, N. (2016). Experimental design for the optimization of preparation conditions of highly efficient activated carbon from *Glebionis coronaria L*. and heavy metals removal ability. *Process Safety and Environmental Protection*, 102, 710–723.
- Tounsadi, H., Khalidi, A., Farnane, M., Machrouhi, A., Elhalil, A., & Barka, N. (2019). Efficient removal of heavy metals by KOH activated *Diplotaxis harra* biomass: Experimental design optimization. *Environmental Engineering and Management Journal*, 18(3), 651–664.
- Xie, Z., Yang, J., Huang, X., & Huang, Y. (1999). Microwave processing and properties of ceramics with different dielectric loss. *Journal of the European Ceramic Society*, 19(3), 381-387.
- Xin-hui, D., Srinivasakannan, C., Jin-hui, P., Li-bo, Z., & Zheng-yong, Z. (2011). Comparison of activated carbon prepared from Jatropha hull by conventional heating and microwave heating. *Biomass and Bioenergy*, 35, 3920-3926.
- Ukanwa, K. S., Patchigolla, K., Sakrabani, R., Anthony, E., & Mandavgane, S. (2019). A review of chemicals to produce activated carbon from agricultural waste biomass. *Sustainability (Switzerland)*, 11(22), 1–35.
- Vargas-delgadillo, D. P., Giraldo, L., & Moreno-piraján, J. C. (2010). Preparation and characterisation of activated carbon monoliths with potential application as phenol adsorbents. *E-Journal of Chemistry*, 7(2), 531–539.
- conversion of agriculture waste shells to activated carbon via microwave-assisted
- Wang, X., Chi, Q., Liu, X., & Wang, Y. (2019). Influence of pyrolysis temperature on characteristics and environmental risk of heavy metals in pyrolyzed biochar made from hydrothermally treated sewage sludge. *Chemosphere*, 216, 698–706.
- Wei, J., Liang, G., Alex, J., Zhang, T., & Ma, C. (2020). Research progress of energy utilization of agricultural waste in China. *Sustainability (Switzerland)*, 12(3), Article#812.
- Yaacoubi, H., & Songlin, Z. (2019). Effect of Ammonia Modification on Activated Carbons for the Removal of Acidic Anthraquinone Dyes. *International Journal of Chemical Reactor Engineering*, 17(8), 1-13.
- Yang, K., Peng, J., Xia, H., Zhang, L., Srinivasakannan, C., & Guo, S. (2010). Textural characteristics of activated carbon by single step CO₂ activation from coconut shells. *Journal of the Taiwan Institute of Chemical Engineers*, 41(3), 367–372.
- Yang, X., Wan, Y., Zheng, Y., He, F., Yu, Z., Huang, J. & Gao, B. (2019). Surface functional groups of carbon-based adsorbents and their roles in the removal of heavy metals from aqueous solutions: A critical review. *Chemical Engineering Journal*, 366(January), 608–621.
- Yunus, Z. M., G, Y., Al-Gheethi, A., Othman, N., Hamdan, R., & Ruslan, N. N. (2020). Advanced methods for activated carbon from agriculture wastes; a comprehensive review. *International Journal of Environmental Analytical Chemistry*, 1–25.

- Zhang Z., Qu W., Peng J., Zhang L., Ma X., Zhang Z., Li W. (2009). Comparison between microwave and conventional thermal reactivations of spent activated carbon generated from vinyl acetate synthesis, *Desalination*, 249, 247–252.
- Zhao, X., Zeng, X., Qin, Y., Li, X., Zhu, T., & Tang, X. (2018). An experimental and theoretical study of the adsorption removal of toluene and chlorobenzene on coconut shell derived carbon. *Chemosphere*, 206, 285–292.
- Zhou, Y., Zhang, L., & Cheng, Z. (2015). Removal of organic pollutants from aqueous solution using agricultural wastes: A review. *Journal of Molecular Liquids*, 212, 739–762.
- Zafar, S. (2019, November 8). *Agricultural biomass in Malaysia*. Retrieved on 1st December 2019 from https://www.bioenergyconsult.com/agricultural-biomass-in-malaysia/
- Zailani, R., Ghafar, H., & So'aib, M. S. (2013). The Influence of oxygen in the carbonization of oil palm shell on bio-char yield and properties. *Applied Mechanics and Materials*, 393, 499–504.